Journal of Materials Chemistry C

ROYAL SOCIETY OF CHEMISTRY

REVIEW

View Article Online
View Journal

Cite this: DOI: 10.1039/d6tc00938g

Carbazole-based host materials for red to near-infrared OLEDs: molecular design strategies and structure–property relationships

Nurul Ridho Al Amin,[a] Premkumar Gnanasekaran,[b] Yuan Jay Chang *[b] and Chih-Hao Chang *[a]

Achieving high efficiency and long-term stability in red-to-near-infrared (NIR) organic light-emitting diodes (OLEDs) remains challenging due to narrow bandgaps, severe exciton quenching, and charge imbalance. Designing a suitable host is essential to overcome these limitations, as the host dictates exciton confinement, charge transport, and energy transfer to the emitter. Among various candidates, carbazole derivatives stand out as promising scaffolds owing to their excellent hole-transporting properties, tunable optoelectronic characteristics, low oxidation potential, and structural versatility. This review categorizes carbazole-based hosts into four main architectural designs: push–pull, symmetric, asymmetric, and special frameworks. We examine reported carbazole-based hosts used for red-emitters with emissive peaks above 600 nm and analyze the relationship between molecular architecture and device performance. Furthermore, we highlight how each architectural design influences charge balance, exciton confinement, and host–guest interaction in red-to-NIR OLEDs. By mapping the demonstrated carbazole-based hosts into a unified architectural framework, this review establishes structure–function principles and outlines future directions for the development of carbazole-based hosts tailored for high-performance red-to-NIR OLEDs.

Received 23rd March 2026,
Accepted 26th May 2026

DOI: 10.1039/d6tc00938g

rsc.li/materials-c

1. Introduction

1.1. Photophysical constraints and design requirements for red-to-NIR OLEDs

Emission extending beyond 600 nm in red-to-near-infrared (NIR) organic light-emitting diodes (OLEDs) provides distinct advantages for technological and biomedical applications, offering richer display color depth and deeper tissue penetration

[a] Department of Electrical Engineering, Yuan Ze University, Taoyuan 32003, Taiwan. E-mail: chc@saturn.yzu.edu.tw
[b] Department of Chemistry, Tunghai University, Taichung 40704, Taiwan. E-mail: jaychang@thu.edu.tw

Nurul Ridho Al Amin

Nurul Ridho Al Amin received his PhD in Electronic Engineering from the National Taiwan University of Science and Technology, Taiwan in 2024. He is currently a postdoctoral researcher in Prof. Chih-Hao Chang's group at Yuan Ze University. His research mainly focuses on fundamental characterization and optimization of organic optoelectronic devices.

Premkumar Gnanasekaran

Premkumar Gnanasekaran received his PhD in Chemistry from National Tsing Hua University, Taiwan. He is currently a postdoctoral researcher in Prof. Yuan Jay Chang's group at Tunghai University. He is currently conducting advanced molecule designing for self-assembled monolayers, OLED emitters, host materials, and perovskite solar cells.

for bioimaging and phototherapy.[1–6] However, their efficiency and stability are restricted by fundamental photophysical limitations. As emission shifts to longer wavelengths, the energy-gap law leads to an exponential increase in non-radiative decay.[7] At the same time, exciton-loss pathways such as triplet–triplet annihilation (TTA) and exciton–polaron quenching (EPQ) become more pronounced. Red-to-NIR emitters also require host materials with narrower bandgaps, which typically exhibit lower triplet energies. This property could increase the likelihood of back-energy transfer from the emitter to the host, thereby reducing radiative efficiency. Furthermore, lower bandgaps often correspond to deeper lowest unoccupied molecular orbital (LUMO) levels in the host material, causing charge imbalance and contributing to efficiency roll-off.[8–11] Overcoming these limitations requires a deeper understanding of host material molecular design, which is critical for the development of high-performance red-to-NIR OLEDs.[12–14]

An effective host material, particularly for red-to-NIR OLEDs, plays a crucial role not only as a medium for dispersing emitters but also in determining key device processes such as exciton confinement, charge balance, and recombination zone formation. Proper alignment of frontier molecular orbitals between the host and transport layers facilitates efficient charge injection and transport, while sufficiently high triplet energy levels are necessary to prevent exciton back-transfer from the emitter to the host. Consequently, the molecular design of host materials strongly influences the overall efficiency and operational stability of OLED devices. To achieve these requirements, a host material should satisfy four primary criteria: (i) appropriate management of singlet (S_1) and triplet energy (T_1) energy levels, (ii) balanced charge transport properties, (iii) suitable alignment of frontier molecular orbital energy levels, and (iv) high thermal and morphological stability.[15–18] Fig. 1 illustrates the energy-level diagram of a multilayer device structure, bandgap requirements for different emission colors, and the energy-transfer mechanism from the host material to various emitter types.

The selection of a host material should properly manage S_1/T_1 energy levels compatible with the employed emitter type, as each imposes distinct photophysical requirements. For a fluorescent emitter, the host S_1 level must be higher than the guest S_1 level to enable Förster resonance energy transfer (FRET), which is often constrained by the energy gap law. As the guest emission redshifts into the red-to-NIR region, the host fluorescence must be carefully engineered to maintain a significant spectral overlap with the guest absorption, while also optimizing the relative orientation of their transition dipoles. For phosphorescent emitters, a sufficiently high host T_1 level is required to facilitate energy transfer and suppress back-transfer. Unlike long-range FRET, Dexter energy transfer (DET) requires direct orbital overlap for harvesting triplet excitons and is strongly influenced by the host's steric environment. In contrast, thermally activated delayed fluorescence (TADF) emitters require both host S_1 and T_1 levels to be higher than the guest's to prevent singlet and triplet exciton leakage. Ultimately, minimizing energy loss and optimizing the spatial arrangement of the dopant ensures that excitons are efficiently transferred to the red-to-NIR emitter rather than being lost to non-radiative quenching.[19]

Additionally, balanced charge transport is also crucial for efficient exciton formation. This can be achieved using bipolar host materials, co-host systems that combine hole- and electron-transport materials, or host architectures designed to form exciplexes. Equally important is the alignment of frontier molecular orbital energy levels between host and adjacent transport layers to enable efficient charge injection and transfer to the guest emitter. Specifically, close matching of the highest occupied molecular orbital (HOMO) level to the hole-transport layer (HTL), as well as alignment of the LUMO level with the electron-transport layer (ETL), is essential to minimize charge-injection barriers and suppress recombination losses. Finally, the host material must exhibit high thermal and morphological stability. A high decomposition temperature (T_d) is essential to withstand vacuum thermal evaporation, while a sufficiently high glass transition temperature (T_g) is required to maintain

Yuan Jay Chang

Yuan Jay Chang received his PhD in Chemistry from National Taiwan University in 2009. He was a visiting scholar at Kyushu University, Japan, in 2011 and 2025, and joined Tunghai University in 2012. His research focuses on the design and synthesis of advanced materials for self-assembled monolayers, hole-transport materials and passivators of perovskite solar cells, OLEDs, photocatalytic hydrogen production, and organic photovoltaics.

Chih-Hao Chang

Chih-Hao Chang received his PhD in Electro-Optical Engineering from National Taiwan University in 2009 and subsequently joined Yuan Ze University, where he is currently a Distinguished Professor in the Department of Electrical Engineering. His research focuses on the development of organic semiconductor materials and their integration into advanced optoelectronic devices, including metal oxides, flexible organic optoelectronics, and gas sensors, with particular emphasis on OLED technologies for display, lighting, and phototherapy.

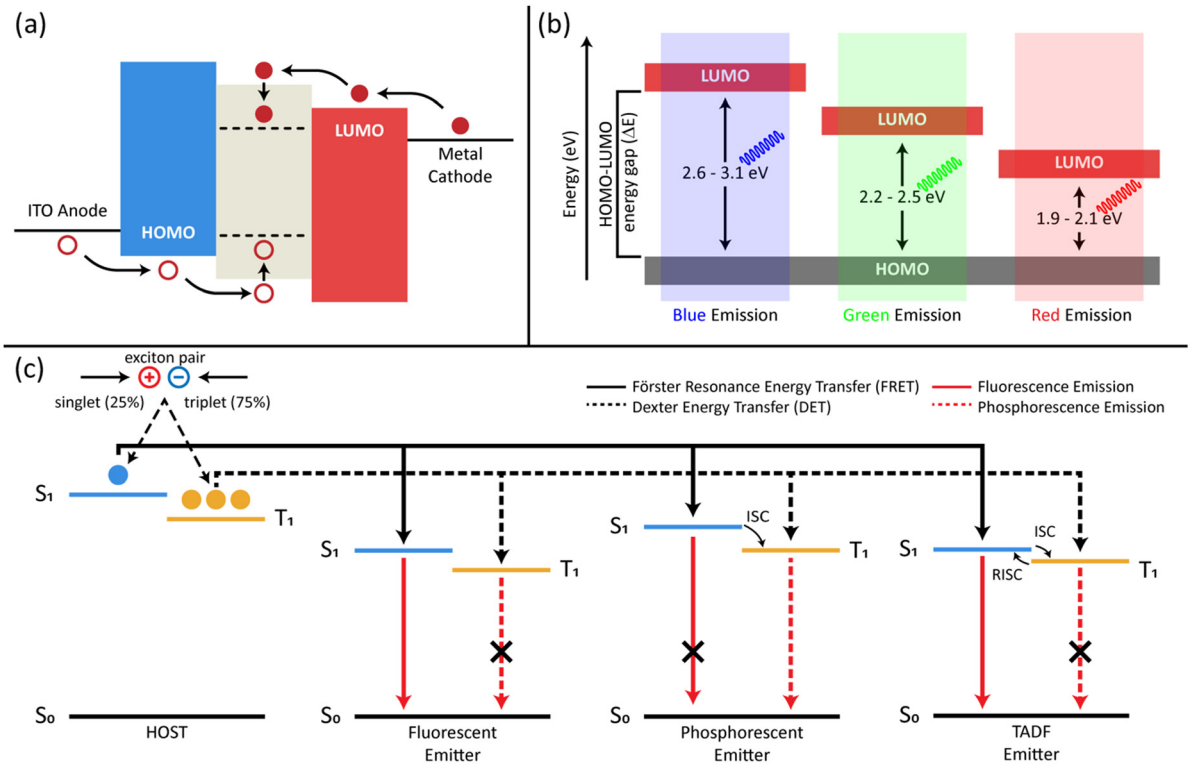

Fig. 1 (a) Energy-level diagram of a multilayer OLED structure. (b) HOMO–LUMO energy gaps (ΔE) for different emitter colors. (c) Energy transfer mechanism from the host material to various emitter types.

film amorphousness and suppress crystallization or aggregation, thereby ensuring long-term device stability.[20–22]

Beyond fundamental energy-level alignment and exciton confinement, the performance of red-to-NIR OLEDs is strongly governed by the nuances of host–guest interactions in the emissive layer. Achieving optimal polarity matching between the host and guest is essential for minimizing phase separation and ensuring a homogeneous dopant distribution, which prevents the formation of local high-concentration regions that can trigger exciton quenching. Furthermore, molecular packing and intermolecular interactions (such as π–π stacking) must be carefully controlled through host design, as they strongly influence exciton diffusion, aggregation behavior, and non-radiative decay pathways.

1.2. Intrinsic advantages and strategic development of the carbazole moiety

Among the diverse molecular scaffolds investigated, carbazole-based derivatives have attracted significant attention as versatile host materials capable of fulfilling the host requirements for high-performance devices.[23] These derivatives have long served as foundational building blocks in the development of highly efficient optoelectronic materials. Their advantages in material design and synthesis arise from several intrinsic advantages: (i) cost-effectiveness, (ii) the presence of multiple reactive sites on both the aromatic rings and the nitrogen atoms, (iii) facile functionalization of the aromatic framework relative to the nitrogen atom, and (iv) rigid fused-ring structures that confers enhanced physical and chemical stability under various operating conditions.[24,25] Moreover, in comparison with other nitrogen-containing amino-heterocyclic donors, carbazole exhibits relatively weaker π-donating character, leading to higher S_1 and T_1 energy levels. Carbazole derivatives can therefore display multifunctional characteristics, including light emission, hole injection, and charge transport.[26]

The development of carbazole-based derivatives spans over several decades, beginning with the early characterization of the carbazole molecule[27–29] and its integration into OLED host systems.[30–33] A major milestone was the introduction of CBP (4,4′-bis(*N*-carbazolyl)biphenyl) in 1999,[34] which remains one of the most widely used host materials to date.[35] Subsequent molecular architectures, such as TCTA[36,37] (tris(4-carbazoyl-9-ylphenyl)amine) and mCP[38] (1,3-bis(*N*-carbazolyl)benzene), marked significant transitions in the structural evolution of carbazole-based derivatives. While early host materials, including CBP and mCP, facilitated the development of efficient OLED emissions ranging from blue to red,[39–44] developments in the 2010s expanded to bi- and tri-carbazole scaffolds as well as donor–acceptor (D–A) hybrid systems.[45–50] During this period, D–A carbazole-based hosts attracted considerable attention by leveraging the strong hole-transporting properties of carbazole units in combination with electron-accepting moieties to improve charge balance and device stability. In the 2020s, research has increasingly shifted toward rigidified, asymmetric, and fused carbazole-based derivatives to deliver a massive push for high-efficiency OLEDs.[16,51–53] These scaffolds suppress

vibrational quenching and non-radiative decay, making them ideal for hosting deep-red and NIR emitters. Despite this extensive progress, systematic analyses correlating carbazole molecular architectures with host performance in red-to-NIR OLEDs remain limited.

Although carbazole derivatives have been widely explored in OLED research and several review articles have summarized carbazole-based materials or OLED host systems, systematic analyses focusing specifically on carbazole-based host materials for red-to-NIR OLEDs remain limited. In particular, the relationship between molecular architecture, optoelectronic properties, and host performance has not been comprehensively discussed. In this review, we offer new insights and perspectives by summarizing recent progress in carbazole-based host materials and categorizing them into four structural classes, namely push–pull, symmetric, asymmetric, and special architectures. By correlating molecular structures with key parameters, including material characterization metrics and device performance characteristics, this review aims to provide a clearer understanding of the design principles governing high-performance host materials for red-to-NIR OLED applications. While host materials have been widely studied for various OLED emitters, this review primarily focuses on host systems used with phosphorescent red-to-NIR emitters, which remain challenging due to the energy-gap law and increased non-radiative decay. In addition, several examples involving TADF emitters are also discussed to illustrate emerging trends in host material design. Recent studies published in the past few years have also been incorporated to ensure that this review reflects the latest progress in carbazole-based host materials.

2. Structural taxonomy of carbazole derivatives

Carbazole and its derivatives are among the most frequently used electron-donating units in organic optoelectronic materials.[54–58] This aromatic heterocycle consists of three fused rings, where two benzene rings are fused to a central pyrrole ring. It exhibits a high triplet energy ($\sim$2.9 eV for unsubstituted carbazole), good thermal stability, and strong hole-transporting capability.[59] Moreover, their molecular framework provides substantial structural versatility, with multiple accessible substitution sites (particularly at the 1, 3, 6, 8, and 9 positions), enabling integration into a broad range of different architectures. This structural tunability enables modulation of photophysical properties, including exciton confinement, energy transfer, and film morphology. These advantages arise from the scaffold's ability to support π-extended conjugation, allowing fine adjustment of molecular and optical properties through rational structural modification. Consequently, a clear understanding of carbazole's structural taxonomy is essential for the rational design of host materials capable of supporting red-to-NIR OLED emissions.[60–62]

Fig. 2 illustrates the molecular structure of 9*H*-carbazole and structural features of carbazole derivatives, including the core framework, representative π-bridges, typical fused architectures, and their molecular geometry characteristics. The nitrogen atoms in the 9*H*-carbazole core can be functionalized with various substituents, such as alkyl, aryl, and acyl groups, forming *N*-substituted carbazole derivatives. Furthermore, the carbazole framework can be further modified through numerous well-established organic reactions, including (i) electrophilic aromatic substitution (S_EAr) (*e.g.*, halogenation or Friedel–Crafts alkylation or acylation), (ii) Ullmann coupling reaction, (iii) Suzuki–Miyaura cross-coupling reaction, (iv) Mannich reaction, (v) Miyaura–Borylation, and (vi) Buchwald–Hartwig amination. These synthetic reactions enable the introduction of electron-donating and electron-withdrawing moieties at specific positions, thereby facilitating the rational design and synthesis of host materials with elevated singlet and triplet energy.[63,64] In the following sections, the influence of these structural modifications on device performance is systematically examined. Particular attention is placed on substitution patterns, the effects of non-fused *versus* fused ring scaffolds, and the intrinsic molecular geometries of carbazole-based derivatives.

2.1. Position of substitutions on carbazole frameworks

Substitution on the carbazole framework critically influences both molecular structure and photophysical behavior.[23] The principal sites for modification are the 3,6-position on the aromatic core and the 9-position (*N*-substitution) on the nitrogen atom. The introduction of the aromatic rings at the 3,6-positions aligns with the carbazole's π-conjugated pathways, thereby facilitating extended electronic delocalization and intensifying the molecular donor strength. This structural configuration not only enhances hole-transport characteristics but also provides a versatile platform for the systematic tuning of the frontier molecular orbitals.[65] In addition, these sites facilitate strong electronic coupling and alter the electronic energy levels of the carbazole when functionalized with electron-donating or electron-withdrawing moieties such as methoxy (–OMe),[66,67] *tert*-butyl (–^{t}Bu),[68–70] and/or cyano (–CN).[71–73] However, increased electronic delocalization tends to lower the triplet energy level compared to unsubstituted carbazole, which can be detrimental to exciton confinement. For red-to-NIR OLEDs, increasing or extending conjugation at these positions can lower the triplet energy and red-shift the emission, so careful tuning is required. Excessive delocalization may promote exciton leakage from the emitter to the host and degrade device efficiency. Therefore, molecular design at the 3,6-positions must balance enhanced charge transport with sufficient triplet confinement to ensure stable, efficient emission.

In contrast, substitution at the 9-position lies orthogonal to the π-plane, modulating electronic density distribution and introducing a steric environment that influences molecular planarity.[74] Although such substitution largely preserves the triplet energy, it can significantly influence intermolecular interaction and molecular packing, thereby enhancing thermal stability and morphological uniformity. Alkyl or aryl substituents at the nitrogen atom provide an effective means to tune

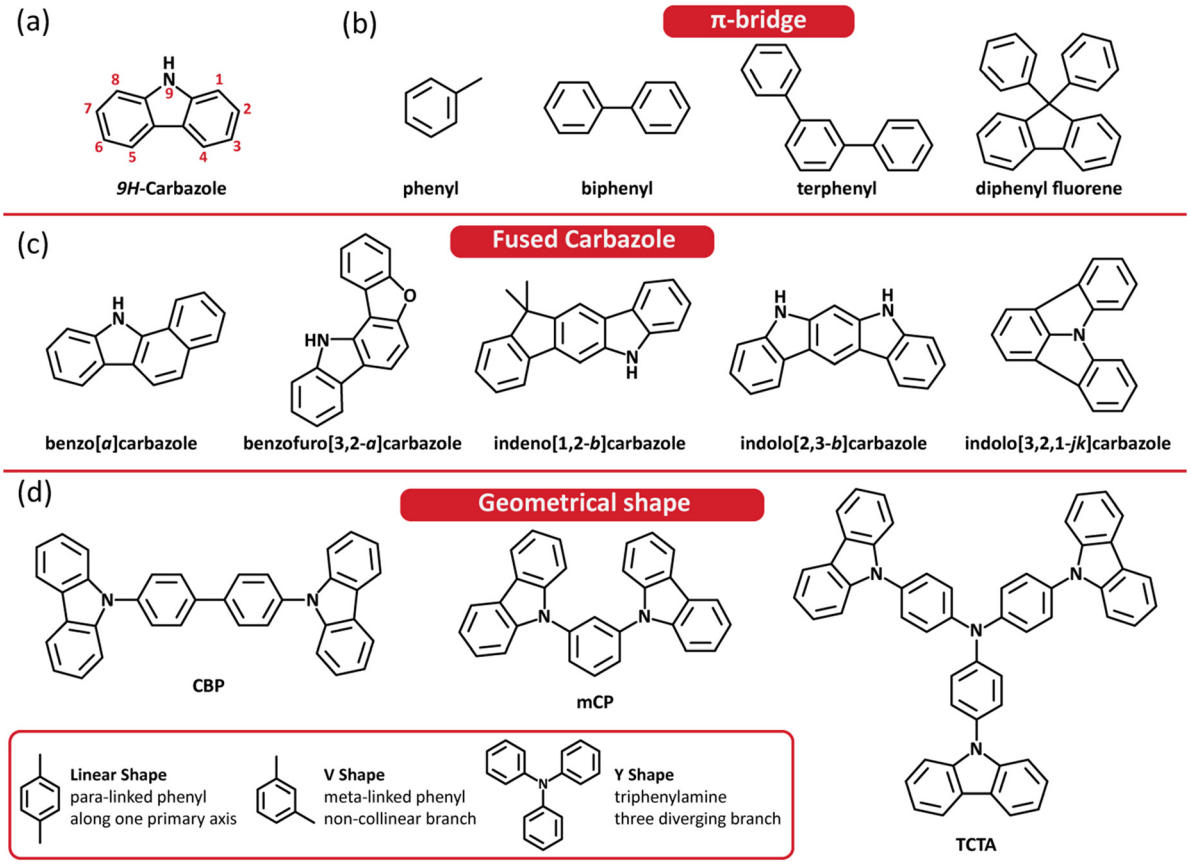

Fig. 2 (a) Chemical structure of 9*H*-carbazole. (b) Representative π-bridge commonly incorporated in carbazole-based systems. (c) Chemical structure of representative fused carbazole derivatives discussed in this manuscript. (d) Common geometrical shapes observed in the carbazole-based materials: linear (CBP), V-shaped (mCP), and Y-shaped (TCTA).

intermolecular interactions, morphological stability, and the spatial distribution of the HOMO. For instance, incorporation of a phenyl group at the *N*-substitution (*N*-phenylcarbazole derivatives) increases rigidity, suppresses molecular aggregation, and improves film-forming stability. In contrast, flexible *N*-alkyl substituents enhance solubility and solution-process ability but may diminish packing order and charge-transport efficiency due to their greater conformational freedom. Consequently, *N*-functionalization exerts a substantial influence on molecular geometry and electronic coupling, thereby shaping optical gaps, charge mobility, and exciton dynamics.

Ultimately, substitution at different positions on the carbazole framework determines the critical balance between electronic properties and structural stability. Substitution at the 3,6-positions primarily tunes the electronic structure through extended π-conjugation, thereby enhancing molecular donor strength and facilitating efficient charge transport. However, as conjugation tends to lower triplet energy, careful tuning is required to maintain a sufficient energy gap for effective exciton confinement. Substitution at the 9-position mainly regulates molecular geometry and intermolecular interactions *via* steric hindrance, thereby increasing the triplet energy by inducing a more twisted conformation that restricts conjugation. While this maintains morphological stability and exciton confinement, excessive steric bulk tends to disrupt intermolecular π–π stacking, thereby reducing charge-carrier mobility. This position-specific design approach enables a balanced optimization of charge transport, exciton confinement, and device stability, providing a rational framework for the development of high-performance OLED host materials.

2.2. Non-fused and fused ring carbazole scaffolds

Carbazole derivatives can be broadly categorized into non-fused and fused-ring architectures, each imparting distinct photophysical and morphological characteristics.[16] Non-fused carbazole derivatives, such as CBP, TCTA, and mCP, consist of carbazole donor units connected through σ-bonds or phenylene linkers. These structures preserve the intrinsically high triplet energies of the carbazole core and allow versatile substitution patterns, offering broad tunability across different emission colors. The partial conformational flexibility and rotational freedom between conjugated segments contribute to effective exciton confinement. However, this non-fused topology also introduces conformational variability that reduces molecular rigidity and increases susceptibility to aggregation-caused quenching (ACQ), particularly at high exciton densities. As a result, such materials may exhibit limited morphological stability and uneven film microstructures.

Fused-ring carbazole derivatives, such as ICz (indolo[3,2,1-*jk*]carbazole) and benzo[*a*]carbazole, feature rigidified frameworks that promote extended π-conjugation and enhanced molecular planarity.[75–77] Ring fusion significantly improves charge-carrier mobility, thermal stability, and film-forming quality, while suppressing morphological degradation during device operation. The resulting rigid and coplanar structures suppress non-radiative vibrational losses, thereby facilitating efficient charge transport and exciton confinement. However, increased π-extension and exciton delocalization generally lead to reduced triplet energy. Consequently, controlled fusion strategies, such as partial or selective ring fusion, are essential to enhance molecular rigidity and thermal stability while preserving the high triplet energy required for effective exciton confinement. Modulating conjugation length through partial ring fusion or the incorporation of non-conjugated spacers therefore provides a practical design strategy to improve structural stability without significantly compromising triplet energy.

2.3. Geometrical shapes of carbazole derivatives

Beyond the chemical connectivity of substituents, the overall molecular geometry of carbazole-based host materials plays a decisive role in shaping their photophysical and morphological characteristics.[74] The geometrical classification of carbazole-based host materials can be broadly categorized into linear, V-shaped, and Y-shaped architectures. These geometries arise from the spatial arrangement of carbazole units or peripheral aryl linkers around a central core, thereby determining molecular symmetry, dipole distribution, and steric environment. In linear-shape architecture, carbazole moieties are connected end-to-end *via para*-linker or rod-like conjugation pathways, which promote strong π–π stacking interactions that enhance charge-transport ability. CBP represents a typical linear-shape architecture and is widely recognized for exhibiting good hole mobility and promoting carrier delocalization. However, the extended π-conjugation in the linear system increases exciton diffusion, weakens exciton confinement, and facilitates molecular aggregation. These effects elevate the quenching probability of exciton–exciton or exciton–polaron, leading to enhanced non-radiative decay. V-shaped architectures, such as mCP, introduce a bent conjugation pathway that is typically achieved through *meta*-linkages or angular core units. This bent shape helps to reduce excessive π–π stacking, minimize intermolecular interaction, and maintain sufficient electronic connectivity between donor sites. The resulting steric hindrance improves amorphous stability, suppresses ACQ, enhances exciton confinement, and preserves high triplet energy. Y-shaped geometries are typically constructed *via* triarylamine-type cores, such as TCTA, which introduce angular deviations and steric hindrance. This inherently disrupts molecular packing, suppresses ACQ, and improves film uniformity and morphological stability. Increased branching or steric bulk effectively promotes site isolation, thereby weakening intermolecular interactions, reducing EPQ and enhancing emission efficiency. However, excessive steric hindrance or highly asymmetric geometries can disrupt charge percolation, highlighting the necessity to balance molecular rigidity with sufficient spacing to maintain both transport efficiency and optical purity.

The molecular geometry, determined by the phenyl linkage position, has been reported to significantly influence both intermolecular interaction and exciton behavior in the carbazole/benzimidazole[78] and carbazole/triazine[79] systems. The *para*-linkage has a more linear geometry, with a longer effective π-electron conjugation length and typically smaller dihedral angles than the *meta*-linkage. This configuration facilitates greater spectral overlap between the HOMO and LUMO, leading to a higher radiative decay rate and improved photoluminescence quantum yield (PLQY). In contrast, *meta*-linkage induces a bent, V-shaped geometry that restricts conjugation and contributes to higher triplet energy compared to its *para*-linked counterpart. Another example of twisted geometry achieved *via* a Y-shaped configuration is reported in a series of electro-active carbazole-based compounds.[80] In this case, the host molecular design incorporates bulky structures to create steric hindrance, which impedes close molecular packing and aggregation. This non-planar molecular configuration possesses significant structural rigidity, resulting in a morphologically stable molecule. Similarly, another unique Y-shaped material integrating imidazole and triphenylamine demonstrates that greater steric hindrance plays a crucial role in introducing a fully twisted geometry, which ultimately enhances thermal stability and emission efficiency.[81] Understanding how molecular geometry governs intermolecular packing and exciton behavior thus provides a critical foundation for the rational design of carbazole-based host materials for red-to-NIR OLEDs.

3. Electronic architectures of carbazole derivatives

Strategic molecular architecture is essential for carbazole derivatives, as the specific positioning of the carbazole units dictates the material's electronic and thermal properties.[23] Since architectural design critically influences OLED device performance, the following section categorizes carbazole derivatives by structural complexity, progressing from fundamental cores to increasingly complex configurations. This classification integrates both electronic architecture and molecular topology, which jointly determine transport and exciton confinement in carbazole-based hosts. To provide a systematic perspective on molecular design strategies, the carbazole-based host materials discussed in this review are categorized into four architectural classes: push–pull, symmetric, asymmetric, and special frameworks. This classification integrates two important aspects of molecular design: electronic architecture and molecular topology. The push–pull architecture primarily emphasizes the electronic distribution introduced by D–A interactions, which can facilitate bipolar charge transport. In contrast, symmetric and asymmetric architectures highlight the influence of molecular topology and steric configuration on parameters such as molecular packing, triplet energy levels, and charge mobility. The final category, special architectures,

includes structures that cannot be readily described by the previous categories but offer unique design features. This classification, therefore, provides a practical framework for understanding how different structural motifs influence the optoelectronic properties and device performance of carbazole-based host materials.

The molecular design strategies discussed herein aim to mitigate the limitations imposed by the energy gap law in the red-to-NIR region, where a reduction in the energy gap from ~2.0 eV to ~1.2 eV can increase non-radiative decay rates by several orders of magnitude, significantly quenching the host singlet or triplet excited state before energy transfer can occur. This fundamental limitation is critical for host materials, as accelerated non-radiative decay competes with efficient FRET or DET to the guest emitter, ultimately reducing the overall device efficiency.[7,82] While strong D–A interactions in push–pull architectures effectively reduce energy gaps to match NIR emitters, they often amplify non-radiative decay. In contrast, symmetric architectures typically exhibit more balanced electronic distributions and comparatively larger energy gaps, which can help suppress vibrationally assisted decay pathways. Asymmetric systems provide an intermediate regime, enabling more precise balance between energetic alignment and the suppression of non-radiative loss. Furthermore, special architectures (particularly those incorporating rigid or sterically constrained frameworks) can mitigate non-radiative decay by limiting structural relaxation, ensuring that the host maintains the necessary excited-state energy to drive guest emission. These highlight that while the energy-gap law remains a fundamental constraint, its impact can be significantly modulated through deliberate molecular design strategies.

In this review, we analyze how optoelectronic and morphological properties depend on the molecular design strategy. An ideal host material should simultaneously exhibit high thermal stability, balanced charge-transport capability, and efficient energy transfer. By correlating the architectural features of carbazole derivatives with material characterization metrics such as thermal stability (T_d/T_g), HOMO/LUMO energy levels, and singlet/triplet (S_1/T_1) energy levels, this study aims to establish clear design rules for identifing effective carbazole-based host materials for red-to-NIR OLEDs. In addition, OLED device characteristics, such as the emitter type, electroluminescence peak (λ_{max}), external quantum efficiency (EQE), current efficiency (CE), power efficiency (PE), and the Commission Internationale de l'Éclairage (CIE) color coordinates, are compiled to facilitate a comprehensive evaluation of host material performance.

3.1. Push–pull architectures: molecular design strategies for energy-level tuning and bipolar transport

Push–pull architecture represents the most fundamental electronic design strategies in molecular architectures.[60,83,84] Their photophysical properties are governed primarily by the D–A interaction. In this configuration, a carbazole donor is linked to an electron-accepting unit either *via* a single bond or through a π-bridge spacer. Carbazole functions as a moderately strong electron donor, offering high triplet energy and excellent structural stability, while the attached acceptor governs the distribution of the frontier molecular orbital. When the acceptor possesses a sufficiently deep LUMO level, balanced charge transport can be achieved without excessive exciton quenching, thereby enabling bipolar host behavior. The incorporation of a π-bridge connection in the system modulates the spatial separation between the HOMO/LUMO and influences transition dipole characteristics. By controlling spacer length and rigidity, key parameters such as the optical bandgap, vibronic coupling, and molecular planarity can be systematically tuned. This design enables adjustable emission while maintaining morphological stability and suppressing ACQ. Moreover, the spacer regulates D–A coupling to prevent excessively strong charge-transfer character that would diminish radiative decay. Fig. 3 illustrates representative host materials employing push–pull architecture for red-to-NIR OLEDs, organized by carbazole connection at the C3 position, while Table 1 summarizes their material properties and OLED device characterization data. Among these materials, most exhibit moderate to high thermal stability (T_d/T_g) and well-tuned HOMO–LUMO energy levels, making them well-suited for red-to-NIR emission. The S_1 energy levels generally exceed 3.00 eV, while the T_1 energy levels vary across different materials, likely reflecting the influence of different acceptor moieties and π-bridge configurations. Device performance, including EQE, CE, and PE, varies significantly with the emitter type and EML configuration employed.

As an initial example of push–pull architecture, Qiu *et al.* synthesized two bipolar host materials, **2CzMC (1)** and **4CzMC (2)**, in which carbazole donors are fused to pyranone acceptor units.[85] Although no distinct π-bridge formally separates the donor and acceptor, the molecule incorporates a styryl moiety that effectively serves as a conjugated π-bridge, with the linkage position determining the extent of conjugation and the strength of the intramolecular charge transfer (ICT) character. Both materials exhibit relatively high triplet energy owing to the carbazole donor. Specifically, **2CzMC (1)**, with linkage at the 2,3-positions, exhibits a T_1 of 2.83 eV, whereas **4CzMC (2)**, linked at 3,4-positions, shows a slightly higher T_1 of 2.90 eV, due to the shorter effective conjugation length and weaker ICT character. In addition, both molecules display weak π–π interactions due to the peripheral phenyl group significantly twisted out of the plane (52° and 54°) of the carbazole-based conjugated framework. This pronounced twisting prevents the formation of extended planar structures required for strong π–π stacking. Although these high T_1 values are more favorable for blue phosphorescent emitters, the author also demonstrates device performance using the red phosphorescent emitter $Ir(MDQ)_2$-(acac). The resulting OLEDs achieved EQEs (CEs and PEs) of 11.6% (17.0 cd A^{-1} and 16.6 lm W^{-1}) for **2CzMC (1)** and 11.4% (16.0 cd A^{-1} and 16.8 lm W^{-1}) for **4CzMC (2)**. Although the materials are not optimized for red emission, they function effectively as universal host materials.

Our group reported four series of imidazolyl-phenylcarbazole host materials and evaluated two of the best-performing materials (**im-CzP (3)** and **im-OCzP (4)**) for potential red

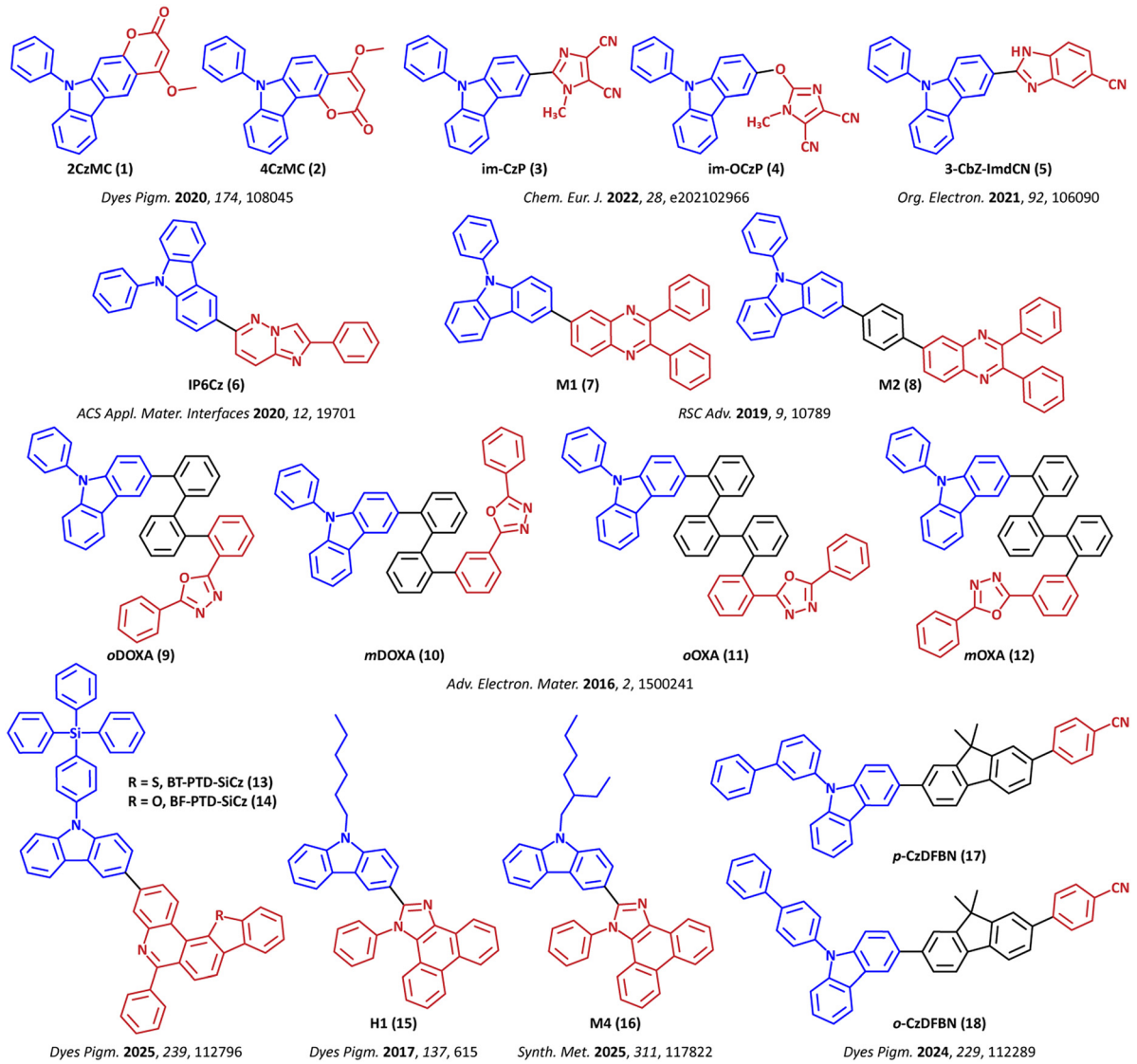

Fig. 3 Chemical structures of carbazole-based host materials employing a push–pull architecture for red-to-NIR OLEDs, grouped according to carbazole substitution at the C3 position. (The highlighted colors correspond to blue for the carbazole donor, red for the acceptor moieties, and black for the π-bridge linkers).

phosphorescent OLED (PhOLED) applications using the $Ir(piq)_2$(acac) emitter.[86] While the T_1 of $Ir(piq)_2$(acac) is approximately 2.25 eV, both host materials exhibit a higher T_1 value of above 2.90 eV. Although such high triplet energies are sufficient to prevent reverse energy transfer from the emitter to the host, they may indirectly increase the risk of efficiency roll-off at higher current densities. Ideally, the host T_1 should exceed emitter T_1 by at least 0.3 eV to suppress back-energy transfer. However, the large energy gap between the host and the emitter can lead to charge carrier trapping in the emitter, which may promote undesirable triplet–polaron quenching (TPQ) (due to interaction between trapped charge (polaron) and triplet exciton on emitter) and TTA (due to increasing local triplet exciton concentration at higher current densities). One strategy to mitigate these efficiency losses is to implement a co-host system to broaden the recombination zone and balance charge transport. The red PhOLEDs incorporating the co-host approach demonstrate superior performance compared to single-host devices based on **im-CzP (3)** and **im-OCzP (4)**. Single-host devices achieved a performance of 14.0% (9.0 cd A^{-1} and 10.9 lm W^{-1}) for **im-CzP (3)** and 14.1% (9.0 cd A^{-1} and 10.1 lm W^{-1}) for **im-OCzP (4)**. Using a co-host system with B3PyMPM, performance improved to 15.2% (9.4 cd A^{-1} and 12.3 lm W^{-1}) and 16.5% (10.2 cd A^{-1} and 13.4 lm W^{-1}), respectively. Despite having a similar HOMO/LUMO (−5.64/−2.19 eV for **im-CzP (3)** and −5.54/−2.08 eV for **im-OCzP (4)**), the presence of an oxygen atom in **im-OCzP (4)** appears to facilitate a more effective carrier balance in the co-host system.

Patil *et al.* introduced a simple D–A architecture host material, **3-Cbz-imdCN (5)**, composed of a carbazole donor and a cyanobenzimidazole acceptor unit.[72] This material exhibits good thermal stability with a T_d of 390 °C, indicating suitability

Table 1 Summary of materials' properties and OLED device performance parameters for the compounds depicted in Fig. 3

		Material characterization			OLED characterization					
Material		T_d/T_g [°C]	HOMO/LUMO [eV]	S_1/T_1 [eV]	EML type	Emitter	λ_{max} [nm]	EQE/CE/PE [%, cd A^{-1}, lm W^{-1}]	CIE [x,y]	Ref.
1	**2CzMC**	297/119	−5.73/−2.34	3.39/2.83	Single	$Ir(MDQ)_2(acac)$	611	11.6/17.0/16.6	0.62, 0.38	85
2	**4CzMC**	304/104	−5.74/−2.29	3.45/2.90				11.4/16.0/16.8		
3	**im-CzP**	321/—	−5.64/−2.19	3.45/2.92	Single	$Ir(piq)_2(acac)$	—	14.0/9.0/10.9	0.68, 0.31	86
					Co-host			15.2/9.4/12.3		
4	**im-OCzP**	321/—	−5.54/−2.08	3.46/2.91	Single			14.1/9.0/10.1		
					Co-host			16.5/10.2/13.4		
5	**3-Cbz-imdCN**	390/—	−5.65/−3.31	—/2.71	Single	$Ir(piq)_2(acac)$	—	6.3/5.9/6.6	0.67, 0.33	72
6	**IP6Cz**	357/91	−5.44/−1.66	—/2.33	Single	$Ir(pq)_2(acac)$	600	26.9/49.9/46.7	0.60, 0.39	87
						$Ir(piq)_2(acac)$	625	20.5/16.7/14.9	0.68, 0.32	
7	**M1**	321/176	−5.60/−3.09	2.51/2.24	Single	$Ir(pq)_2(acac)$	—	14.7/28.6/19.9	0.58, 0.39	88
8	**M2**	415/218	−5.60/−3.21	2.39/2.24				15.1/29.3/20.5	—	
9	***o*DOXA**	354/93	−5.64/−2.54	3.44/2.70	Single	$Os(bpftz)_2(PPhMe_2)_2$	—	15.1/18.1/14.5	0.64, 0.35	89
10	***m*DOXA**	349/101	−5.64/−2.32	3.42/2.71				17.1/20.6/20.7		
11	***o*OXA**	348/103	−5.64/−2.25	3.44/2.71				19.0/21.7/18.2	0.65, 0.35	
12	***m*OXA**	334/132	−5.68/−2.31	3.44/2.69				19.5/22.6/13.7		
13	**BT-PTD-SiCz**	470/—	−5.52/−2.68	3.12/2.59	Single	$Ir(piq)_2(acac)$	—	8.2/4.6/—	—	90
14	**BF-PTD-SiCz**	474/—	−5.51/−2.66	3.16/2.61				13.9/8.0/—		
15	**H1**	386/52	−5.40/−2.18	3.22/2.46	Single	$Ir(MDQ)_2(acac)$	609	5.5/8.5/6.5	0.60, 0.40	91
16	**M4**	391/73	—/—1.61	—/2.56	Single	TPA-DCPP	625	5.6/—/—	—	92
17	***p*-CzDFBN**	393/127	−5.60/−2.31	3.29/2.47	Single	$Ir(piq)_2(acac)$	624	27.2/23.8/25.2	0.68, 0.31	93
18	***o*-CzDFBN**	400/135	−5.59/−2.30	3.29/2.48				25.9/22.3/24.1		

for vacuum thermal deposition and the ability to maintain amorphous film formation. The molecule also displays a long-wavelength π–π electronic transition due to extended π-conjugation, resulting in a relatively low T_1 value of 2.71 eV and a narrow HOMO/LUMO gap of −5.65/−3.31 eV. Analysis of the hole and electron reorganization energies provides insight into the molecule's charge-transport properties. The result shows that **3-Cbz-imdCN (5)** has a lower hole reorganization energy (λ_h), which generally corresponds to higher hole mobility, suggesting that this host material is better suited for hole transport. However, as charge balance is not fully achieved, the performance of the red PhOLED employing this single host is limited, reaching 6.3% (5.9 cd A^{-1} and 6.6 lm W^{-1}).

In a subsequent study, Song *et al.* introduced imidazo[1,2-*b*]-pyridazine (IP) as a novel electron-withdrawing unit for the development of bipolar host materials.[87] Four bipolar host materials were synthesized, including one classified as a push–pull architecture (**IP6Cz (6)** in Fig. 3), one belonging to the multi D–A category (**IP368Cz (41)** in Fig. 6), and two asymmetric architectures (**IP36Cz (80)** and **IP68Cz (81)** in Fig. 8). Among these, the **IP6Cz (6)** host material demonstrates exceptional device performance when paired with the $Ir(pq)_2$-(acac) emitter, achieving 26.9% (49.9 cd A^{-1} and 46.7 lm W^{-1}). For deep-red emission using the $Ir(piq)_2(acac)$ emitter, **IP6Cz (6)**-based devices still delivered a high performance of 20.5% (16.7 cd A^{-1} and 14.9 lm W^{-1}). The superior performance of the **IP6Cz (6)** host material can be attributed to its well-matched HOMO/LUMO of −5.44/−1.66 eV, an appropriate T_1 of 2.33 eV, and balanced charge transport, as confirmed by carrier mobility measurements. This balanced bipolar behavior arises from the strong electron-accepting nature of the IP unit. At the same time, substitution at the 6-position effectively suppresses excessive extension of π-conjugation, thereby facilitating efficient energy transfer to the emitter. Such balanced charge transport broadens the exciton recombination zones and effectively suppresses efficiency roll-off in red PhOLEDs.

Feng *et al.* investigated the influence of a phenyl π-bridge on the photophysical properties of host materials composed of a carbazole donor and diphenylquinoxaline acceptor units by comparing **M1 (7)** (without a π-bridge) and **M2 (8)** (with a phenyl π-bridge).[88] These host materials were specifically designed for red PhOLED devices and exhibit appropriate T_1 at 2.24 eV. The introduction of the phenyl π-bridge modulates the π-electron conjugation and significantly influences the LUMO energy level, shifting it from −3.09 eV in **M1 (7)** to −3.21 eV in **M2 (8)**. In comparison, the HOMO energy levels of both materials remain similar at −5.60 eV. These results confirm that the carbazole donor predominantly governs the HOMO, regardless of the presence of the phenyl π-bridge. In addition, the incorporation of the phenyl π-bridge presents a more sterically hindered molecular structure to **M2 (8)**, resulting in a substantially enhanced thermal stability (T_d/T_g) of 415/218 °C compared to 321/176 °C for **M1 (7)**. Both materials exhibited good device performance in red PhOLEDs employing the $Ir(pq)_2(acac)$ emitter. The single-host device based on **M2 (8)** achieved higher performance at 15.1% (29.3 cd A^{-1}, 20.5 lm W^{-1}), compared to 14.7% (28.6 cd A^{-1}, 19.9 lm W^{-1}) for **M1 (7)**. The lower LUMO energy level of the **M2 (8)** host material facilitates more efficient electron injection into the EML and improves charge balance, thereby enhancing device efficiency.

The study by Cheng *et al.* demonstrated that carbazole-oxadiazole hybrid molecules can function as versatile bipolar host materials with considerable performance in red PhOLEDs.[89] Four novel bipolar hosts, ***o*DOXA (9)**, ***m*DOXA (10)**, ***o*OXA (11)**, and ***m*OXA (12)**, were synthesized by incorporating different π-bridges

(biphenyl or *o*-terphenyl) and connection topologies (*ortho*- or *meta*-positions). The key design strategy of this study lies in tailoring the connectivity between the oxadiazole acceptor and the carbazole donor through diverse π-bridges. This approach induces highly distorted molecular geometries that effectively decouple the donor and acceptor units, thereby suppressing direct electronic interactions. This structural distortion enables the preservation of a high T_1 of approximately 2.70 eV. The twisted molecular geometries result in weak electronic coupling, which is beneficial for achieving pronounced HOMO–LUMO separation, where the HOMO is strictly localized on the donor moiety and the LUMO is confined to the acceptor unit. Consequently, the utilization of the *meta*-linked *o*-terphenyl π-bridge achieves best red PhOLED performance, as exemplified by ***m*OXA (12)**, which achieves 19.5% (22.6 cd A^{-1} and 13.7 lm W^{-1}). Meanwhile, the ***o*OXA (11)** host material exhibits the most balanced performance across a broad emission range (blue, green, yellow, orange, and red), delivering a red PhOLED performance of 19.0% (21.7 cd A^{-1} and 18.2 lm W^{-1}).

The following study by Park *et al.* reported the synthesis of two phenanthridine-based host materials, benzothieno-substituted **BT-PTD-SiCz (13)** and benzofuro-substituted **BF-PTD-SiCz (14)**, with an interesting tetraphenylsilane unit attached at the 9-position of the carbazole donor.[90] The introduction of the bulky tetraphenylsilane group was intended to suppress intermolecular packing, dopant aggregation, and excimer formation, which may arise from the rigid and planar fused structures of the benzofuro- and benzothieno-penanthridine acceptor core. As a result, both materials exhibit excellent thermal stability, with T_d exceeding 470 °C. The **BT-PTD-SiCz (13)** host, containing an electron-rich benzothieno moiety, exhibits enhanced electron-transport characteristics. However, this leads to an imbalance in charge transport and results in inferior red PhOLED performance of 8.2% and 4.6 cd A^{-1} when using the $Ir(piq)_2(acac)$ emitter. In contrast, **BF-PTD-SiCz (14)** exhibits more balanced charge transport, enabling significantly improved device performance of 13.9% and 8.0 cd A^{-1}.

Grigalevicius's group published two studies employing phenanthro[9,10-*d*]imidazole-based materials as hosts, with the primary structural difference being the alkyl spacer attached to the *N*-substituted carbazole donor. The nature of the attached spacer can significantly influence the electronic properties and charge transport behavior of host materials. In these studies, host **H1 (15)** incorporates a hexyl substituent,[91] whereas host **M4 (16)** contains an ethylhexyl group at the 9-position of the carbazole donor.[92] The material characterization shows that both materials exhibit good thermal stability with T_d exceeding 385 °C. However, relatively low T_g values are observed, with 52 °C for **H1 (15)** and 73 °C for **M4 (16)**. When employed as a host in red PhOLEDs, a single-host device using host **H1 (15)** doped with an $Ir(MDQ)_2(acac)$ emitter achieves a performance of 5.5% (8.5 cd A^{-1} and 6.5 lm W^{-1}), while **M4 (16)** doped with the TPA-DCPP emitter achieves a maximum EQE of 5.6%. The presence of flexible alkyl spacers appears to reduce current density and impair carrier transport capability, which in turn contributes to the relatively modest device performance observed in both systems.

Highly efficient red PhOLED performance is reported by Hu *et al.*, who compared two host compounds, ***p*-CzDFBN (17)** and ***o*-CzDFBN (18)**, synthesized using 9,9-dimethylfluorene as a π-bridge and benzonitrile as an acceptor unit.[93] The primary structural difference between the two compounds lies in the steric spacer attached at the *N*-substitution of the carbazole donor (biphenyl group) connected through either the *para*- or the *meta*-position. Both materials exhibit high thermal stability with T_d/T_g exceeding 390/125 °C. The T_1 values of ***p*-CzDFBN (17)** and ***o*-CzDFBN (18)** were determined to be 2.47 eV and 2.48 eV, respectively, confirming their suitability as host materials for red PhOLEDs. The device employing the $Ir(piq)_2(acac)$ emitter achieved a peak performance of 27.2% (23.8 cd A^{-1} and 25.2 lm W^{-1}) for ***p*-CzDFBN (17)** and 25.9% (22.3 cd A^{-1} and 24.1 lm W^{-1}) for ***o*-CzDFBN (18)**. Since there is a negligible difference in the HOMO/LUMO and T_1 energy levels between the two hosts, the superior performance of ***p*-CzDFBN (17)** is likely attributed to the *meta*-connected biphenyl spacer. This structural feature promotes a more favorable spatial orientation, facilitates efficient energy transfer, and enables more balanced bipolar charge transport compared to ***o*-CzDFBN (18)**.

Fig. 4 illustrates host materials employing a simple push–pull architecture for red-to-NIR OLEDs, organized according to the carbazole connection at the 9-position. Table 2 summarizes the corresponding material properties and OLED device characterization. Compared with the data presented in Table 1, the S_1 energy levels are slightly lower, whereas the T_1 energy levels vary across materials, likely reflecting the influence of distinct acceptor moieties and π-bridge configurations. Atul Askar's group has reported two publications on structurally similar materials that compare acceptor cores with phenylcarbazole donors at the N9 and C3 positions. The first study, published in 2018, coupled phenylcarbazole donors to a pyrrolo[1,2-*a*]quinoxaline acceptor unit, yielding two synthesized materials, **3CBZ-PQ (19)** and **4CZB-PQ (20)**.[94] In **3CBZ-PQ (19)**, the phenyl group at the *N*-substitution of carbazole acts as a steric spacer, whereas in **4CZB-PQ (20)** it functions as a π-bridge directly linking the donor and acceptor. The **4CBZ-PQ (20)** host material exhibited best performance in red PhOLEDs using the $Os(bpftz)_2(PPhMe_2)_2$ emitter, achieving 15.1% (18.1 cd A^{-1} and 12.9 lm W^{-1}), compared to only 4.75% (1.9 cd A^{-1} and 1.8 lm W^{-1}) for **3CBZ-PQ (19)**. This improvement is attributed not only to enhanced carrier balance and energy-transfer efficiency but also to the favorable geometric characteristics and molecular planarity. Although increased planarity can promote π–π stacking that may induce excimer formation and exciton quenching, it also facilitates faster charge hopping, resulting in higher current density within the devices. A significant shift in the λ_{max} is observed between **4CBZ-PQ (20)** (616 nm) and **3CBZ-PQ (19)** (674 nm). Although the emission predominantly originates from the emitter, the host's structural variation can influence the device's charge balance and chemical compatibility with the emitter. Such variation in charge balance significantly influences the host–guess energy transfer and exciton formation dynamics. Furthermore, the chemical structure of the host influences polarity, molecular packing, and intermolecular

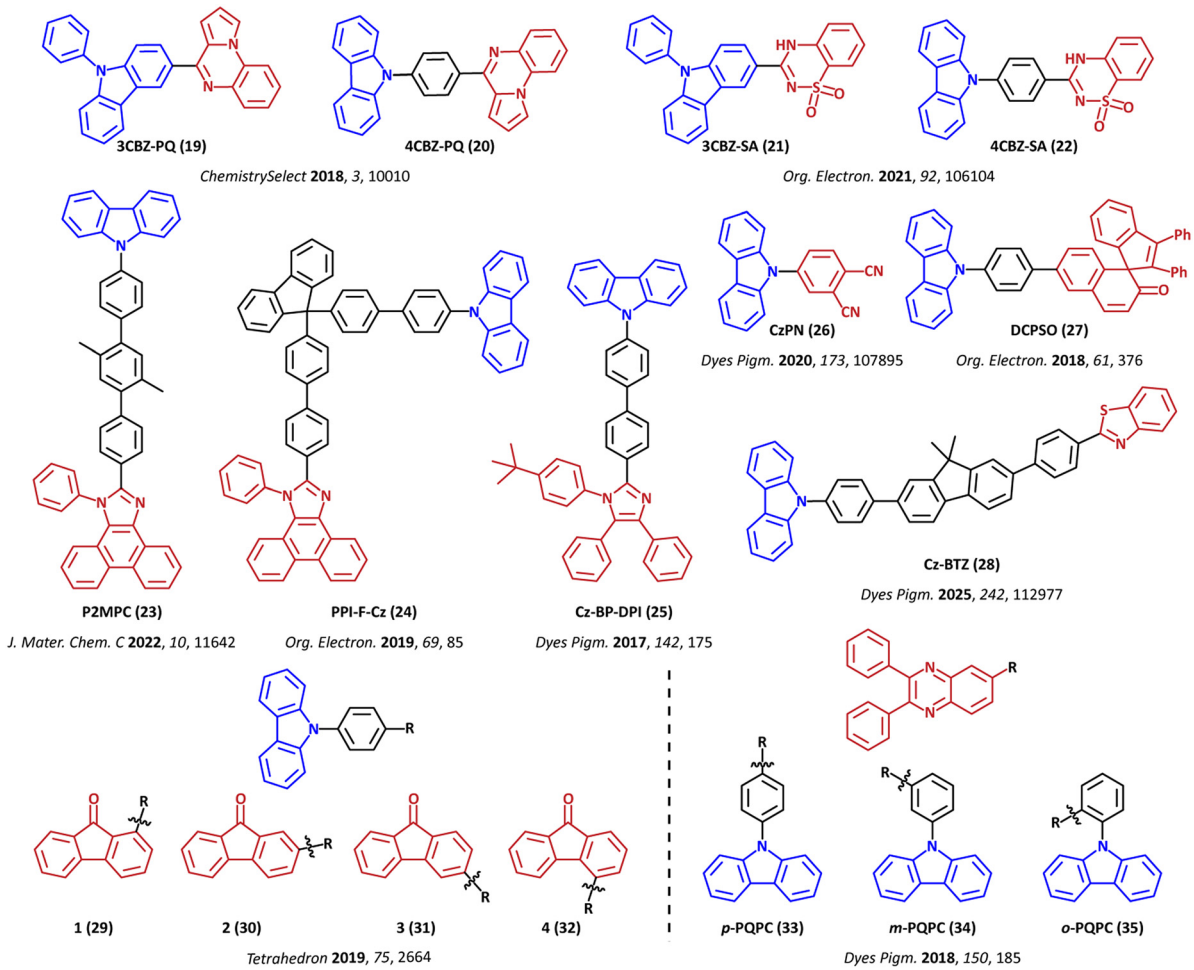

Fig. 4 Chemical structures of carbazole-based host materials employing a push–pull architecture for red-to-NIR OLEDs, grouped according to carbazole substitution at the 9-position. (The highlighted colors correspond to blue for the carbazole donor, red for the acceptor moieties, and black for the π-bridge linkers).

Table 2 Summary of materials' properties and OLED device performance parameters for the compounds depicted in Fig. 4

		Material characterization			OLED characterization					
Material		T_d/T_g [°C]	HOMO/LUMO [eV]	S_1/T_1 [eV]	EML type	Emitter	λ_{max} [nm]	EQE/CE/PE [%, cd A^{-1}, lm W^{-1}]	CIE [x,y]	Ref.
19	**3CBZ-PQ**	207/—	−5.22/−1.35	—/2.77	Single	$Os(bpftz)_2(PPhMe_2)_2$	674	4.75/1.9/1.8	—	94
20	**4CBZ-PQ**	161/156	−5.32/−1.68	—/2.59			616	15.1/18.1/12.9	0.64, 0.35	
21	**3CBZ-SA**	412/235	−5.56/−2.32	—/2.64	Single	$Ir(pq)_2(acac)$	—	10.0/15.2/17.6	—	95
22	**4CBZ-SA**	417/231	−5.61/−2.56					12.7/20.6/22.5		
23	**P2MPC**	475/—	−5.20/−2.22	3.04/2.46	Single	$Ir(MDQ)_2(acac)$	—	23.0/41.0/42.9	0.60, 0.39	96
24	**PPI-F-Cz**	502/217	−5.45/−2.32	—/2.40	Single	$Ir(MDQ)_2(acac)$	624	20.9/25.2/23.3	0.61, 0.38	97
25	**Cz-BP-DPI**	416/140	−5.78/−2.49	—/2.64	Single	PtOEP	—	2.58/0.9/—	0.65, 0.33	98
26	**CzPN**	309/—	−5.76/−2.72	3.03/2.70	Single	$Ir(MDQ)_2(acac)$	604	20.9/41.5/41.1	0.58, 0.40	99
27	**DCPSO**	454/160	−5.40/−2.30	3.10/2.60	Single	$Ir(piq)_2(acac)$	620	16.6/12.4/13.4	—	100
						AQ-Ph-DPAb1	624	13.3/11.1/10.0		
28	**Cz-BTZ**	404/—	−5.40/−2.25	3.15/2.59	Single	$Ir(piq)_2(acac)$	620	27.8/27.2/33.6	0.67, 0.32	101
29	**1**	367/89	−5.55/−2.89	2.66/2.50	Single	$Ir(MDQ)_2(acac)$	616	15.1/20.0/21.4	0.63, 0.37	102
30	**2**	388/—	−5.57/−3.00	2.57/2.36			620	10.5/12.0/14.5	0.64, 0.36	
31	**3**	368/—	−5.58/−2.88	2.70/2.57			620	3.1/4.0/5.4	0.63, 0.36	
32	**4**	356/94	−5.59/−2.85	2.74/2.33			612	3.4/5.0/6.7	0.62, 0.37	
33	***p*-PQPC**	403/112	−5.72/−2.67	3.05/2.37	Single	$Ir(piq)_2(acac)$	602	12.2/11.7/8.7	0.61, 0.38	103
34	***m*-PQPC**	390/107	−5.81/−2.65	3.16/2.40				9.2/8.9/6.6	0.62, 0.38	
35	***o*-PQPC**	357/104	−5.82/−2.65	3.17/2.46				12.2/12.0/8.5		

interaction around the $Os(bpftz)_2(PPhMe_2)_2$ emitter, ultimately leading to the observed spectral shifts.

A similar structural trend was investigated in a 2021 publication, in which benzothiadiazine was employed as the acceptor core to form **3CBZ-SA (21)** and **4CBZ-SA (22)**.[95] The phenyl group at the 9-position of carbazole in **3CBZ-SA (21)** serves as a steric spacer, while in **4CBZ-SA (22)** it acts as a π-bridge. When applied as a host material in red PhOLEDs using the $Ir(pq)_2(acac)$ emitter, **3CBZ-SA (21)** achieved a performance of 10.0% (15.2 cd A^{-1} and 17.6 lm W^{-1}), whereas **4CBZ-SA (22)** achieved 12.7% (20.6 cd A^{-1} and 22.5 lm W^{-1}). In this case, the position difference of the carbazole unit did not significantly affect exciton confinement, as both host materials exhibited an identical high T_1 of 2.64 eV. However, the HOMO level of **4CBZ-SA (22)** (−5.61 eV) is slightly deeper than **3CBZ-SA (21)** (−5.56 eV), suggesting subtle differences in hole transport behavior. The deeper HOMO level of **4CBZ-SA (22)** likely contributes to improved charge balance, resulting in a slight increase in device performance. Overall, the results of these two publications demonstrate that the positional variation of the carbazole unit critically influences molecular rigidity, planarity, and effective conjugation, all of which are key factors governing charge transport and ultimately device efficiency.

Subsequent studies from different research groups further explored the phenanthroimidazole acceptor moiety by varying the π-bridge architecture while retaining the same donor and acceptor units. These works highlight the critical role of π-bridge design in regulating molecular conformation, conjugation length, and charge-transport characteristics. Peng *et al.* synthesized a deep-blue bipolar fluorescent material, **P2MPC (23)**, incorporating a terphenyl unit bearing two methyl substituents at the central phenyl ring, which serves as the π-bridge.[96] The material exhibits a HOMO/LUMO of approximately −5.20/−2.22 eV and a T_1 of 2.46 eV, fulfilling the energetic requirement for red PhOLED host applications. Density functional theory (DFT) calculations indicate that the steric hindrance introduced by the methyl groups induces large dihedral angles (43.41° and 43.61°) along the molecular backbone, effectively suppressing excessive π-conjugation extension. The device employing $Ir(MDQ)_2(acac)$ as the emitter demonstrates excellent performance of 23.0% (41.0 cd A^{-1} and 42.9 lm W^{-1}), reflecting effective exciton confinement and host–guest energy transfer.

In a related work, Wang *et al.* reported a bipolar host material, **PPI-F-Cz (24)**, incorporating a 9,9-diphenyl-9*H*-fluorene unit as the π-bridge.[97] This host material displays a comparable HOMO/LUMO of −5.45/−2.32 eV, and a T_1 of 2.40 eV, which is sufficient to confine triplet excitons in red PhOLEDs. Unlike the methyl-substituted terphenyl bridge, the bulky 9,9-diphenyl-9*H*-fluorene unit as a π-bridge disrupts molecular planarity through steric congestion and torsional twisting, thereby suppressing exciton quenching and limiting ICT within the molecule. The device based on **PPI-F-Cz (24)** and $Ir(MDQ)_2(acac)$ as the emitter achieved an excellent performance of 20.9% (25.2 cd A^{-1} and 23.3 lm W^{-1}), confirming the effectiveness of this π-bridge strategy.

Wang *et al.* demonstrated a D–A material, **Cz-BP-DPI (25)**, consisting of a diphenylimidazole acceptor unit and a biphenyl π-bridge connected to a carbazole donor unit.[98] In terms of material characteristics, **Cz-BP-DPI (25)** exhibits high thermal stability with a T_d/T_g of 416/140 °C, and high T_1 estimated at 2.64 eV. Theoretical calculations indicated that **Cz-BP-DPI (25)** possesses a hybridized local and charge-transfer (HLCT) excited-state character. Despite these favorable material properties, device performance with PtOEP as the emitter was relatively poor, with EL efficiencies of 2.58% and 0.9 cd A^{-1}, accompanied by pronounced efficiency roll-off. This behavior was possibly attributed to TTA, yet the specific factors contributing to the poor device performance remain unexplored. We attribute the limited performance to the interplay between charge trapping and an imbalance in charge carriers within the emission zone. Given the sufficiently high triplet energy of the host, back-energy transfer is unlikely to be the dominant loss pathway. Instead, there is a substantial mismatch between the host and emitter energy level, where **Cz-BP-DPI (25)** exhibits a HOMO/LUMO of −5.78/−2.49 eV compared to approximately −5.3/−3.0 eV for PtOEP. This result suggests that the dopant molecule might induce charge trapping, thereby hampering charge transport and reducing overall recombination efficiency.

Wu *et al.* synthesized a host material by directly coupling a carbazole donor to a phthalonitrile acceptor unit without the incorporation of a π-bridge.[99] The resulting material, **CzPN (26)**, exhibits an optical bandgap of 3.00 eV and a HOMO of −5.76 eV. DFT calculations further reveal bipolar charge-transport characteristics, along with an S_1/T_1 of 3.03/2.70 eV, respectively. When doped with the $Ir(MDQ)_2(acac)$ emitter, **CzPN (26)** demonstrates a high PLQY of 0.72, indicating efficient host–guest energy transfer. Red PhOLEDs fabricated using **CzPN (26)** as the host achieved a device performance of 20.9% (41.5 cd A^{-1} and 41.1 lm W^{-1}). These results underscore the importance of appropriate energy-level alignment with adjacent transport layers, efficient energy transfer, and balanced charge transport in achieving high device performance through effective charge balance within the emitting layer.

Wang *et al.* reported the **DCPSO (27)** material, featuring a spironaphthalenone acceptor unit connected to a carbazole donor moiety *via* a phenyl π-bridge.[100] The resulting host exhibits excellent thermal properties with a T_d/T_g of 454/160 °C and a sufficiently high T_1 of 2.60 eV to effectively confine both the phosphorescent emitter $Ir(piq)_2(acac)$ and TADF emitter AQ-Ph-DPAb1. The spiro-D architecture was intentionally employed to induce a highly twisted molecular conformation, thereby interrupting π-conjugation and promoting spatial separation of the frontier molecular orbitals. The OLED devices utilizing **DCPSO (27)** as the host achieve a performance of 16.6% (12.4 cd A^{-1} and 13.4 lm W^{-1}) for phosphorescent devices with a λ_{max} at 620nm. For TADF devices, the performance is 13.3% (11.1 cd A^{-1} and 10.0 lm W^{-1}) for the TADF type with a λ_{max} at 624 nm. The electroluminescence (EL) spectra closely follow the emission profiles of the respective emitters, indicating efficient energy transfer from the host to the dopant.

Hou *et al.* synthesized the **Cz-BTZ (28)** host material by incorporating a benzothiazole acceptor linked to a carbazole donor moiety through a dimethylfluorene π-bridge.[101] This material exhibited outstanding performance in a red PhOLED, achieving a performance of 27.8% (27.2 cd A^{-1} and 33.6 lm W^{-1}) using an $Ir(piq)_2(acac)$ emitter. Thermal analysis revealed high thermal stability with a T_d of 404 °C. The HOMO/LUMO of **Cz-BTZ (28)** were determined to be −5.40/−2.25 eV, which align well with those of commonly used hole-transporting materials. The well-aligned frontier molecular orbitals are conducive to minimizing energy loss and reducing charge-injection barriers. The T_1 value of **Cz-BTZ (28)** was estimated to be 2.59 eV, suggesting its suitability as a host for red PhOLEDs. Furthermore, hole-only and electron-only device measurements demonstrate high current densities and confirm the bipolar charge transport capability of **Cz-BTZ (28)**, which is a critical factor contributing to its high device efficiency.

Fei *et al.* introduced a series of bipolar host materials (compounds **1** to **4 (29–32)**) based on fluorenone derivatives with different regioisomeric connection patterns to investigate the influence of linkage position on material properties and device performances.[102] All four compounds exhibit good thermal stability with T_d ranging from 356–388 °C, indicating their suitability for vacuum deposition. In addition, the materials possess high T_1 values of 2.33–2.57 eV, suggesting their potential as hosts for red PhOLEDs. Their HOMO levels are distributed within a narrow range from −5.55 to −5.59 eV. DFT calculations reveal that the HOMO is primarily localized on the carbazole donor moiety and the LUMO on the fluorenone acceptor unit. Among the synthesized hosts, compound **1 (29)** exhibited the best performance when employed with the $Ir(MDQ)_2(acac)$ emitter, achieving an efficiency of 15.1% (20.0 cd A^{-1} and 21.4 lm W^{-1}). This enhanced performance is attributed to the highly twisted molecular geometry. The author further noted that regioisomerism between the fluorenone and carbazole units significantly influences molecular conformation and the singlet–triplet energy difference (ΔE_{ST}). Specifically, the most twisted compound, **1 (29)**, exhibits the smallest ΔE_{ST} of 0.02 eV, followed by compounds **2 (30)**, **3 (31)**, and **4 (32)** with ΔE_{ST} values of 0.05, 0.10, and 0.04 eV, respectively. These values are consistent with the observed device performance trends. The disparity between the CIE coordinates and λ_{max} for compounds **1–4 (29–32)** is likely due to the different aggregation behavior of the guest material within the host, arising from the regioisomeric effect of the host materials. Overall, this study demonstrates that regioisomeric engineering is an effective strategy for tuning molecular planarity, excited-state energetics, and device efficiency.

Hu *et al.* synthesized three bipolar host materials (***p*-PQPC (33)**, ***m*-PQPC (34)**, and ***o*-PQPC (35)**) based on a quinoxaline acceptor linked to a carbazole donor through phenyl π-bridges with *para*-, *meta*-, and *ortho*-substitution patterns, respectively.[103] Overall, these materials exhibit favorable physical properties, including high thermal stability and suitable HOMO/LUMO energy levels for red PhOLED applications. Modulation of the π-bridge connection position significantly alters molecular geometry, transitioning from a relatively planar structure in the *para*-substituted compound to a highly twisted conformation in the *ortho*-substituted analogue. Planar structures generally exhibit higher T_d due to extended π-conjugation and stronger intermolecular interactions, which require greater energy to disrupt, but often possess lower triplet energies. In contrast, twisted geometries maintain higher triplet energies by interrupting π-conjugation. The trade-off for this restricted electron delocalization is often a decrease in bond dissociation energy and thermal stability. The *para*-, *meta*-, and *ortho*-substituted hosts exhibited a T_d of 403, 390, and 357 °C and a T_1 value of 2.37, 2.40, and 2.46 eV, respectively.

The device employing ***p*-PQPC (33)** achieved the highest performance of 12.2% (11.7 cd A^{-1} and 8.7 lm W^{-1}) using an $Ir(piq)_2(acac)$ emitter. This high performance is attributed to the close alignment of the ***p*-PQPC (33)** LUMO level (−2.67 eV) with the TPBi ETL (−2.7 eV), which facilitates efficient electron injection. The device based on ***o*-PQPC (35)** exhibited a comparable performance of 12.2% (12.0 cd A^{-1} and 8.5 lm W^{-1}), owing to balanced charge transport, as revealed by hole-only and electron-only device measurements. The enhanced triplet energy and disrupted π-conjugation in ***o*-PQPC (35)**, resulting from increased steric hindrance, further contribute to its effective exciton confinement. In contrast, the device with the ***m*-PQPC (34)** host displayed the lowest efficiency of 9.2% (8.9 cd A^{-1} and 6.6 lm W^{-1}), attributed to unbalanced bipolar transport, characterized by excessive hole current and insufficient electron transport.

Fig. 5 presents carbazol-based host materials employing a push–pull architecture for red-to-NIR OLEDs, categorized according to the fused carbazole donor unit, while Table 3 summarizes the corresponding material properties and OLED device characterization data. Interestingly, the S_1 energy levels vary across materials, likely reflecting the influence of the different fused carbazole donor units employed. Li *et al.* reported two studies introducing a fused carbazole donor, specifically indole[2,3-*a*]carbazole, combined with a triazine acceptor. The key structural difference lies in the acceptor extension: **BBPICT (36)** incorporates a bisbiphenyl unit,[104] whereas **BCPICT (37)** employs a biscyanophenyl unit to extend the π-conjugation of the acceptor moiety.[105] Time-of-flight (TOF) measurements reveal that both materials exhibit comparable hole and electron mobility, indicating balanced charge transport. Upon closure inspection, **BBPICT (36)** exhibits a hole mobility (μ_h) of approximately 1.8×10^{-4} cm^2 V^{-1} s^{-1} and an electron mobility (μ_e) of approximately 7.0×10^{-4} cm^2 V^{-1} s^{-1}, whereas **BCPICT (37)** shows a higher hole mobility of approximately 7.8×10^{-4} cm^2 V^{-1} s^{-1} and a lower electron mobility of approximately 2.3×10^{-4} cm^2 V^{-1} s^{-1}. Neither study reported the thermal stability of the material. The HOMO/LUMO are similar for both hosts, with values of −5.60/−2.50 eV for **BBPICT (36)** and −5.64/−2.63 eV for **BCPICT (37)**. In a red PhOLED device employing $Ir(mphmq)_2(tmd)$ as the emitter, **BBPICT (36)** demonstrates superior performance, achieving 20.9% (22.1 cd A^{-1} and 29.6 lm W^{-1}), compared to **BCPICT (37)**, which exhibits a performance of 10.7% (12.8 cd A^{-1} and 8.9 lm W^{-1}).

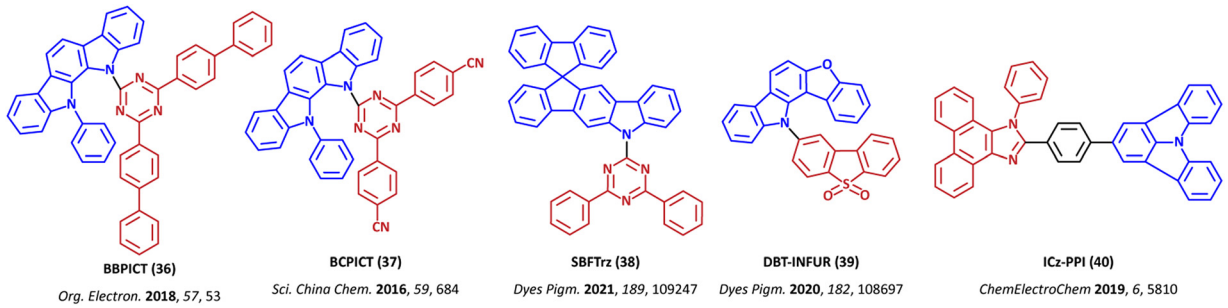

Fig. 5 Chemical structures of carbazole-based host materials employing a push–pull architecture for red-to-NIR OLEDs, grouped according to the fused carbazole donor. (The highlighted colors correspond to blue for carbazole donor, red for the acceptor moieties, and black for the π-bridge linkers.)

Table 3 Summary of materials' properties and OLED device performance parameters for the compounds depicted in Fig. 5

		Material characterization				OLED characterization				
Material		T_d/T_g [°C]	HOMO/LUMO [eV]	S_1/T_1 [eV]	EML type	Emitter	λ_{max} [nm]	EQE/CE/PE [%, cd A^{-1}, lm W^{-1}]	CIE [x,y]	Ref.
36	**BBPICT**	—/—	−5.60/−2.50	2.74/2.58	Single	$Ir(mphmq)_2(tmd)$	620	20.9/22.1/29.6	—	104
37	**BCPICT**	—/—	−5.64/−2.63	2.88/2.76	Single	$Ir(mphmq)_2(tmd)$	624	10.7/12.8/8.9	—	105
38	**SBFTrz**	487/134	−5.88/−3.24	3.63/2.74	Co-host	$Ir(mphmq)_2(tmd)$	610	26.2/37.9/32.7	0.65, 0.35	106
39	**DBT-INFUR**	371/—	−5.87/−2.61	3.26/2.71	Single	$Ir(mphmq)_2(tmd)$	—	12.4/15.5/8.9	0.64, 0.35	107
40	**ICz-PPI**	431/173	−5.46/−2.16	—/2.48	Single	$Ir(MDQ)_2(acac)$	—	19.4/25.7/26.9	0.63, 0.37	108

Since both materials were evaluated using identical device architectures and doping concentrations, this suggests that device efficiency is limited by structural or charge-transport factors rather than by simple HOMO/LUMO and triplet energy-level alignment. From a comparative perspective, although **BCPICT (37)** possesses a higher T_1 than **BBPICT (36)**, its device performance is significantly lower. This discrepancy suggests that the biscyanophenyl extension, while effective at increasing T_1 and deepening the LUMO, may introduce detrimental effects, such as dipole-induced quenching or an imbalanced charge distribution. In contrast, **BBPICT (36)** exhibits superior electron mobility, which likely facilitates a more centrally located recombination zone and suppresses triplet-polaron annihilation, resulting in nearly double the device performance. Conversely, the higher hole mobility in **BCPICT (37)** may shift the recombination zone toward the interface, promoting TPQ and reducing overall efficiency.

Patil *et al.* synthesized a novel n-type host material, **SBFTrz (38)**, featuring a fused donor unit based on spirobifluorene carbazole combined with diphenyltriazine acceptor units.[106] This host material exhibits high thermal stability with a T_d/T_g of 487/134 °C, which is attributed to its rigid molecular framework. The material shows an S_1/T_1 of 3.63/2.74 eV, and DFT calculations indicate a HOMO/LUMO of −5.88/−3.24 eV. This n-type host was subsequently combined with the p-type host BPBPCz to form an exciplex host system with an S_1/T_1 of 2.94/2.59 eV, which is well-suited for red PhOLED applications. The device employing $Ir(mphmq)_2(tmd)$ as the emitter achieved superior efficiencies of 26.2% (37.9 cd A^{-1} and 32.7 lm W^{-1}), with λ_{max} at 610 nm, consistent with the emission profile of the emitter. Furthermore, the authors demonstrated that the exciplex-based device (Device D) exhibited a lifetime enhancement of up to fivefold compared with the corresponding single-host device (Device F). This outcome confirms the superior device performance of the exciplex system due to improved charge balance. The spiro unit in **SBFTrz (38)** induces a highly twisted molecular geometry, which aids in controlling film morphology and reducing unfavorable intermolecular interaction with the BPBPCz host material.

Jang *et al.* introduced a bipolar host material, **DBT-INFUR (39)**, constructed using a fused donor unit based on benzofurocarbazole linked to a dibenzothiophene acceptor.[107] This material exhibits a T_1 of 2.71 eV and a HOMO/LUMO of −5.87/−2.61 eV. **DBT-INFUR (39)** also demonstrates good thermal stability, with a T_d of 371 °C, which is lower than that of other reported host materials but remains sufficient for device fabrication. DFT calculations reveal a dihedral angle of approximately 64° between donor and acceptor units. The frontier molecular orbital distributions confirm the bipolar characteristic in the material, with the HOMO predominantly localized on the donor unit and the LUMO on the acceptor unit. This indicates that the host material exhibits good charge separation due to its bipolar nature. Red PhOLEDs employing **DBT-INFUR (39)** as a single host and $Ir(mphmq)_2(acac)$ as the emitter achieve a performance of 12.4% (15.5 cd A^{-1} and 8.9 lm W^{-1}).

Zheng *et al.* reported a bipolar host material, **ICz-PPI (40)**, that combines a fused indolo[3,2,1-*jk*]carbazole (ICz) donor and a phenanthro[9,10-*d*]imidazole (**PI**) acceptor connected by a phenyl π-bridge.[108] This host material exhibits suitable a HOMO/LUMO of −5.46/−2.16 eV and a high T_1 value of 2.48 eV, along with excellent thermal stability of T_d/T_g at 431/173 °C, which

is favorable for device efficiency and operational stability. **ICz-PPI (40)** exhibits weak ICT character, attributed to its rigid, highly twisted molecular structure. The relatively simpler D–π–A architecture promotes balanced charge transport, which is essential for achieving higher device efficiency and contributes to its superior electroluminescence performance. When employed as a single host in red PhOLEDs using $Ir(MDQ)_2(acac)$ as the emitter, **ICz-PPI (40)** achieves a maximum device performance of 19.4% (25.7 cd A^{-1} and 26.9 lm W^{-1}), with low efficiency roll-off and maintaining an EQE of 14.9% at a high luminance of 10 000 cd m^{-2}. This improved device performance is attributed to the favorable carrier transport balance and effective exciton confinement provided by the host material.

Finally, within the framework of push–pull architecture, multi-branch and star-shaped architectures are also included in this category. Multi-branched and star-shaped architectures incorporate multiple carbazole donor units around a central core to disrupt molecular stacking. This geometry promotes amorphous film formation and preserves high triplet energies. Additionally, the high branching density helps balance charge transport and suppresses non-radiative decay. These traits make such architectures particularly effective for red-to-NIR applications, which are highly sensitive to energy loss. Fig. 6 presents host materials employing push–pull architecture for red-to-NIR OLEDs, organized according to a multi-D–A classification, while Table 4 summarizes the corresponding material properties and OLED device performance. Most materials exhibit high thermal stability (T_d/T_g), attributed to their multi-branched/star-shaped molecular geometry. The T_1 energy levels are also notably higher than those of other push–pull-architecture materials discussed above, where such elevated triplet energies are typically associated with wide-bandgap hosts, which may be suboptimal for red phosphorescent emitters.

The host material **IP368Cz (41)**, reported by Song *et al.*, represents a push–pull architecture featuring a multi-D–A using multiple carbazole donor units tethered to an imidazo[1,2-*b*]pyridazine (IP) acceptor core.[87] This star-shaped molecular geometry substantially increases molecular mass, thereby enhancing the thermal stability of T_d/T_g, reaching 456/162 °C. The calculated HOMO and LUMO are −5.13 and −1.66 eV, respectively, accompanied by a T_1 of 2.28 eV. Red PhOLEDs employing $Ir(pq)_2(acac)$ as the emitter exhibit a performance of 12.4% (22.2 cd A^{-1} and 18.8 lm W^{-1}), which is the lowest among the hosts reported in the multi-D–A classification series. This inferior device efficiency is attributed to the introduction of carbazole substituents at the 3-position of the acceptor core, which extends the overall π-conjugation and induces pronounced steric hindrance. Such steric effects impair electron transport and diminish the efficiency of energy transfer within the devices.

In a subsequent study by the Grazulevicius group, two star-shaped host materials (compounds **3 (42)** and **4 (43)**) were developed based on a central carbazole donor core directly connected to multiple peripheral arms comprising two carbazole donor units and two imidazole acceptor units.[109] The structural distinction between these two compounds arises from the presence of a *tert*-butyl-substituted carbazolyl moiety in compound **4 (43)**. This substitution imparts enhanced thermal stability; compound **4 (43)** exhibits higher thermal stability (T_d/T_g = 487/172 °C) than compound **3 (42)** (T_d/T_g = 477/151 °C). Both materials possess high T_1 values (3.08 eV for compound **3 (42)** and 3.05 eV for compound **4 (43)**), which are sufficient to suppress back energy transfer from the emissive dopant. However, such elevated triplet energies are typically associated with wide-bandgap hosts, which are suboptimal for red phosphorescent emitters due to substantial energetic

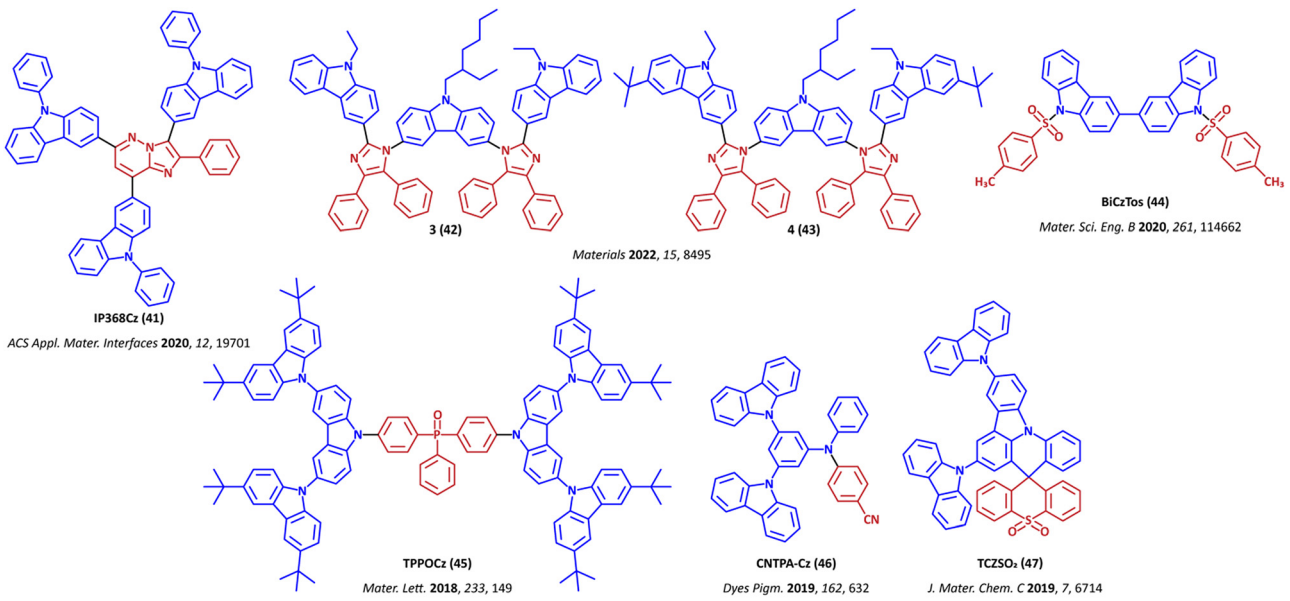

Fig. 6 Chemical structures of carbazole-based host materials employing a push–pull architecture for red-to-NIR OLEDs, grouped according to multi-D–A classification. (The highlighted colors correspond to blue for the carbazole donor, red for the acceptor moieties, and black for the π-bridge linkers.)

Table 4 Summary of materials' properties and OLED device performance parameters for the compounds depicted in Fig. 6

		Material characterization			OLED characterization					
Material		T_d/T_g [°C]	HOMO/LUMO [eV]	S_1/T_1 [eV]	EML type	Emitter	λ_{max} [nm]	EQE/CE/PE [%, cd A^{-1}, lm W^{-1}]	CIE [x,y]	Ref.
41	**IP368Cz**	456/162	−5.13/−1.66	2.46/2.28	Single	$Ir(pq)_2(acac)$	600	12.4/22.2/18.8	0.61, 0.39	87
42	**3**	477/151	−5.26/−1.92	—/3.08	Single	$Ir(piq)_2(acac)$	632	6.4/4.4/3.3	0.67, 0.32	109
43	**4**	487/172	−5.25/−1.94	—/3.05			629	4.5/3.9/1.7	0.63, 0.31	
44	**BiCzTos**	349/126	−5.73/−2.10	3.35/2.90	Single	$Ir(piq)_2(acac)$	—	2.2/1.3/0.9	—	110
45	**TPPOCz**	427/213	−5.49/−2.27	3.20/2.98	Single	$Ir(2\text{-phq})_2(acac)$	612	12.4/20.1/—	0.62, 0.37	111
46	**CNTPA-Cz**	427/121	−5.29/−1.82	3.11/2.76	Single	$Ir(MDQ)_2(acac)$	—	20.3/34.5/25.9	0.61, 0.39	112
47	**$TCZSO_2$**	487/236	−5.44/−2.31	3.13/2.86	Single	$Ir(MDQ)_2(acac)$	615	21.0/28.7/21.9	0.63, 0.37	113

misalignment at the host–guest interaction. This mismatch can lead to increased operating voltage, inefficient charge transport, and pronounced charge imbalance within the emissive layer. Consequently, a red PhOLED device incorporating $Ir(piq)_2(acac)$ as the emitter exhibits a poor performance of 6.4% (4.4 cd A^{-1} and 3.3 lm W^{-1}) for compound **3 (42)** and 4.5% (3.9 cd A^{-1} and 1.7 lm W^{-1}) for compound **4 (43)**.

In a related publication, a new multi-D–A host material, **BiCzTos (44)**, was synthesized by integrating carbazole donor units with a toluenesulfonyl acceptor moiety.[110] **BiCzTos (44)** exhibits a moderate thermal stability of T_d/T_g of 349/126 °C and a T_1 of 2.9 eV. The electrochemical properties show a HOMO/LUMO of −5.73/−2.10 eV. While **BiCzTos (44)** features a high T_1 value and good thermal stability, this host exhibits inefficient charge transport, resulting in inferior red PhOLED performance. The device utilizing $Ir(piq)_2(acac)$ as the phosphorescent emitter achieves a performance of 2.2% (1.3 cd A^{-1} and 0.9 lm W^{-1}). This performance is significantly inferior to the reference device based on an mCP host. Consequently, a higher turn-on voltage (V_{on}) of 4.5 V was recorded, further highlighting the impact of the host's transport limitations.

Wang *et al.* reported a multi-D–A host with a dendritic architecture, **TPPOCz (45)**, in which carbazole units function as electron-donating units and a phenylphosphine oxide moiety serves as the central electron-accepting core.[111] The dendritic molecular design endows **TPPOCz (45)** with enhanced thermal stability due to its large molecular weight and rigid framework. In addition, the pronounced steric hindrance introduced by the peripheral carbazole units effectively suppresses π–π stacking interaction, thereby stabilizing the amorphous solid state. Thermal analysis reveals high thermal stability, with a T_d/T_g of 427/213 °C, and is accompanied by a high T_1 value of 2.98 eV. The calculated HOMO/LUMO are −5.49/−2.27 eV, with the LUMO predominantly originating from the electron-withdrawing phosphine oxide core. The red PhOLED device employing **TPPOCz (45)** as the host and $Ir(2\text{-phq})_2(acac)$ as the phosphorescent dopant exhibits a maximum EQE of 12.4% and a current efficiency of 20.1 cd A^{-1}.

Ran *et al.* reported a tripodal bipolar material, **CNTPA-Cz (46)**, constructed from two carbazole donor units and a triphenylamine core in which one peripheral phenyl ring is substituted with a benzonitrile acceptor.[112] This configuration endows the molecule with pronounced bipolar charge transport characteristics. When employed as a host for the red phosphorescent emitter $Ir(MDQ)_2(acac)$, **CNTPA-Cz (46)** delivered a high device performance, achieving 20.3% (34.5 cd A^{-1} and 25.9 lm W^{-1}). The superior performance is further corroborated by hole-only and electron-only device measurements, which confirm balanced hole and electron transport. The charge balance is an essential factor for efficient exciton formation and reduced charge accumulation. In addition, **CNTPA-Cz (46)** exhibits high thermal stability, with a T_d/T_g of 427/121 °C, and a sufficiently high T_1 of 2.76 eV to ensure effective energy transfer to the phosphorescent dopant. The HOMO and LUMO are −5.29 and −1.82 eV, respectively, which facilitate efficient charge injection. Notably, the HOMO is predominantly localized on the carbazole units, while the LUMO is primarily distributed over the central benzonitrile-containing core, thereby supporting efficient hole and electron transport pathways.

Concluding the discussion on multi-D–A host systems, Zhu *et al.* reported a spiro-configuration host material called **$TCZSO_2$ (47)**.[113] This host delivers reasonable performance in red PhOLEDs, achieving 21.0% (28.7 cd A^{-1} and 21.9 lm W^{-1}) when doped with the $Ir(MDQ)_2(acac)$ emitter. **$TCZSO_2$ (47)** is designed using a spiro-type molecular architecture that integrates a tercarbazole donor unit with a thioxanthene 10,10-dioxide acceptor. This molecular design strategy targets universal host functionality, as **$TCZSO_2$ (47)** demonstrated EQEs exceeding 20% in blue, green, and red PhOLEDs. Closer examination reveals that **$TCZSO_2$ (47)** possesses relatively high triplet energy (T_1 = 2.86 eV), which is critical for effective triplet exciton confinement and for suppressing reverse energy transfer from the emitter to the host. The spiro-type configuration imparts exceptional thermal stability with T_d/T_g reaching 487/236 °C. The orthogonal geometry and rigid frameworks inherent to spiro compounds effectively inhibit intermolecular π–π stacking and crystallization, thereby promoting a stable and uniform amorphous morphology even under thermal stress. The HOMO/LUMO (−5.44/−2.31 eV) are well aligned to facilitate balanced charge injection, transportation, and recombination.

In this system, the tercarbazole moiety enhances hole injection and transport, whereas the sulfone-containing thioxanthene 10,10-dioxide acceptor promotes efficient electron injection and transport. Charge carrier mobility measurements further corroborate the achievement of balanced bipolar transport. Nevertheless, in the context of red PhOLED applications, the relatively high triplet energy and wide bandgap associated with the universal-host design may be electronically inefficient.

These characteristics can exacerbate energy-level mismatches with red emitters, leading to reduced overall performance and pronounced efficiency roll-off at high luminance. This behavior is reflected in the device performance, where the maximum performance of 21.0% (28.7 cd A^{-1} and 21.9 lm W^{-1}) decreased to 19.3% (26.4 cd A^{-1} and 15.9 lm W^{-1}) at 1000 cd m^{-2} and further to 14.9% (20.4 cd A^{-1} and 9.4 lm W^{-1}) at 5000 cd m^{-2}. Notably, this efficiency roll-off is more pronounced than that observed in the blue and green devices, underscoring trade-offs associated with universal host designs for red PhOLEDs.

3.2. Symmetric architectures: molecular design strategies for rigidification and balanced charge transport

The use of symmetric architectures, including donor–acceptor–donor (D–A–D) and acceptor–donor–acceptor (A–D–A) configurations, represents an advanced structural design strategy in carbazole-based molecules. In these systems, identical donor or acceptor units are symmetrically arranged around a central core, resulting in a balanced electronic framework and well-defined frontier orbital distribution.[114–117] D–A–D architectures typically favor hole transport by reinforcing HOMO localization on the paired carbazole donors, while the central acceptor modulates the bandgap and stabilizes the excitonic state. Conversely, A–D–A architectures impart enhanced electron-transporting characteristics and enable precise tuning of HOMO/LUMO energy levels. Symmetrically arranged molecules often exhibit high rigidity and shape-persistent geometries due to the use of a rigid central core and peripheral units that constrain conformational freedom and lock the molecule into a well-defined structure. This has benefits for suppressing morphological changes that can otherwise lead to material degradation, compromised device stability, and increased efficiency roll-off under prolonged operation. Moreover, symmetric architectures effectively regulate the spatial distribution of electron orbitals (HOMO/LUMO), thereby promoting balanced charge transport and suppressing exciton quenching. This structural control results in more homogeneous films and improved long-term device performance. Fig. 7 illustrates host materials with symmetric architectures for red-to-NIR OLEDs, while Table 5 summarizes their corresponding material properties and OLED device performance. Owing to their symmetric architecture, most exhibit high thermal stability (T_d/T_g) and well-tuned HOMO–LUMO energy levels, well-suited for red-to-NIR emission.

The first study discussed herein was conducted by our group, in which six host materials based on symmetric D–A–D architectures were synthesized.[118] These materials incorporate

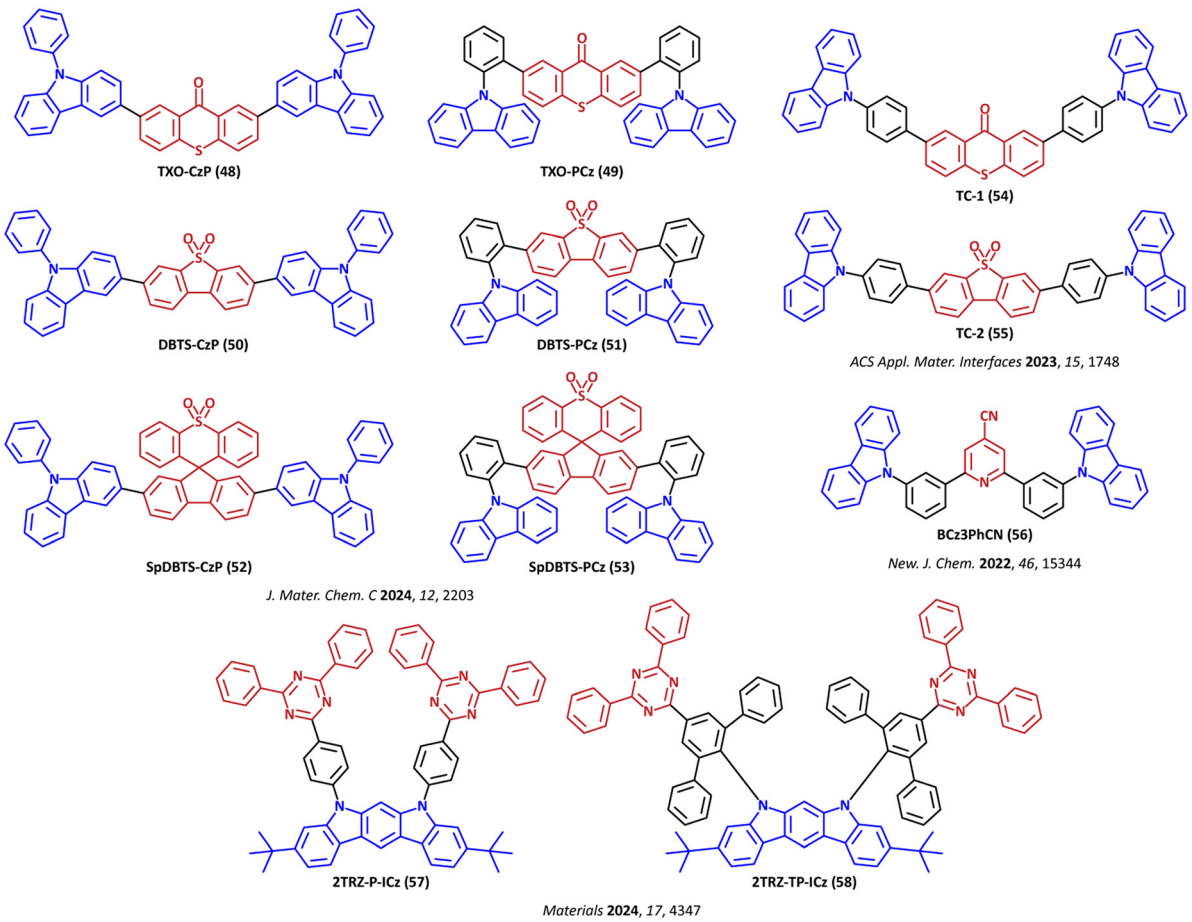

Fig. 7 Chemical structures of carbazole-based host materials employing a symmetric architecture for red-to-NIR OLEDs. (The highlighted colors correspond to blue for the carbazole donor, red for the acceptor moieties, and black for the π-bridge linkers.)

Table 5 Summary of materials' properties and OLED device performance parameters for the compound depicted in Fig. 7

Material		Material characterization			OLED characterization					
		T_d/T_g [°C]	HOMO/LUMO [eV]	S_1/T_1 [eV]	EML type	Emitter	λ_{max} [nm]	EQE/CE/PE [%, cd A^{-1}, lm W^{-1}]	CIE [*x*,*y*]	Ref.
48	**TXO-CzP**	428/—	−5.14/−2.32	2.82/2.39	Co-host	$Ir(piq)_2(acac)$	629	18.6/12.7/15.7	0.68, 0.32	118
49	**TXO-PCz**	397/—	−5.14/−2.13	2.93/2.65			635	21.1/11.8/16.2	0.69, 0.31	
50	**DBTS-CzP**	431/—	−5.16/−2.17	2.99/2.13			634	21.7/13.4/18.4		
51	**DBTS-PCz**	426/—	−5.13/−1.84	3.23/2.45			633	19.1/10.9/15.2		
52	**SpDBTS-CzP**	462/—	−5.15/−2.01	3.01/2.31			633	20.2/11.3/15.8		
53	**SpDBTS-PCz**	451/—	−5.15/−1.65	3.46/2.47			631	20.1/12.7/17.8	0.68, 0.31	
54	**TC-1**	480/—	−5.28/−2.36	2.93/2.53	Single	$Ir(piq)_2(acac)$	636	21.6/12.0/12.5	0.69, 0.31	119
55	**TC-2**	440/—	−5.27/−2.21	3.06/2.12				22.9/14.0/15.7		
56	**BCz3PhCN**	460/126	−5.67/−2.55	—/2.76	Single	$Ir(pq)_2(acac)$	606	26.8/41.1/47.9	0.62, 0.38	120
57	**2TRZ-P-ICz**	504/—	−5.50/−2.70	2.93/2.72	Single	$Ir(piq)_2(acac)$	630	9.6/6.8/3.6	0.68, 0.32	121
58	**2TRZ-TP-ICz**	518/—	−5.59/−2.84	2.83/2.75			626	13.7/9.9/5.5		

three distinct acceptor cores: thioxanthone (TXO), diphenyl sulfone (DBTS), and spiro[fluorine-9,9′-thioxanthene]-10′,10′-dioxide (SpDBTS). In each design, carbazole donors were linked to the acceptor core either at the C3 position (CzP), favoring a more planar molecular conformation, or at the *N*-substitution (PCz), inducing a twisted geometry. Accordingly, the six host materials—**TXO-CzP (48)**, **TXO-PCz (49)**, **DBTS-CzP (50)**, **DBTS-PCz (51)**, **SpDBTS-CzP (52)**, and **SpDBTS-PCz (53)**—were successfully synthesized. Frontier molecular orbital calculations reveal that all compounds exhibit similar HOMO levels in the range of −5.13 to −5.16 eV, predominantly originating from the carbazole donor units. Computational analyses further indicate that the twisted hosts (**TXO-PCz (49)** and **DBTS-PCz (51)**) exhibit pronounced orbital separation, with the HOMO localized on the carbazole donors and the LUMO confined to the acceptor cores. In contrast, the more linear CzP-linked host exhibits reduced torsional angles and partial HOMO–LUMO overlap, consistent with locally excited (LE) electronic characteristics. All materials demonstrate high thermal stability, with T_d exceeding 397 °C, and a marginally enhanced T_d observed for CzP-linked derivatives relative to their PCz counterparts. The calculated T_1 value spans from 2.19 to 2.65 eV, rendering these hosts suitable for use in red PhOLED structures.

Device performance evaluations employing a co-host system with CN-T2T and $Ir(piq)_2(acac)$ as the phosphorescent emitter reveal favorable electroluminescence performance. All six devices exhibit emission characteristics consistent with $Ir(piq)_2(acac)$, confirming that exciton generation occurs predominantly within the EML. Minor shifts observed in λ_{max} are attributed to variations in the host material, which modify the optical pathways and microcavity effects of the device. Specifically, differences in charge transport properties, energy levels, and interfacial interactions with the CN-T2T co-host and adjacent layers modulate the electron–hole recombination zone, thereby influencing the resulting EL spectra. Among the series, **TXO-CzP (48)** exhibits the lowest efficiency, achieving 18.6% (12.7 cd A^{-1} and 15.7 lm W^{-1}), whereas **DBTS-CzP (50)** delivers the highest performance of 21.7% (13.4 cd A^{-1} and 18.4 lm W^{-1}). The relatively inferior performance of **TXO-CzP (48)** is attributed to disrupted π-conjugation arising from the sulfur linkage within the acceptor core. In contrast, the superior performance of **DBTS-CzP (50)** underscores the advantage of a linear molecular arrangement, which promotes stronger intermolecular π–π stacking interaction and facilitates TTA up-conversion. Moreover, the linear geometry enables a more uniform electron distribution and reinforces the LE character, thereby enhancing energy-transfer efficiency within the device.

Our group also reported symmetric architecture host materials based on carbazole donor units combined with different acceptor cores, namely **TC-1 (54)**, incorporating a thioxanthone acceptor, and **TC-2 (55)**, incorporating a dibenzo[*b*,*d*]thiophene 5,5-dioxide acceptor.[119] In both systems, a phenyl π-bridge was employed to connect the donor and acceptor segments. Notably, these two hosts exhibit distinct molecular packing behaviors: **TC-1 (54)** adopts a more distorted molecule arrangement that suppresses intermolecular π–π stacking interactions, where **TC-2 (55)** forms a more favorable oriented packing motif with pronounced π–π stacking, which enhances TTA up-conversion processes. Both hosts demonstrate excellent thermal stability, with T_d values of 480 °C for **TC-1 (54)** and 440 °C for **TC-2 (55)**, which are suitable for thermal vacuum deposition. The HOMO/LUMO and T_1 values of **TC-1 (54)** are −5.28/−2.36 eV and 2.53 eV, respectively, while those of the **TC-2 (55)** host are −5.27/−2.21 eV and 2.12 eV. Device studies confirm that these hosts are highly effective for red PhOLED applications. Red PhOLEDs using $Ir(piq)_2(acac)$ as the emitter achieved a performance of 21.6% (12.0 cd A^{-1} and 12.5 lm W^{-1}) for **TC-1 (54)** and 22.9% (14.0 cd A^{-1} and 15.7 lm W^{-1}) for **TC-2 (55)**. Overall, both materials exhibit high performance, highlighting the critical role of balanced charge transport enabled by a bipolar, symmetrical architecture. In particular, the superior performance of **TC-2 (55)** underscores the effectiveness of controlled molecular packing and π–π stacking interactions as a molecular design strategy for high-efficiency OLED host materials.

Zhou *et al.* synthesized a universal bipolar host material, **BCz3PhCN (56)**, constructed by integrating carbazole donor units with an isonicotinonitrile acceptor and a phenyl π-bridge.[120] This material exhibits excellent thermal stability with a T_d/T_g of 460/126 °C and a T_1 of 2.76 eV, making it suitable for red PhOLED applications. DFT calculations confirm the bipolar nature of **BCz3PhCN (56)**, revealing an almost complete spatial

separation of the frontier molecular orbitals, with the HOMO/LUMO located at −5.67 and −2.55 eV, respectively. Red PhOLED devices employing $Ir(pq)_2(acac)$ as the emitter demonstrate outstanding electroluminescence performance, achieving a maximum performance of 26.8% (41.1 cd A^{-1} and 47.9 lm W^{-1}). This superior performance is attributed to the planar molecular configuration, which minimized steric hindrance between the cyano group and adjacent phenyl rings, thereby lowering the LUMO energy level. The reduced LUMO facilitates electron injection and transport by decreasing the energy barrier and improving charge balance within the emissive layer. The cyano (–CN) group is particularly effective in introducing strong electron-withdrawing character without significantly increasing molecular bulk or steric congestion. Overall, the exceptional OLED performance of **BCz3PhCN (56)** is closely associated with its well-balanced bipolar charge-transport properties.

Park *et al.* introduced two host materials based on an indolocarbazole donor core, forming a symmetric A–D–A architecture with triazine acceptor units.[121] The two hosts differ in the nature of the π-bridge: **2TRZ-P-ICz (57)** incorporates a phenyl linker, whereas **2TRZ-TP-ICz (58)** employs a terphenyl bridge. Both materials exhibit TADF characteristics; **2TRZ-P-ICz (57)** shows a ΔE_{ST} of 0.21 eV with a T_1 value of 2.72 eV, while **2TRZ-TP-ICz (58)** displays a smaller ΔE_{ST} of 0.08 eV and a slightly higher T_1 value of 2.75 eV. Both hosts demonstrate exceptional thermal stability with T_d exceeding 504 °C. Theoretical calculations reveal that the HOMO is predominantly localized on the indolocarbazole donor moiety, whereas the LUMO is mainly distributed over the triazine acceptor and π-bridge segments. The calculated HOMO/LUMO are −5.50/−2.70 eV for **2TRZ-P-ICz (57)** and −5.59/−2.84 eV for **2TRZ-TP-ICz (58)**. In red PhOLED devices employing $Ir(piq)_2(acac)$ as the phosphorescent emitter, the **2TRZ-P-ICz (57)**-based host achieved a performance of 9.6% (6.8 cd A^{-1} and 3.6 lm W^{-1}), where devices using **2TRZ-TP-ICz (58)** deliver a higher performance of 13.7% (9.9 cd A^{-1} and 5.5 lm W^{-1}). The higher performance of **2TRZ-TP-ICz (58)** is attributed to the sterically bulky terphenyl bridge, which effectively suppresses intramolecular rotation and vibration relaxation, thereby reducing non-radiative decay pathways while maintaining high triplet energy. This result highlights the critical role of π-bridge engineering in regulating excited-state dynamics and device efficiency in red PhOLED host materials.

3.3. Asymmetric architectures: molecular design strategies for ICT regulation and exciton management

Asymmetric architectures, including non-symmetric D–A–D, donor–donor–acceptor (D–D–A), and donor–acceptor–acceptor (D–A–A), deliberately disrupt both electronic and structural symmetry to achieve properties that are unattainable in fully symmetric architecture.[122–125] These designs expand molecular design by the strategic combination of donor or acceptor moieties with varying electronic strength, steric demand, and conjugation length. Incorporation of two distinct peripheral units or placement of donor and acceptor groups at non-equivalent locations allows precise modulation of charge distribution and HOMO/LUMO alignment. Consequently, carrier injection pathways can be systematically tuned to optimize charge balance and enhance exciton confinement within the EML. In the D–A–D and D–D–A architectures, the incorporation of two distinct donor moieties aims to facilitate hole transport, owing to the higher density of electron-rich sites. These multiple-donor units typically raise the HOMO level, promoting electron donation to the acceptor and leading to a strong ICT state. Conversely, in the D–A–A configuration, the donor is coupled to two acceptor moieties, increasing electron affinity and providing additional pathways for electron hopping, which significantly enhance electron transport characteristics. Furthermore, the presence of multiple acceptors typically stabilizes the LUMO energy level, thereby narrowing the optical bandgap, which is advantageous for red-to-NIR OLEDs.

In the development of red-to-NIR OLEDs, asymmetric material design is critical for overcoming efficiency limitations associated with the energy-gap law and concentration quenching.[126,127] The utilization of structurally disparate donors disrupts intermolecular π–π stacking, thereby suppressing exciton diffusion and minimizing non-radiative quenching losses. Collectively, these attributes enable performance levels that are unattainable with symmetric hosts. They provide a versatile platform for optimizing charge transport, exciton management, and energy alignment in high-efficiency red-to-NIR OLEDs. Fig. 8 illustrates host materials employing an asymmetric architecture for red-to-NIR OLEDs, organized around an asymmetric D–A–D structural motif, while Table 6 summarizes their corresponding material properties and OLED device performance. The data reveal that most materials exhibit moderate to high thermal stability (T_d/T_g). The elevated S_1 energy levels are likely attributed to the structural asymmetry, which limits intramolecular charge transfer and localizes the frontier molecular orbitals.

As an initial example of an asymmetrical architecture, as presented in Fig. 8, Bezvikonnyi *et al.* reported two asymmetric D–A–D-type hosts (compounds **1 (59)** and **2 (60)**) incorporating carbazole and diphenyl imidazole units.[109] Molecular asymmetry was achieved by introducing *N*-ethyl carbazole at different positions of the diphenyl imidazole core, while *tert*-butyl substitution further modulated compound **2 (60)**. Both hosts exhibit high thermal stability (T_d/T_g) and high T_1 values of 399/134 °C and 3.18 eV for compound **1 (59)**, and 400/147 °C and 3.16 eV for compound **2 (60)**, rendering them suitable for red phosphorescent OLEDs. The diphenyl imidazole fragment facilitates bipolar charge transport. However, similar to compounds **3 (42)** and **4 (43)** (in Fig. 6) discussed in the section on push–pull architecture, such elevated triplet energies are typically associated with wide bandgap hosts, which are suboptimal for red phosphorescent emitters due to substantial energetic misalignment at the host–guest interaction. This mismatch can lead to increased operating voltage, inefficient charge transport, and pronounced charge imbalance within the emissive layer, where these hosts doped with $Ir(piq)_2(acac)$ achieved maximum EQEs of 3.0% (2.7 cd A^{-1} and 0.9 lm W^{-1}) and 2.7% (2.6 cd A^{-1} and 1.4 lm W^{-1}), respectively.

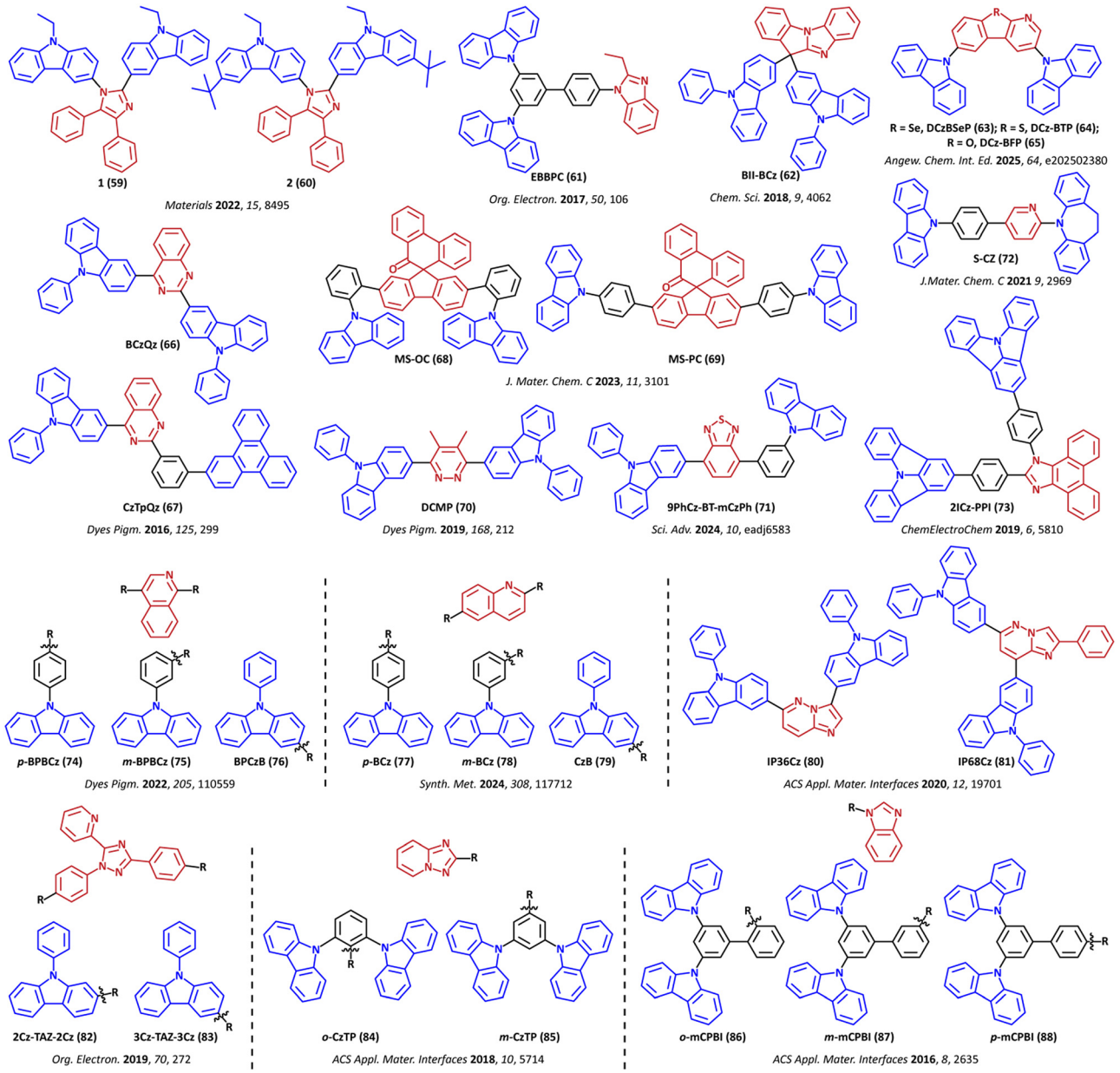

Fig. 8 Chemical structure of carbazole-based host materials employing an asymmetric architecture for red-to-NIR OLEDs, grouped according to the asymmetric D–A–D structural motif. (The highlighted colors correspond to blue for the carbazole donor, red for the acceptor moieties, and black for the π-bridge linkers).

Zang *et al.* designed an asymmetric host, **EBBPC (61)**, comprising two carbazole units attached at the 3- and 5-positions of a central phenyl core, with a benzimidazole moiety as the electron-accepting unit and a biphenyl serving as the π-bridge.[128] The biphenyl linkage induces a non-planar geometry that effectively suppresses aggregation and enhances thermal stability, with a T_d/T_g of 431/142 °C. In addition, the incorporation of an ethyl substituent at the 2-position of the benzimidazole ring restricts π-conjugation, thereby preserving a high T_1 value of 2.74 eV, which is essential for efficient triplet exciton confinement and energy transfer in PhOLEDs. The frontier molecular orbitals of **EBBPC (61)** (HOMO/LUMO = −5.71/−2.36 eV) are well aligned with those of the adjacent layer, thereby minimizing energy barriers and improving charge balance. Designed as a universal host for white PhOLEDs, **EBBPC (61)**, when combined with the red emitter $Ir(MDQ)_2(acac)$, delivered a maximum performance of 14.9% (23.5 cd A^{-1} and 21.1 lm W^{-1}). Admittance spectroscopy further revealed bipolar transport behavior with electron-dominant charge transport (μ_e of $\sim 2 \times 10^{-5}$ cm^2 V^{-1} s^{-1}), nearly twice that of the hole mobility, enabling **EBBPC (61)** to function effectively as both a host and an electron-transporting material.

Chen *et al.* synthesized a novel host material, **BII–BCz (62)**, by linking two phenylcarbazole units at the 3-position of

Table 6 Summary of materials' properties and OLED device performance parameters for the compounds depicted in Fig. 8

		Material characterization			OLED characterization					
Material		T_d/T_g [°C]	HOMO/LUMO [eV]	S_1/T_1 [eV]	EML type	Emitter	λ_{max} [nm]	EQE/CE/PE [%, cd A^{-1}, lm W^{-1}]	CIE [x,y]	Ref.
59	**1**	399/134	−5.25/−1.81	—/3.18	Single	$Ir(piq)_2(acac)$	625	3.0/2.7/0.9	0.56, 0.29	109
60	**2**	400/147	−5.21/−1.87	—/3.16				2.7/2.6/1.4	0.59, 0.29	
61	**EBBPC**	431/142	−5.71/−2.36	3.10/2.74	Single	$Ir(MDQ)_2(acac)$	—	14.9/23.5/21.1	0.61, 0.39	128
62	**BII-BCz**	438/177	−5.70/−2.26	3.44/2.98	Single	$Ir(piq)_2(acac)$	—	22.7/15.8/16.5	0.68, 0.31	129
63	**DCz-BSeP**	410/137	−5.70/−2.20	3.40/2.90	Single	DBP	611	21.0/—/28.3	0.62, 0.35	130
64	**DCz-BTP**	425/143					609	15.4/—/24.7	0.62, 0.38	
65	**DCz-BFP**	380/135					611	16.9/—/28.0		
66	**BCzQz**	438/148	−5.71/−2.64	3.05/2.36	Single	$Ir(mphmq)_2(acac)$	618	17.4/16.7/15.7	—	131
67	**CzTpQz**	447/153	−5.75/−2.69	3.09/2.40			619	18.4/17.6/19.3		
68	**MS-OC**	426/179	−5.20/−1.81	3.31/2.66	Single	$Ir(piq)_2(acac)$	—	14.9/8.7/10.5	0.69, 0.31	132
					Co-host			20.1/12.0/16.6		
69	**MS-PC**	396/—	−5.19/−2.08	3.14/2.55	Single			14.4/8.1/10.5		
					Co-host			18.8/10.7/15.3		
70	**DCMP**	425/102	-5.58/-2.11	3.47/2.62	Single	$Ir(pq)_2(acac)$	—	20.0/37.0/28.2	0.62, 0.38	133
71	**9-PhCz-BT-mCzPh**	—/122	−6.05/−3.7	—/2.20	Co-host (bottom)	BBT-TPA	891	1.7/—/—	—	134
					Co-host (top)		930	1.6/—/—		
72	**S-CZ**	414/116	−5.40/−1.93	3.48/2.80	Single	$Ir(MDQ)_2(acac)$	—	23.0/34.0/33.5	0.63, 0.38	135
73	**2ICz-PPI**	511/—	−5.48/−2.37	—/2.80	Single	$Ir(MDQ)_2(acac)$	—	17.1/25.7/26.9	0.62, 0.38	108
74	***p*-BPBCz**	529/143	−5.65/−2.57	—/2.35	Single	$Ir(pq)_2(acac)$	600	15.0/26.3/22.9	0.60, 0.38	136
75	***m*-BPBCz**	495/123	−5.63/−2.62	—/2.47				17.2/29.6/22.6		
76	**BPCzB**	481/141	−5.57/−2.37	—/2.40				12.6/21.4/19.8	0.61, 0.38	
77	***p*-BCz**	476/97	−5.61/−2.64	3.25/2.39	Single	$Ir(piq)_2(acac)$	624	14.1/10.9/8.6	0.67, 0.33	137
78	***m*-BCz**	532/123	−5.62/−2.63	3.47/2.40				12.7/9.2/5.3		
79	**CzB**	475/128	−5.50/−2.45	3.09/2.36				10.3/7.7/3.9		
80	**IP36Cz**	427/156	−5.18/−2.51	2.67/2.27	Single	$Ir(pq)_2(acac)$	600	16.2/30.3/31.4	0.60, 0.39	87
81	**IP68Cz**	473/158	−5.34/−2.39	2.95/2.28				25.2/46.0/44.7	0.61, 0.39	
						$Ir(piq)_2(acac)$	625	19.9/15.6/13.2	0.68, 0.32	
82	**2Cz-TAZ-2Cz**	457/—	−5.56/−2.37	3.19/2.66	Single	$Ir(piq)_2(acac)$	626	16.6/12.4/12.7	—	138
83	**3Cz-TAZ-3Cz**	432/109	−5.40/−2.12	3.28/2.65				11.4/9.7/8.9		
84	***o*-CzTP**	417/130	−5.38/−1.78	3.39/2.93	Single	$Ir(pq)_2(acac)$	600	15.8/29.9/24.9	0.60, 0.39	139
85	***m*-CzTP**	435/—	−5.34/−1.78	3.58/2.92				17.2/29.6/16.9	0.61, 0.38	
86	***o*-mCPBI**	400/130	−5.44/−1.86	—/3.00	Single	$(PPQ)_2Ir(acac)$	—	19.8/24.5/21.4	0.64, 0.36	140
87	***m*-mCPBI**	394/124	−5.40/−1.84	—/2.80				18.7/23.6/21.8		
88	***p*-mCPBI**	429/141	−5.44/−1.89	—/2.71				12.8/15.1/15.8	0.65, 0.35	

carbazole to the central acceptor core of 11H-benzo[4,5]-imidazo[1,2-*a*]indole (BII).[129] The BII moiety imparts a strong electron–withdrawing character derived from the benzimidazole framework, while the phenyl substituent connected through a non-conjugated C–N bond efficiently suppresses ICT between the carbazole donor and BII acceptor. This suppression is critical for preserving a high T_1 of 2.98 eV, enabling **BII-BCz (62)** to function as a universal host for PhOLEDs. DFT calculations reveal spatial separation of the frontier molecular orbitals, with the HOMO and LUMO localized on donor and acceptor units (−5.70/−2.26 eV), suggesting favorable charge injection and transport characteristics. Owing to its bulky and rigid three-dimensional (3D) configuration, **BII-BCz (62)** exhibits excellent thermal stability (T_d/T_g of 438/177 °C) and reduced structural relaxation-induced exciton quenching. As a result, devices based on this host achieve outstanding EQE, exceeding 20% from blue to red PhOLEDs, and demonstrate stable EL spectra in white devices. In particular, a red PhOLED employing the **BII-BCz (62)** host with $Ir(piq)_2(acac)$ emitter achieves a performance of 22.7% (15.8 cd A^{-1} and 16.5 lm W^{-1}).

Wang *et al.* reported an asymmetric host material, **DCz-BSeP (63)**, consisting of two carbazole units linked at the 3- and 6- positions of a benzo[4,5]selenopheno[2,3-*b*]pyridine acceptor core, where selenium incorporation was employed to investigate the external heavy-atom effect (EHAE) in OLED hosts.[130] For comparison, two analogous hosts were synthesized by replacing selenium with sulfur (**DCz-BTP (64)**) and oxygen (**DCz-BFP (65)**). Selenium incorporation enhanced spin-orbital coupling *via* the heavy-atom effect and increased the reverse intersystem crossing (RISC) rate by a factor of 3. This acceleration effectively reduces triplet exciton lifetimes, suppresses triplet-related quenching, and mitigates efficiency roll-off. Consequently, **DCz-BSeP (63)** exhibited superior bipolar charge-transport characteristics compared to the oxygen- and sulfur-based counterparts. Furthermore, the higher molecular polarizability imparted by the selenium atom promotes electronic coupling despite pronounced geometric distortion. Together with its intrinsically asymmetric D–A–D framework, **DCz-BSeP (63)** facilitates balanced carrier injection and transport, making it suitable for red-to-NIR emitters. All hosts exhibited high thermal stability (T_d: 380–425 °C; T_g: 135–143 °C), similar HOMOs/LUMOs (−5.7/−2.2 eV), and comparable S_1/T_1 energies (3.4/2.9 eV), confirming minimal perturbation of frontier orbitals upon selenium substitution. In TADF-sensitized red fluorescent OLEDs

employing DBP as the emitter, **DCz-BSeP (63)** achieved a maximum device performance of 21.0% and 28.3 lm W^{-1}, surpassing **DCz-BTP (64)** (15.4%, 24.7 lm W^{-1}) and **DCz-BFP (65)** (16.9%, 28.0 lm W^{-1}). These results demonstrate the effectiveness of selenium-induced EHAE in host molecular design.

Zhang *et al.* developed two asymmetric D–A–D host molecules featuring a quinazoline electron-accepting core with phenylcarbazole units attached at the 3-position.[131] **BCzQz (66)** contains two phenylcarbazole groups (T_d/T_g of 438/148 °C), where **CzTpQz (67)** replaces one phenylcarbazole with a bulky triphenylene-phenyl moiety, where the *meta*-linkage phenyl spacer induces a conjugation breaker, further enhancing thermal stability (T_d/T_g of 447/153 °C). DFT analysis indicates that the LUMO is primarily localized on the quinazoline core, and the HOMO on the carbazole unit, for both hosts. **BCzQz (66)** exhibits pronounced hole-transporting character due to its two carbazole units, while **CzTpQz (67)** displays more balanced charge transport due to the phenyl spacer, which disrupts conjugation between triphenylene and quinazoline, thereby modulating the electronic structure. Both materials possess a high T_1 level (2.40 and 2.36 eV), rendering them suitable for red PhOLEDs employing $Ir(mphmq)_2(acac)$ as the emitter. Devices based on **BCzQz (66)** and **CzTpQz (67)** achieved a maximum performance of 17.4% (17.4 cd A^{-1} and 15.7 lm W^{-1}) and 18.4% (17.6 cd A^{-1} and 19.3 lm W^{-1}), respectively. Their bipolar characteristics promote balanced carrier injection and high efficiency, with **CzTpQz (67)**-based devices exhibiting higher luminescence and reduced efficiency roll-off, suggesting improved charge balance under high operating voltages.

In our previous report, we designed and synthesized two bipolar host materials, **MS-OC (68)** and **MS-PC (69)**, incorporating spiro[fluorene-9,9′-phenanthrene-10′-one] as the acceptor and *ortho*- (**MS-OC (68)**) or *para*- (**MS-PC (69)**) phenylcarbazole as the donor units.[132] Both materials exhibit high thermal stability, with a T_d/T_g of 426/179 °C for **MS-OC (68)**, while **MS-PC (69)** has a T_d of 396 °C but no T_g observed. **MS-OC (68)** shows slightly higher S_1/T_1 at 3.31/2.66 eV, respectively, compared to **MS-PC (69)** with 3.14/2.55 eV, due to the disruption of π-conjugation between the acceptor and donor in **MS-OC (68)**. First, both materials were used as single hosts in red OLEDs with $Ir(piq)_2(acac)$ as the emitter, achieving efficiencies of 14.9% (8.7 cd A^{-1} and 10.5 lm W^{-1}) for **MS-OC (68)** and 14.4% (8.1 cd A^{-1} and 10.5 lm W^{-1}) for **MS-PC (69)**. To improve electron transport, the co-host CN-T2T was incorporated, leading to an enhanced device performance of 20.1% (12.0 cd A^{-1} and 16.6 lm W^{-1}) for **MS-OC (68)** and 18.8% (10.7 cd A^{-1} and 15.3 lm W^{-1}) for **MS-PC (69)**. These findings highlight that the *ortho*-substituted donor unit in **MS-OC (68)** provides superior performance compared to the *para*-substituted phenylcarbazole in the construction of efficient red OLED host materials.

Jia *et al.* developed a novel host material, **DCMP (70)**, featuring 4,5-dimethylpyridazine as the electron-accepting unit and two phenylcarbazole donor moieties.[133] The combination of the rigid carbazole framework with the methyl-substituted pyridazine induces a highly twisted molecular structure. The methyl substituents on the pyridazine increase steric hindrance, thereby suppressing ICT character and enhancing the T_1 level. **DCMP (70)** exhibits high thermal stability, with a T_d/T_g of 425/102 °C and a high T_1 value of 2.62 eV, making it suitable as a host for red PhOLEDs. DFT calculations confirm pronounced spatial separation of the frontier molecular orbitals, with the HOMO (−5.58 eV) localized on the carbazole unit and the LUMO (−2.11 eV) on the pyridazine core, highlighting the material's balanced bipolar carrier-transport characteristics. When employed as a host material for red PhOLEDs with $Ir(pq)_2(acac)$ as the emitter, **DCMP (70)** achieved a remarkable device performance of 20.0% (37.0 cd A^{-1} and 28.2 lm W^{-1}), demonstrating strong potential as an efficient host material for high-performance red PhOLED applications.

Yamada *et al.* reported the design and synthesis of a specialized bipolar host material, **9PhCz-BT-mCzPH (71)**, which incorporates a benzo[*c*][1,2,5]thiadiazole (BTD) acceptor and two isomeric phenylcarbazole donor units.[134] This material was specifically engineered to function as a narrow energy-gap host. With HOMO/LUMO energy levels of −6.05/−3.7 eV and a T_1 value of 2.2 eV, **9PhCz-BT-mCzPH (71)** exhibits favorable electronic properties for efficient energy transfer. When used as the host in NIR OLEDs, **9PhCz-BT-mCzPH (71)** effectively supports BBT-TPA, a NIR fluorescent emitter, along with TPA-PZTCN as a TADF co-dopant. The top-emissive (TE) of NIR OLED achieved an intense λ_{max} recorded at 930 nm with an EQE of 1.6%. This TE-type device demonstrated excellent operational stability, with the lifetime exceeding 300 hours without significant degradation. These results highlight the potential of **9PhCz-BT-mCzPH (71)** as an efficient narrow-energy-gap host material for TE-type NIR OLEDs, combining high performance with exceptional device stability.

Sun *et al.* designed and synthesized a novel host material, **S-CZ (72)**, which incorporates a 10,11-dihydro-5*H*-dibenzo[*b*,*f*]-azepine (AZ) motif and a carbazole donor moiety, connected to phenyl-pyridine acceptor units.[135] The study investigates the impact of the structure on the material's thermal and photophysical properties. **S-CZ (72)** exhibits high thermal stability, with T_d/T_g reaching 414/116 °C. The material also demonstrates favourable electronic characteristics, with a HOMO/LUMO of −5.4/−1.93 eV and high S_1/T_1 values of 3.48 eV and 2.80 eV, respectively. These properties make **S-CZ (72)** well-suited for use in red phosphorescent OLEDs. When used in conjunction with the red phosphorescent emitter $Ir(MDQ)_2(acac)$, the OLED device fabricated with **S-CZ (72)** achieved an exceptional device performance of 23.2% (34.0 cd A^{-1} and 33.5 lm W^{-1}). Notably, the device demonstrated a minimal efficiency roll-off of only 2.6% at 1000 cd m^{-2}, indicating that **S-CZ (72)** is a highly stable and efficient host material for red phosphorescent OLED applications.

Zheng *et al.* reported an asymmetrical bipolar host material, **2ICz-PPI (73)**, incorporating two fused indolo[3,2,1-*jk*]carbazole (ICz) donors and a phenanthro[9,10-*d*]imidazole (**PI**) acceptor.[108] The donor units were introduced at the 1- and 2-positions of the imidazole core, resulting in an asymmetrical architecture. Notably, **2ICz-PPI (73)** exhibits exceptional thermal stability with a T_d of 511 °C and no observable glass-transition temperature,

alongside a suitable HOMO/LUMO of −5.48/−2.37 eV and a high T_1 of 2.80 eV. Similar to the **ICz-PPI (40)** counterpart in the push–pull architecture (Fig. 5), **2ICz-PPI (73)** also exhibits weak ICT character, which is attributed to its rigid, highly twisted molecular structure. Furthermore, the incorporation of an additional ICz group in **2ICz-PPI (73)** enhances triplet energy but reduces PLQY, thereby directly contributing to lower device performance. These additional ICz substituents introduce stronger steric and electron-blocking effects on the PI acceptor, thereby weakening its electron-transport capability and disrupting charge balance. As a result, OLED devices employing $Ir(MDQ)_2(acac)$ as the emitter achieved a moderate performance of 17.1% (25.7 cd A^{-1} and 26.9 lm W^{-1}), reflecting slightly off-balance carrier transport properties compared to the corresponding **ICz-PPI (40)** host system.

Xie *et al.* developed three bipolar host materials—***p*-BPBCz (74)**, ***m*-BPBCz (75)**, and **BPCzB (76)**—based on positional isomers of phenylcarbazole donors combined with an isoquinoline acceptor.[136] All hosts exhibit excellent thermal stability, with a T_d of 529, 495, and 481 °C and a T_g of 143, 123, and 141 °C, respectively. The ***p*-BPBCz (74)** and ***m*-BPBCz (75)** isomers show similar HOMO/LUMO/T_1 energy levels (−5.65/−2.57/2.35 eV and −5.63/−2.56/2.47 eV), owing to their comparable molecular structures and π-conjugation along the *N*-linked carbazole–acceptor backbone. In contrast, **BPCzB (76)** exhibits a slightly shallower HOMO and higher LUMO (−5.57/−2.37/2.40 eV), attributed to its more extended π-conjugation. Benefiting from suitable energy alignment and high triplet energies, these materials function effectively as single hosts for red PhOLEDs using $Ir(pq)_2(acac)$ ($\lambda_{max} \approx$ 600 nm). Devices based on ***p*-BPBCz (74)**, ***m*-BPBCz (75)**, and **BPCzB (76)** achieved maximum EQEs of 15.0%, 17.2%, and 12.6%, with corresponding CEs of 26.31, 29.60, and 21.39 cd A^{-1} and PEs of 22.95, 22.58, and 19.75 lm W^{-1}.

In a subsequent study from the same group, Hu *et al.* designed a series of bipolar host materials—***p*-BCz (77)**, ***m*-BCz (78)**, and **CzB (79)**—based on three positional isomers of phenylcarbazole donors coupled with a quinoline acceptor.[137] All three materials exhibit excellent thermal stability, with a T_d of 476, 532, and 475 °C and a T_g of 97, 123, and 128 °C, for ***p*-BCz (77)**, ***m*-BCz (78)**, and **CzB (79)**, respectively. The ***p*-BCz (77)** and ***m*-BCz (78)** isomers show similar HOMO/LUMO/S_1/T_1 at −5.61/−2.64/3.25/2.35 and −5.62/−2.63/3.47/2.40 eV, respectively, which can be attributed to their comparable molecular structures and π-conjugation along the molecular backbone, with the carbazole units *N*-linked to the acceptor. In contrast, **CzB (79)** exhibits a HOMO/LUMO/S_1/T_1 of −5.57/−2.37/5.50/2.40 eV, reflecting the extended π-conjugation between the carbazole backbone and the molecular π-system. Owing to their appropriate energy levels, these materials are suitable as single-host systems for red phosphorescent OLEDs using $Ir(piq)_2(acac)$ as the dopant (λ_{max} = 624 nm). Devices based on ***p*-BCz (77)**, ***m*-BCz (78)**, and **CzB (79)** achieved maximum EQEs of 14.1%, 12.7%, and 10.3%, corresponding to CEs of 10.92, 9.19, and 7.68 cd A^{-1}, and PEs of 8.75, 5.31, and 3.87 lm W^{-1}, respectively. Together with related studies, these results highlight the significant isomeric effects of phenyl-carbazole donor units when paired with acceptors such as isoquinoline and quinoline, demonstrating how subtle structural variations strongly influence the thermal, electronic, and device performance of bipolar host materials.

Song *et al.* developed two asymmetrical bipolar host materials, **IP36Cz (80)** and **IP68Cz (81)**, by incorporating imidazo[1,2-*b*]-pyridazine (IP) as the electron-transporting unit and carbazole as the p-type donor.[87] The substitution sites of the IP core were systematically altered to optimize their photophysical and electrochemical properties. Both materials demonstrate excellent thermal stability, with T_d/T_g values of 427/156 °C and 473/158 °C, suitable HOMO/LUMO levels of −5.18/−2.51 eV and −5.34/−2.39 eV, and high T_1 values of 2.27 and 2.28 eV. These characteristics are well-suited for use in red phosphorescent OLEDs, with $Ir(pq)_2(acac)$ as the dopant. Device evaluation reveals that **IP36Cz (80)** achieves the second-lowest device performance of 16.2% (30.3 cd A^{-1} and 31.4 lm W^{-1}), while **IP68Cz (81)** achieves the second-highest efficiency of 25.2% (46.0 cd A^{-1} and 44.7 lm W^{-1}) compared to **IP6Cz (6)** (in Fig. 3) and **IP368Cz (41)** (in Fig. 6) discussed above in the section on push–pull architecture. Structural analysis indicates that carbazole substitution at the 3-position (present in **IP36Cz (80)** and **IP368Cz (41)**) effectively extends π-conjugation and introduces steric hindrance, thereby impairing electron transport and reducing energy transfer from the host to the emitter, as evidenced by residual host emission in the EL spectra. In contrast, substitution at the 6-position (present in **IP6Cz (6)** and **IP68Cz (81)**) provides optimal energy-level alignment, effectively suppressing excessive π-conjugation extension, thereby facilitating efficient energy transfer to the emitter. The study mentions that substitution at the 8-position has a minimal influence on the overall photophysical properties. Furthermore, **IP68Cz (81)** demonstrates excellent performance in deep-red OLEDs employing $Ir(piq)_2(acac)$. Overall, these findings emphasize the critical role of engineering substitution sites in the IP core in governing charge transport, energy transfer, and device efficiency.

Wang *et al.* reported two novel bipolar host materials, **2Cz-TAZ-2Cz (82)** and **3Cz-TAZ-3Cz (83)**, by introducing 1,2,4-triazole at the C2 and C3 positions of 9-phenylcarbazole, respectively.[138] These materials exhibit exceptional thermal stability, with T_d values of 457 °C and 432 °C, respectively. Notably, **3Cz-TAZ-3Cz (83)** displays a T_g value of 109 °C, while **2Cz-TAZ-2Cz (82)** remains stable without a detectable T_g. Leveraging their excellent thermal and photophysical properties, **2Cz-TAZ-2Cz (82)** and **3Cz-TAZ-3Cz (83)** were used as host materials in red phosphorescent OLEDs, with $Ir(piq)_2(acac)$ (λ_{max} = 626 nm) as the emitter. The **2Cz-TAZ-2Cz (82)**-based device achieved efficiencies of 16.6% (12.4 cd A^{-1} and 12.7 lm W^{-1}), while the **3Cz-TAZ-3Cz (83)**-based device reached a lower maximum performance of 11.4% (9.7 cd A^{-1} and 8.9 lm W^{-1}). The superior performance of host materials can be attributed to their improved bipolar charge transport, which enhances both the electron and hole mobilities in the device, leading to higher efficiency and stability.

Song *et al.* designed two novel bipolar host materials, ***o*-CzTP (84)** and ***m*-CzTP (85)**, by incorporating the electron-accepting

[1,2,4]triazolo[1,5-*a*]pyridine (TP) core at the 2- and 5-positions of mCP, respectively.[139] These materials, ***o*-CzTP (84)** and ***m*-CzTP (85)**, exhibit outstanding thermal stability, with a T_d of 417 °C and 432 °C, respectively. Interestingly, ***o*-CzTP (84)** displays a T_g of 130 °C, whereas ***m*-CzTP (85)** remains stable without a detectable T_g, which is attributed to the distinct molecular orientations of the TP units at different positions on the mCP donor backbone. Both ***o*-CzTP (84)** and ***m*-CzTP (85)** exhibit high triplet energies (2.93 and 2.92 eV, respectively) and well-aligned electronic energy levels (HOMO/LUMO: −5.38/−1.78 eV and −5.34/−1.78 eV, respectively), making them ideal candidates for red OLED applications. These favorable properties were harnessed in red OLED devices using $Ir(pq)_2(acac)$ (λ_{max} = 600 nm) as the emitter, achieving device performance of 15.8% (29.9 cd A^{-1} and 24.9 lm W^{-1}) for ***o*-CzTP (84)**, and a slightly improved performance of 17.2% (29.6 cd A^{-1} and 16.9 lm W^{-1}) for ***m*-CzTP (85)**. These results highlight the role of the TP core in enhancing the thermal and morphological stability of the materials, particularly in neat film form, thereby improving the operational stability and efficiency of red phosphorescent OLEDs.

Zhao *et al.* developed three novel benzimidazole-based host materials, ***o*-mCPBI (86)**, ***m*-mCPBI (87)**, and ***p*-mCPBI (88)**, by incorporating a benzimidazole unit into the mCP backbone at the *ortho*-, *meta*-, and *para*-positions of the *N*-phenyl group, respectively.[140] The different linkage positions led to significant variations in their properties. These hosts exhibit high thermal stability, with T_d values ranging from 411 °C to 417 °C and T_g values between 124 °C and 141 °C. Additionally, the hosts demonstrate well-matched electronic energy levels, with HOMO/LUMO values of −5.44/−1.86 eV for ***o*-mCPBI (86)**, −5.40/−1.84 eV for ***m*-mCPBI (87)**, and −5.44/−1.89 eV for ***p*-mCPBI (88)**. Notably, all three hosts have high T_1 values of 3.0 eV for ***o*-mCPBI (86)**, 2.80 eV for ***m*-mCPBI (87)**, and 2.71 eV for ***p*-mCPBI (88)**, making them ideal candidates for red OLED applications. These favorable properties were utilized in red OLED devices using $Ir(PPQ)_2(acac)$ as the emitter, achieving a maximum performance of 19.8% (24.5 cd A^{-1} and 21.4 lm W^{-1}) for ***o*-mCPBI (86)** and 18.7% (29.6 cd A^{-1} and 16.9 lm W^{-1}) for ***m*-mCPBI (87)**. In contrast, the ***p*-mCPBI (88)**-based device exhibited lower performance at 12.8% (15.1 cd A^{-1} and 15.8 lm W^{-1}). Compared with the commonly used mCP host, the introduction of the benzimidazole moiety into the new hosts resulted in higher T_g and more balanced charge fluxes, without reducing triplet energy levels for *ortho*- and *meta*-linkages.

In addition, a variety of asymmetrical D–D–A and D–A–A structured carbazole-based bipolar host materials are presented in Fig. 9, while Table 7 summarizes their corresponding materials' properties and OLED device performance characterization. Interestingly, both the D–D–A and D–A–A structural motifs maintain exceptionally high S_1 and deep LUMO levels, whereas their T_1 energy levels vary across structures due to the distinct influence of the respective acceptor moieties. Zhao *et al.* designed and synthesized two such materials, **DBTPC1 (89)** and **DBTPC2 (90)**, by employing different linkage strategies between the phenyl-carbazole donor and the 2-(dibenzo[*b*,*d*]thiophen-4-yl)pyridine acceptor.[141] Both **DBTPC1 (89)** and **DBTPC2 (90)** exhibit high thermal stability, with T_d ranging from 388 °C to 418 °C and T_g between 113 °C and 110 °C, and high T_1 of 2.93 eV and 2.92 eV, respectively. Additionally, the electronic energy levels of both hosts are well-aligned, with HOMO/LUMO values of −5.83/−2.67 eV for **DBTPC1 (89)** and −5.90/−2.64 eV for **DBTPC2 (90)**, making them highly suitable for red OLED applications. These energy levels enable the use of a single host system in the fabrication of red OLED devices with $Ir(piq)_2(acac)$. **DBTPC1 (89)** and **DBTPC2 (90)** demonstrate a maximum performance of 18.8% (13.2 cd A^{-1} and 13.8 lm W^{-1}) and 13.2% (10.9 cd A^{-1} and 7.8 lm W^{-1}), respectively. In **DBTPC2 (90)**, the HOMO is primarily localized on the carbazole-phenyl fragments, while the LUMO is mainly localized on the phenyl-pyridine-dibenzothiophene moiety. On the other hand, **DBTPC1 (89)**, where the phenyl-3-carbazolyl group is connected to 2-(dibenzo[*b*,*d*]thiophen-4-yl)pyridine, exhibits a more planar molecular structure, with the HOMO/LUMO levels distributed across the entire π-backbone of the carbazole-pyridine-dibenzothiophene architecture. This structural characteristic enhances the film-forming ability of **DBTPC1 (89)**, making it a more efficient host material compared to **DBTPC2 (90)**, as evidenced by its superior performance in OLED devices. Thus, **DBTPC1 (89)** emerges as the more favourable choice due to its better planar configuration and higher efficiency.

Patil *et al.* designed and synthesized two asymmetrical D–A–A host materials, **Cbz-Py-PQ (91)** and **Cbz-Py-SA (92)**, by integrating a carbazole donor through a pyridine auxiliary acceptor to a pyrroloquinoxaline (PQ) or benzothiadiazine 1,1-dioxide (SA) acceptor.[142] The unique 1 : 1 : 1 donor : auxiliary–acceptor : acceptor ratio improves the balance of hole and electron transport, enhancing the materials' bipolar character. Both materials exhibited high thermal stability, with T_d around 400 °C, while only the **Cbz-Py-SA (92)** material had a T_g of 90 °C. **Cbz-Py-PQ (91)** and **Cbz-Py-SA (92)** exhibit deep HOMO levels (−5.66 eV and −5.69 eV), favorable LUMO levels (−3.22 eV and −3.20 eV), and high triplet energies (2.34 eV and 2.44 eV), rendering them suitable for red phosphorescent OLED applications. In OLED device testing with $Ir(piq)_2(acac)$ as the emitter, **Cbz-Py-PQ (91)** achieved a maximum EQE of 13.0%, while **Cbz-Py-SA (92)** reached 6.4%. When $BeBq_2$ was added to the auxiliary emission layer to enhance electron transport, the **Cbz-Py-PQ (91)** device showed improved performance (EQE of 16.4%). However, **Cbz-Py-SA (92)** showed no improvement, likely due to the presence of a free N–H group, which hindered electron transport.

Mao *et al.* developed a series of asymmetrical host materials, **DCzPBI (93)** and **POCzPBI (94)**, constructed by introducing two carbazole donors at the 1- and 2-positions of a benzimidazole acceptor in **DCzPBI (93)**, and by incorporating triphenylphosphine oxide at the 1-position and carbazole at the 2-position of the benzimidazole core in **POCzPBI (94)**.[143] Both materials exhibit excellent thermal stability, with a T_d/T_g of 451/120 °C for **DCzPBI (93)** and 436/127 °C for **POCzPBI (94)**, along with a high T_1 of 2.60 eV and 2.59 eV, respectively. Theoretical

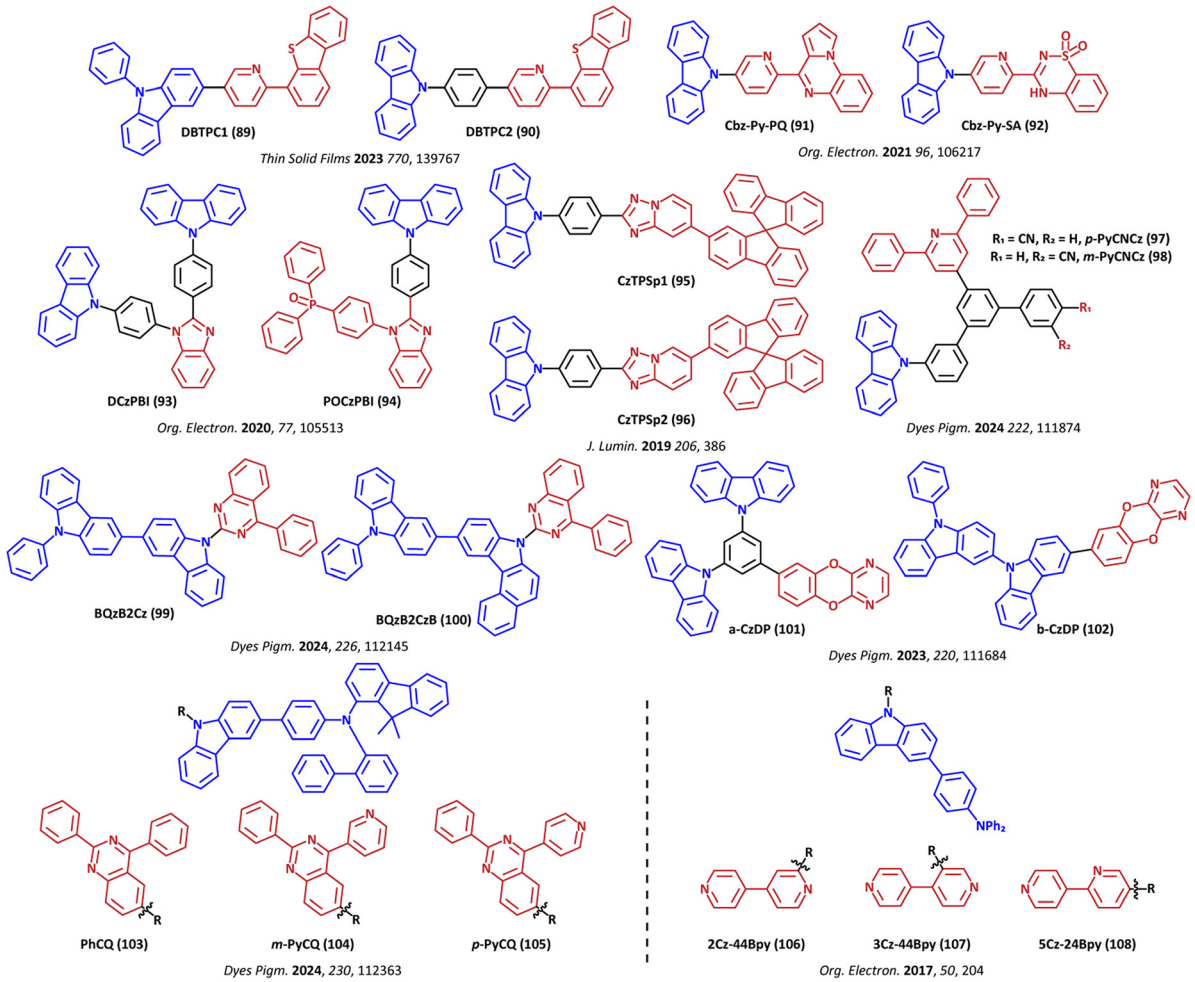

Fig. 9 Chemical structures of carbazole-based host materials employing an asymmetric architecture for red-to-NIR OLEDs, grouped according to asymmetric D–D–A and D–A–A structural motifs. (The highlighted colors correspond to blue for the carbazole donor, red for the acceptor moieties, and black for the π-bridge linkers).

calculations reveal that the LUMO is localized on the benzimidazole, while the HOMO is distributed over the benzimidazole and carbazole moieties, giving a comparable HOMO/LUMO of −5.38/−2.06 eV for **DCzPBI (93)** and −5.37/−2.08 eV for **POCzPBI (94)**. Notably, incorporation of the triphenylphosphine oxide group enhances the electron affinity of **POCzPBI (94)**, resulting in improved electron-transport capability and more balanced charge transport. When used as the host material with Ir(piq)$_2$(acac) as the emitter, **POCzPBI (94)** delivered higher device performance of 10.4% (15.4 cd A^{-1} and 13.8 lm W^{-1}).

Song *et al.* synthesized two asymmetric bipolar host materials, **CzTPSp1 (95)** and **CzTPSp2 (96)**, by incorporating carbazole as a hole-transporting unit and [1,2,4]triazolo[1,5-*a*]pyridine (TP) as an electron-transporting unit.[144] The key difference between the two materials is the position of spirobifluorene fragments attached to the TP core: the *para*-position in **CzTPSp1 (95)** and the *meta*-position in **CzTPSp2 (96)**. These materials exhibit excellent thermal stability, with T_d between 418 °C and 451 °C. **CzTPSp1 (95)** has a T_g of 130 °C, while **CzTPSp2 (96)** shows a higher T_d and no T_g due to the positional difference in the spirobifluorene substitution. **CzTPSp1 (95)** and **CzTPSp2 (96)** exhibit favorable HOMO/LUMO energy levels (−5.38/−2.12 and −5.31/−2.01 eV, respectively) along with high S_1/T_1 energies (3.26/2.43 and 3.30/2.47 eV, respectively). OLED devices using these hosts and Ir(pq)$_2$(acac) as the emitter achieved a high performance of 23.0% (39.2 cd A^{-1} and 26.4 lm W^{-1}) and 22.1% (38.6 cd A^{-1} and 38.5 lm W^{-1}). The devices also showed minimal efficiency roll-off, with EQE values of 22.0% and 21.6% at 1000 cd m^{-2}, and roll-off values of just 4.3% and 2.2%. These results highlight the effectiveness of spirobifluorene decoration in reducing π-interaction, enabling efficient host–guest interactions, and leading to high efficiency with reduced roll-off at high luminance.

Zhang *et al.* synthesized two asymmetric bipolar host materials, ***p*-PyCNCz (97)** and ***m*-PyCNCz (98)**, by incorporating phenyl carbazole as a donor, benzonitrile as the acceptor, and 2,6-diphenylpyridine as an auxiliary acceptor unit.[145] The key difference between the two hosts lies in the position of the electron-withdrawing nitrile (CN) group on the biphenyl core:

Table 7 Summary of materials' properties and OLED device performance parameters for the compounds depicted in Fig. 9

Material		Material characterization			OLED characterization					
		T_d/T_g [°C]	HOMO/LUMO [eV]	S_1/T_1 [eV]	EML type	Emitter	λ_{max} [nm]	EQE/CE/PE [%, cd A^{-1}, lm W^{-1}]	CIE [x, y]	Ref.
89	**DBTPC1**	388/113	−5.83/−2.67	3.16/2.63	Single	$Ir(piq)_2(acac)$	628	18.8/13.2/13.8	0.68, 0.32	141
90	**DBTPC2**	418/110	−5.90/−2.64	3.26/2.63				13.2/10.9/7.8		
91	**Cbz-Py-PQ**	404/—	−5.66/−3.22	2.44/2.34	Single	$Ir(piq)_2(acac)$	—	13.0/7.7/7.4	0.68, 0.32	142
					Co-host			16.4/9.6/9.4	0.69, 0.31	
92	**Cbz-Py-SA**	401/90	−5.69/−3.20	2.49/2.44	Single			6.4/4.4/5.8	0.68, 0.32	
					Co-host			6.5/4.4/5.8		
93	**DCzPBI**	451/120	−5.38/−2.06	3.32/2.60	Single	$Ir(MDQ)_2(acac)$	—	6.2/9.2/8.2	—	143
94	**POCzPBI**	436/127	−5.37/−2.08	3.29/2.59				10.4/15.4/13.8		
95	**CzTPSp1**	418/130	−5.38/−2.12	3.26/2.43	Single	$Ir(pq)_2(acac)$	601	23.0/39.2/26.4	0.62, 0.38	144
96	**CzTPSp2**	451/—	−5.31/−2.01	3.30/2.47				22.1/38.6/38.5		
97	***p*-PyCNCz**	489/135	−5.71/−2.47	3.44/2.75	Single	$Ir(piq)_2(acac)$	624	16.1/14.5/16.3	0.67, 0.31	145
98	***m*-PyCNCz**	493/127	−5.72/−2.45	3.47/2.84				25.3/22.2/24.4		
99	**BQzB2Cz**	422/132	−5.41/−2.17	3.24/2.55	Single	$Ir(piq)_2(acac)$	624	25.1/21.5/24.1	0.68, 0.31	146
100	**BQzB2CzB**	452/144	−5.42/−2.17	3.23/2.55				25.1/21.6/24.2		
101	**a-CzDP**	440/155	−5.31/−1.77	3.54/2.57	Single	$Ir(piq)_2(acac)$	624	10.3/8.2/4.6	0.67, 0.33	147
102	**b-CzDP**	403/147	−5.39/−2.03	3.36/2.55				13.8/9.7/7.27		
103	**PhCQ**	—/—	−5.44/−2.24	2.61/2.46	Single (bottom)	RD-1	624	20.0/20.2/24.01	0.68, 0.32	148
					Single (top)			37.2/49.5/56.01		
104	***m*-PyCQ**	—/—	−5.41/−2.29	2.53/2.36	Single (bottom)			20.0/19.9/23.6		
					Single (top)			34.8/43.9/47.2		
105	***p*-PyCQ**	—/—	−5.40/−2.28	2.34/2.21	Single (bottom)			20.2/17.9/22.02		
					Single (top)			31.8/47.4/43.9		
106	**2Cz-44Bpy**	420/108	−5.48/−2.45	—/2.43	Single	$(Mpq)_2Ir(acac)$	—	17.8/17.9/22.5	0.65, 0.34	149
107	**3Cz-44Bpy**	324/—	−5.49/−2.41	—/2.46				16.8/16.4/17.6		
108	**5Cz-24Bpy**	425/110	−5.47/−2.38	—/2.45				9.0/8.6/12.3		

the *para*-position in ***p*-PyCNCz (97)** and the *meta*-position in ***m*-PyCNCz (98)**. Both materials exhibit excellent thermal stability, with T_d ranging from 489 °C to 493 °C, and a T_g of 135 °C for ***p*-PyCNCz (97)** and 127 °C for ***m*-PyCNCz (98)**. Compared to ***p*-PyCNCz (97)** (λ_{max} = 443 nm), ***m*-PyCNCz (98)** exhibits a narrower and blue-shifted emission maximum at λ_{max} = 429 nm, which is attributed to the weaker conjugation between the biphenyl core and the phenyl carbazole unit in ***m*-PyCNCz (98)**. ***p*-PyCNCz (97)** and ***m*-PyCNCz (98)** exhibit favorable HOMO/LUMO energy levels (−5.71/−2.47 eV and −5.72/−2.45 eV), along with high S_1/T_1 energies (3.44/2.75 eV and 3.47/2.84 eV). OLED devices using ***p*-PyCNCz (97)** as the host and $Ir(piq)_2(acac)$ as the emitter achieved a maximum performance of 16.09% (14.51 cd A^{-1} and 16.28 lm W^{-1}), while ***m*-PyCNCz (98)** showed a significantly improved performance of 25.32% (22.2 cd A^{-1} and 24.38 lm W^{-1}). The improved performance of ***m*-PyCNCz (98)** is attributed to enhanced molecular interactions and more balanced charge transport, highlighting that the position of the CN group significantly influences both molecular properties and OLED performance.

Zhang *et al.* reported two asymmetric bipolar host materials by incorporating 4-phenylquinazoline as an acceptor and either 9-phenyl-9*H*,9′*H*-3,3′-bicarbazole (**BQzB2Cz (99)**) or 10-(9-phenyl-9*H*-carbazol-3-yl)-7H-benzo[*c*]carbazole (**BQzB2CzB (100)**) as the donor units.[146] **BQzB2Cz (99)** and **BQzB2CzB (100)** exhibit excellent thermal stability (T_d/T_g = 422/132 °C and 452/144 °C, respectively) and HOMO/LUMO energy levels well-suited for red OLED applications (−5.41/−2.17 eV and −5.42/−2.17 eV, respectively). Both materials have similar S_1/T_1 values (3.23/2.55 eV and 3.24/2.55 eV, respectively) due to the usage of the same acceptor and similar carbazole-based donor fragments. OLED devices based on **BQzB2Cz (99)** and **BQzB2CzB (100)**, using $Ir(piq)_2(acac)$ as the emitter, showed comparable performance, with a maximum EQE of around 25.10%, a CE of approximately 21.5 cd A^{-1}, and a PE of about 24.3 lm W^{-1}. These results demonstrate that both host materials exhibit similar charge transfer properties and frontier molecular orbital energy levels, contributing to high device efficiency. Notably, replacing carbazole with benzocarbazole in **BQzB2CzB (100)** offers improved stability at high luminance.

Chen *et al.* designed and synthesized two asymmetric bipolar host materials, employing dioxy[2,3-*b*]pyrazine as the electron-accepting unit, with mCP (**a-CzDp (101)**) or 9-phenyl-9*H*-3,9′-bicarbazole (**b-CzDp (102)**) as the donor unit.[147] Both materials exhibit excellent thermal stability, with a T_d/T_g of 440/155 °C for **a-CzDp (101)** and 403/147 °C for **b-CzDp (102)**, along with a high T_1 of 2.57 eV and 2.55 eV, respectively. The DFT reveals that the HOMO is primarily localized on the carbazole moieties, while the LUMO is distributed over the pyrazine-dioxane acceptor unit. For **a-CzDp (101)**, the HOMO/LUMO are −5.31/−1.77 eV, whereas **b-CzDp (102)** shows more pronounced spatial separation of the frontier orbitals (−5.39/−2.03 eV) due to weaker conjugation arising from the increased D–A distance. In red OLED devices employing $Ir(piq)_2(acac)$ as the emitter, **a-CzDp (101)** delivered a maximum performance of 10.32% (8.23 cd A^{-1} and 4.63 lm W^{-1}), while **b-CzDp (102)** achieved an improved performance of 13.82% (9.69 cd A^{-1} and 7.27 lm W^{-1}). The superior performance of **b-CzDp (102)** is attributed to its more balanced charge transport, as confirmed by mobility measurements, which is associated with its distinct

structural configuration that reduces D–A conjugation and promotes broader LUMO distribution compared to **a-CzDp (101)**.

Zang *et al.* introduced a series of TADF host materials by incorporating triphenylamine-substituted carbazole as the donor and quinazoline as the acceptor.[148] The acceptor fragment was modified by introducing a pyridyl ring instead of a benzene ring, with different junction sites—**PhCQ (103)**, ***m*-PyCQ (104)**, and ***p*-PyCQ (105)**—to tune the electron-withdrawing properties and optimize the HOMO/LUMO separation. This modification resulted in a small ΔE_{ST} and efficient RISC. The TADF hosts exhibit well-matched electronic energy levels, with a HOMO/LUMO/S_1/T_1 of −5.31/−2.24/2.61/2.46 eV for **PhCQ (103)**, −5.41/−2.29/2.53/2.36 eV for ***m*-PyCQ (104)**, and −5.40/−2.28/2.34/2.21 eV for ***p*-PyCQ (105)**. The RISC rates for **PhCQ (103)**, ***m*-PyCQ (104)**, and ***p*-PyCQ (105)** were 4.2×10^5, 5.0×10^5, and 3.1×10^5 s^{-1}, respectively, making them ideal candidates for red OLED applications. In OLED devices using RD-1 as the phosphorescent emitter, the **PhCQ (103)**, ***m*-PyCQ (104)**, and ***p*-PyCQ (105)**-based bottom-emission red PhOLED devices achieved maximum performance of 20.0% (20.22 cd A^{-1} and 24.01 lm W^{-1}), 20.0% (19.92 cd A^{-1} and 23.61 lm W^{-1}), and 20.2% (17.95 cd A^{-1} and 22.02 lm W^{-1}), respectively. Top-emission devices with these hosts achieved an exceptional performance of 37.2% (49.54 cd A^{-1} and 56.01 lm W^{-1}), 34.8% (43.96 cd A^{-1} and 47.22 lm W^{-1}), and 31.8% (47.44 cd A^{-1} and 43.89 lm W^{-1}), respectively. Compared with commonly used fluorescent host materials, TADF-based hosts exhibit excellent performance due to efficient charge transfer and the matching of frontier molecular orbitals with red emitters. The **PhCQ (103)**-based OLED device exhibited the best performance, owing to its high FRET efficiency (99.782%) and rapid RISC rate, highlighting the potential of these TADF hosts for high-performance red OLEDs.

In the last section on asymmetric structure host materials, Chatterjee *et al.* designed and synthesized a series of hosts comprising triphenylamine-decorated carbazole as the donor and 4,4′-bipyridine (44Bpy) and 2,4-bipyridine (24Bpy) as the acceptors.[149] The materials were classified based on the position of carbazole substitution: at the 2-position (**2Cz-44Bpy (106)**), 3-position (**3Cz-44Bpy (107)**) of 4,4′-bipyridine, and 5-position (**5Cz-24Bpy (108)**) of 2,4-bipyridine. All three hosts exhibit excellent thermal stability (T_d = 324–425 °C), high T_1 values (2.21–2.46 eV), and well-matched electronic energy levels (HOMO/LUMO = −5.48/−2.45 eV for **2Cz-44Bpy (106)**, −5.49/−2.41 eV for **3Cz-44Bpy (107)**, and −5.47/−2.38 eV for **5Cz-24Bpy (108)**). **2Cz-44Bpy (106)** and **5Cz-24Bpy (108)** show a T_g of 108 °C and 110 °C, respectively, while **3Cz-44Bpy (107)** does not show T_g. Red PhOLED devices using **2Cz-44Bpy (106)**, **3Cz-44Bpy (107)**, and **5Cz-24Bpy (108)** as hosts and $(Mpq)_2Ir(acac)$ as the emitter in a single-host system achieved a performance of 17.8% (17.9 cd A^{-1} and 22.5 lm W^{-1}), 16.8% (16.4 cd A^{-1} and 17.6 lm W^{-1}), and 9.0% (8.6 cd A^{-1} and 12.3 lm W^{-1}), respectively. The devices hosted by **5Cz-24Bpy (108)** performed the poorest, likely due to lower carrier mobility compared to the other two materials.

3.4. Special architecture: molecular design strategies for high triplet energy and exciton-confinement host systems

Special architecture classified here refers to the distinct host-material design of carbazole-based molecules that deviates from the classical push–pull architecture, focusing instead on donor–donor (D–D) or multi-donor configurations. These frameworks typically pair a carbazole moiety with other donor moieties without incorporating intrinsic acceptor units, resulting in hole-transport architectures with minimal internal ICT character.[150–152] By avoiding strong acceptors, these materials retain elevated triplet energies, suppress back-energy transfer from long-wavelength emitters, and reduce the likelihood of non-radiative decay pathways. Their electronic structure promotes localized excited states, supports efficient hole mobility through a well-distributed HOMO framework, and mitigates EPQ under high current densities. Furthermore, the absence of a strong acceptor moiety often results in enhanced morphological stability, particularly in architectures incorporating rigidified or spiro-configurations that inhibit intermolecular π–π stacking. While these attributes are highly valuable for preserving the high T_1 required for blue hosts, they are equally strategic for the red-to-NIR regime where a host must provide robust hole transport without interfering with the emitter's exciton distribution.

However, because these D–D architectures consist of pure donor moieties, they inherently lack electron-transporting character, which can lead to an imbalanced charge transport. To address this, the introduction of acceptor-type–either using ETL or co-host materials–is necessary to improve carrier balance and broaden the recombination zone.[153] In this context, co-host or exciplex-forming systems composed of donor and suitable acceptor-type molecules have demonstrated superior device performance compared to single-host systems, as they facilitate balanced charge injection and transport while maintaining high triplet energy and efficient exciton confinement.[35,154] These attributes are particularly valuable for red-to-NIR OLEDs, where balanced carrier transport and exciton management are critical for achieving high-efficiency devices. Recent studies consistently demonstrate that devices utilizing a co-host/exciplex system outperform those employing a single D–D host, as they combine the high triplet stability of the D–D scaffold with the efficient charge-recombination kinetics required for high-performance red-to-NIR OLEDs. Fig. 10 illustrates carbazole-based host materials employing special architectures for red-to-NIR OLEDs, organized by the D–D structural motif, where Table 8 summarizes the corresponding material properties and OLED device performance characterization. As expected, the donor-only framework exhibits S_1 and T_1 energy levels that are notably higher than those of the other architectures discussed above, consistent with the absence of acceptor moieties in this configuration.

Bezvikonnyi *et al.* designed and synthesized a host material, **BiCzSiPh3 (109)**, by attaching triphenylsilyl moieties to the 9,9′-positions of 3,3′-bicarbazole.[110] Thermal and photophysical studies showed that **BiCzSiPh3 (109)** has excellent thermal stability, with a T_d/T_g of 372/149 °C, respectively. The material

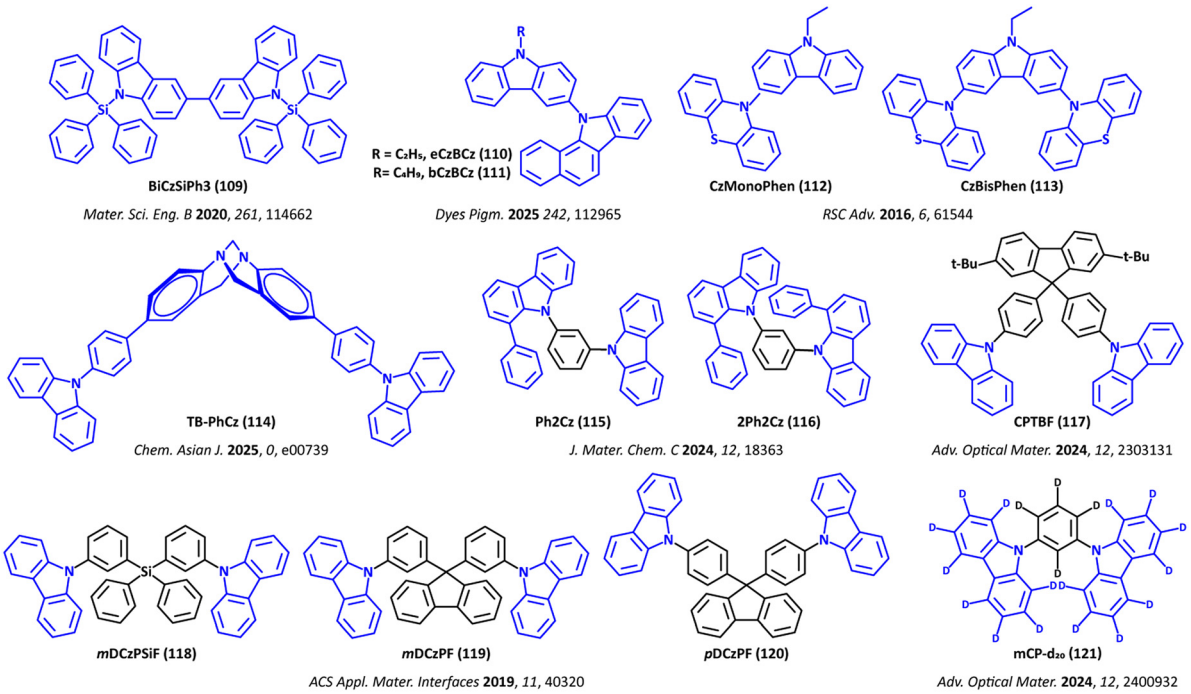

Fig. 10 Chemical structure of carbazole-based host materials employing a special architecture for red-to-NIR OLEDs, grouped according to the D–D structural motif. (The highlighted colors correspond to blue for carbazole donors, red for the acceptor moieties, and black for the π-bridge linkers.)

Table 8 Summary of materials' properties and OLED device performance parameters for the compounds depicted in Fig. 10

		Material characterization			OLED characterization					
Material		T_d/T_g [°C]	HOMO/LUMO [eV]	S_1/T_1 [eV]	EML type	Emitter	λ_{max} nm]	EQE/CE/PE [%, cd A^{-1}, lm W^{-1}]	CIE [x, y]	Ref.
109	**BiCzSiPh3**	372/149	−5.43/−2.13	3.34/2.91	Single	$Ir(piq)_2(acac)$	—	7.7/5.4/3.5	—	110
110	**eCzBCz**	344/107	−5.79/−2.27	3.47/2.53	Single	$Ir(piq)_2(acac)$	631	16.8/10.8/12.1	0.69, 0.31	77
					Co-host			20.7/12.9/18.0	0.68, 0.32	
111	**bCzBCz**	350/80	−5.79/−2.27	3.47/2.50	Single		628	9.2/6.4/8.4	0.68, 0.31	
					Co-host		634	21.2/11.9/15.8	0.69, 0.30	
112	**CzMonoPhen**	327/—	−4.85/−1.45	3.09/2.60	Single	$Ir(piq)_2(acac)$	—	10.5/37.4/29.6	0.68, 0.31	155
113	**CzBisPhen**	419/—	−4.86/−1.55	3.03/2.61				7.2/28.2/40.6		
114	**TB-PhCz**	358/—	−5.17/−1.76	3.41/2.68	Single	$Ir(piq)_2(acac)$	628	6.1/4.0/5.3	0.68, 0.32	156
					Exciplex		631	9.2/5.5/7.4	0.68, 0.31	
115	**Ph2Cz**	339/90	−5.68/−2.19	3.49/3.06	Exciplex	NZDFT	619	10.8/15.7/17.6	0.60, 0.39	157
116	**2Ph2Cz**	353/—	−5.68/−2.24	3.44/3.00				11.3/16.4/17.6		
117	**CPTBF**	—/—	—/—	—/—	Exciplex (*p*-CN)	DCzPBBT	736	6.85/—/—	—	158
					Exciplex (m-CN)		740	8.45/—/—		
118	***m*DCzPSiF**	—/—	−5.75/−2.16	—/3.03	Single	PtN3N-ptb	—	8.6/—/—	0.62, 0.38	50
119	***m*DCzPF**	450/—	−5.38/−1.80	—/2.88				9.4/—/—	0.63, 0.37	
120	***p*DCzPF**	480/—	−5.32/−1.82					9.5/—/—		
121	***m*CP-d20**	—/—	—/—	—/—	Co-host	BBT-TPA-d28	899	2.3/—/—	—	159

has well-matched electronic energy levels, with a HOMO/LUMO of −5.43/−2.13 eV and a high T_1 of 2.91 eV. A similar case with **BiCzTos (44)** (in Fig. 6) in a push–pull architecture, **BiCzSiPh3 (109)** features high triplet energy and good thermal stability. Still, this host suffers from inefficient charge transport, resulting in inferior red PhOLED performance. Red OLED devices using $Ir(piq)_2(acac)$ as the red PhOLED emitter achieved a device performance of 7.7% (5.4 cd A^{-1} and 3.5 lm W^{-1}). This low performance is likely due to lower carrier mobility in **BiCzSiPh3 (109)**.

Tavgeniene *et al.* synthesized carbazole-benzo[*a*]carbazole-based compounds with controlled alkyl substitution as hole-transporting hosts.[77] These materials, featuring ethyl (**eCzBCz (110)**) and butyl (**bCzBCz (111)**) side chains, exhibited good thermal stability ($T_d \approx 350$ °C) and the ability to form stable, amorphous layers. Notably, **eCzBCz (110)** and **bCzBCz (111)** demonstrated high T_g values of 107 °C and 80 °C, respectively. The HOMO/LUMO of both materials are well-suited for red OLED applications, with values of −5.79/−2.27 eV for both

eCzBCz (110) and **bCzBCz (111)** and favourable T_1 values of 2.53 eV and 2.50 eV, respectively. Red PhOLEDs using $Ir(piq)_2$-(acac) as the emitter on **eCzBCz (110)** achieved an efficiency of 16.8% (10.8 cd A^{-1} and 12.1 lm W^{-1}), while **bCzBCz (111)** showed a performance of 9.2% (6.4 cd A^{-1} and 8.4 lm W^{-1}). These performances were attributed to their strong hole-transport properties but relatively weak electron-transport capabilities. To enhance electron transport, a co-host system incorporating CN-T2T with **eCzBCz (110)** and **bCzBCz (111)** was explored. This approach resulted in significant performance improvements, with a performance of 20.7% (12.9 cd A^{-1} and 18.0 lm W^{-1}) and 21.2% (11.9 cd A^{-1} and 15.8 lm W^{-1}), respectively. The addition of alkyl chains to improve film-forming properties led to better charge balance, higher efficiency, and reduced efficiency roll-off.

Bagdziunas *et al.* introduced two novel host materials, **CzMonoPhen (112)** (D–D) and **CzBisPhen (113)** (D–D–D), incorporating carbazole as the donor and phenothiazine as the second donor.[155] Both materials exhibited excellent thermal stability, with a T_d of 327 °C and 419 °C for **CzMonoPhen (112)** and **CzBisPhen (113)**, respectively, and no observable glass transition. All host materials exhibit well-suited HOMO/LUMO (−4.85/−1.45 eV and −4.86/−1.55 eV) and favourable T_1 values (2.60 eV and 2.61 eV), making them ideal candidates for red OLEDs using $Ir(piq)_2$(acac) as the emitter. OLED devices based on **CzMonoPhen (112)** achieved impressive performance, with a maximum efficiency of 10.5% (37.4 cd A^{-1} and 29.6 lm W^{-1}), while **CzBisPhen (113)** exhibited 7.2% (28.2 cd A^{-1} and 40.6 lm W^{-1}). However, the observed efficiency roll-off and relatively low performance were attributed to quenching processes, such as TTA and TPQ, which are linked to inefficient electron transfer within the host materials.

Our group introduced a series of materials incorporating Tröger's base (TB) and phenyl carbazole (PhCz) isomers, with **TB-PhCz (114)** specifically employed as a host material for the red-emitting $Ir(piq)_2$(acac) emitter.[156] Notably, this host material demonstrated good thermal stability, with a T_d of 358 °C and no observable T_g, making it a promising candidate for OLED applications. The HOMO/LUMO were measured at −5.17/−1.76 eV, and the S_1/T_1 were found to be 3.41/2.68 eV. The **TB-PhCz (114)**:CNT2T (1:1) co-host system demonstrated a favourable S_1/T_1 of 3.03/2.66 eV, respectively. This co-host system exhibited typical exciplex behaviour, with both prompt and delayed fluorescence emissions. **TB-PhCz (114)** achieved promising results, with a maximum performance of 6.1% (4.0 cd A^{-1} and 5.3 lm W^{-1}) where the **TB-PhCz (114)**:CNT2T (1:1) co-host system led to a significantly improved performance of 9.2% (5.5 cd A^{-1} and 7.4 lm W^{-1}). This study underscores the advantage of using co-host systems, as they notably enhance OLED performance by optimizing carrier transport and exciton confinement. The co-host device exhibited a remarkable 50% increase in EQE compared to the single-host device, reaching 9.2%. This improvement confirms that the co-host configuration provides more balanced carrier transport and efficient energy transfer.

Yi *et al.* synthesized two novel carbazole-based donor materials, **Ph2Cz (115)** and **2Ph2Cz (116)**, which were derived from mCP by introducing a phenyl group at the 1-position of the carbazole in mCP.[157] These donor materials were then blended with a triazine-centered acceptor (PO-T2T) to facilitate exciplex formation and explore their potential application as exciplex hosts in deep red-fluorescent OLEDs with NZDFT (λ_{max} = 619 nm) as the emitter. The material demonstrated high thermal stability, with a T_d/T_g of 339/90 °C for **Ph2Cz (115)**, while **2Ph2Cz (116)** showed a T_d of 353 °C with no observable T_g. Single-crystal studies of both materials revealed that the phenyl groups were oriented perpendicular to the central phenyl ring, disrupting molecular planarity in the Cz-Ph-Cz plane and confirming significant structural distortion. The HOMO/LUMO of **Ph2Cz (115)** were −5.68/−2.19 eV, respectively, while **2Ph2Cz (16)** exhibited slightly more negative LUMO levels (−5.68/−2.24 eV). Both compounds exhibited favourable T_1 values of 3.06 eV (for **Ph2Cz (115)**) and 3.00 eV (for **2Ph2Cz (116)**). OLED devices incorporating the exciplex-host system **Ph2Cz (115)**:PO-T2T achieved a performance of 10.78% (15.72 cd A^{-1} and 17.64 lm W^{-1}), where **2Ph2Cz (116)**:PO-T2T achieved a slightly enhanced performance of 11.30% (16.40 cd A^{-1} and 17.64 lm W^{-1}).

Chen *et al.* demonstrated a carbazole-based donor molecule, **CPTBF (117)**, and two dicyanopyrazine-based acceptor molecules, *m*-CN and *p*-CN, to explore exciplex formation.[158] While no thermal or electrochemical properties had been reported for the individual molecules, the photophysical properties of the blended exciplexes were thoroughly characterized. The blends of **CPTBF (117)** with *m*-CN and *p*-CN exhibited distinctive, red-shifted emission spectra and showed delayed fluorescence in time-resolved measurements, demonstrating the TADF characteristics. This unique behavior makes these blends promising candidates for high-efficiency OLEDs. In terms of device performance, the **CPTBF (117)**:*m*-CN blend achieved an EQE of 5.22% with λ_{max} at 607 nm. In contrast, the **CPTBF (117)**:*p*-CN blend showed an EQE of 2.05% with a longer λ_{max} at 625 nm. From the onset of the phosphorescence spectra, the corresponding T_1 values were calculated to be 2.61 eV for **CPTBF (117)**:*m*-CN and 2.57 eV for **CPTBF (117)**:*p*-CN, further supporting the feasibility of using these exciplexes in OLED devices. The exciplex emitter blends were further explored in deep red to NIR OLEDs by incorporating the NIR fluorescent emitter DCzPBBT, which has an emission maximum at 816 nm. Devices where the EML consisted of **CPTBF (117)**:*m*-CN blended with 1 wt% DCzPBBT achieved a high EQE of 8.45% with a λ_{max} of 758 nm. Similarly, the **CPTBF (117)**:*p*-CN blend with 1 wt% DCzPBBT achieved a solid EQE of 6.85%, with a λ_{max} at 736 nm. Further increasing the doping concentration of DCzPBBT to 10 wt% led to a bathochromic shift in the EL spectrum to 772 nm, covering 94% of the NIR region (>700 nm). While the EQE decreased slightly to 4.06%, the device's performance remained robust.

Li *et al.* reported three carbazole-based host materials featuring a fluorene core: reference M-type (***m*DCzPSiF (118)**), M-type (***m*DCzPF (119)**), and V-type (***p*DCzPF (120)**).[50] Both ***m*DCzPF (119)** and ***p*DCzPF (120)** demonstrated excellent thermal stability, with T_d values of 450 °C and 480 °C, respectively,

and no observable T_g, making them promising candidates for OLED applications. The three host materials displayed HOMO/LUMO/T_1 values of −5.75/−2.16/3.03 eV for ***m*DCzPSiF (118)**, −5.38/−1.80/2.88 eV for ***m*DCzPF (119)**, and −5.32/−1.82/2.88 eV for ***p*DCzPF (120)**. OLED devices using ***m*DCzPSiF (118)**, ***m*DCzPF (119)**, and ***p*DCzPF (120)** as hosts and PtN3N-ptb as the emitter in a single-host configuration achieved an EQE of 8.6%, 9.4%, and 9.5%, respectively. Interestingly, the red phosphorescent OLED utilizing the "M"-type ***m*DCzPF (119)** as the host showed a remarkable 10-fold improvement in operational lifetime compared to the "V"-type ***p*DCzPF (120)**-based OLED.

Yu *et al.* explored the impact of deuteration on the NIR photoluminescence (PL) and EL properties of both host and guest materials, revealing significant performance enhancements.[159] Two deuterated compounds were synthesized, the host material **mCP-d_{20} (121)** and the NIR emitter BBT-TPA-d_{28}. Incorporation of deuterium into both materials improved their photophysical characteristics, particularly in electroluminescent devices. The co-deposited thin film with 1 wt% of BBT-TPA-d_{28} and **mCP-d_{20} (121)** exhibited a remarkable PLQY of 15 ± 2%, with a peak emission at ∼900 nm, representing an approximately three times increase compared to the undeuterated counterpart. Crucially, deuteration of only one component—either the host or the guest—did not achieve this level of enhancement, indicating that the combined deuteration of both materials is essential for suppressing nonradiative decay and enhancing radiative efficiency. The deuterated co-deposited film as the EML achieved an EQE of 2.3 ± 0.2% at ∼900 nm, significantly outperforming conventional undeuterated OLEDs. Furthermore, the use of **mCP-d_{20} (121)** as the host for a 10 wt% TPA-PZTCN emitter resulted in an increased PLQY of 46 ± 2%, compared to 39 ± 2% in the undeuterated mCP matrix. This result further emphasizes the role of deuteration in enhancing the photophysical performance, reducing energy losses, and improving the overall efficiency of OLED and TADF-based systems.

Finally, within the framework of special architecture, multi-donor structures for red-to-NIR OLEDs are shown in Fig. 11, while Table 9 summarizes the corresponding material properties and OLED device performance. Interestingly, variations in the HOMO and LUMO energy levels are observed among the donor-only carbazole-based materials. This behavior is primarily governed by the degree of intermolecular electronic coupling and orbital splitting between the adjacent carbazole units. Hasan *et al.* designed and synthesized a novel carbazole-based dendrimer, namely **tpc-CDBP (122)**.[160] This compound demonstrates excellent thermal stability, with a T_d/T_g of 487/283 °C, making it a robust candidate for use in organic electronic devices. The electronic properties of **tpc-CDBP (122)** were carefully characterized. The HOMO/LUMO was determined to be −5.24/−2.02 eV, and T_1 was found to be 2.83 eV.

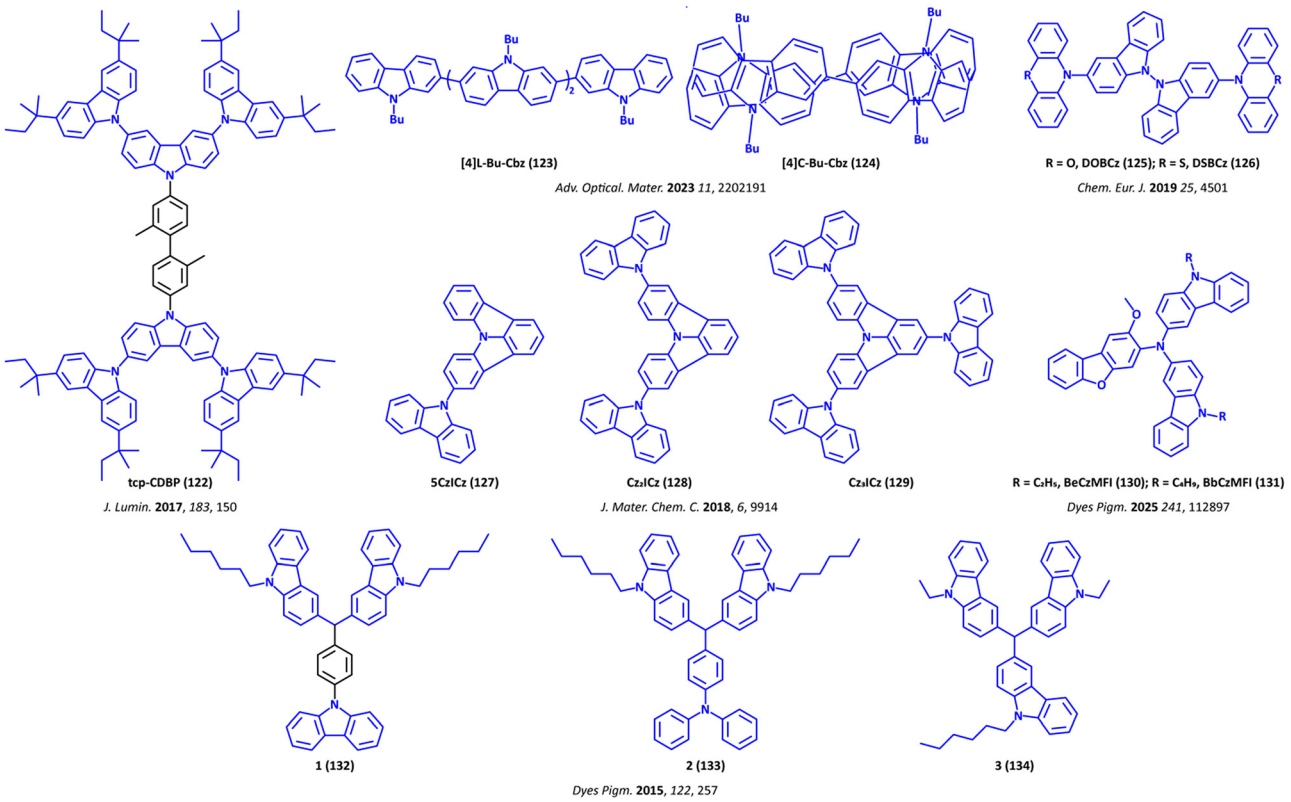

Fig. 11 Chemical structures of carbazole-based host materials employing a special architecture for red-to-NIR OLEDs, grouped according to multi-donor structural motifs. (The highlighted colors correspond to blue for carbazole donors, red for the acceptor moieties, and black for the π-bridge linkers.)

Table 9 Summary of materials' properties and OLED device performance parameters for the compounds depicted in Fig. 11

Material		Material characterization			OLED characterization					
		T_d/T_g [°C]	HOMO/LUMO [eV]	S_1/T_1 [eV]	EML type	Emitter	λ_{max} [nm]	EQE/CE/PE [%, cd A^{-1}, lm W^{-1}]	CIE [x, y]	Ref.
122	**tcp-CDBP**	487/283	−5.24/−2.02	—/2.83	Single	Hex-Ir(phq)$_3$	—	—/9.9/3.3	0.57, 0.43	160
123	**[4]L-Bu-Cbz**	—	−5.30/−2.17	—/2.38	Single	Ir(MDQ)$_2$(acac)	620	11.1/13.0/15.7	0.65, 0.35	161
124	**[4]C-Bu-Cbz**		−5.18/−2.40	—/2.26				17.0/20.6/25.8		
125	**DOBCz**	394/170	−4.96/−1.86	3.10/2.70	Single	Ir(MDQ)$_2$(acac)	—	13.3/22.0/13.1	0.61, 0.39	162
126	**DSBCz**	394/180	−4.97/−1.87	3.10/2.65				11.7/19.5/11.3		
127	**5CzICz**	450/101	−5.57/−2.47	—/2.83	Single	Ir(MDQ)$_2$(acac)	—	20.2/32.7/31.0	—	76
128	**Cz$_2$ICz**	>500/171	−5.54/−2.47	—/2.82				20.4/30.0/29.3		
129	**Cz$_3$ICz**	>500/327	−5.63/−2.59	—/2.80				17.6/24.9/25.2		
130	**BeCzMFI**	360/132	−5.21/−2.42	2.86/2.45	Single	Ir(piq)$_2$(acac)	631	8.0/5.0/5.7	0.69, 0.31	163
					Co-host			10.9/7.7/10.7	0.68, 0.31	
					Exciplex			11.9/7.1/9.0	0.69, 0.31	
131	**BbCzMFI**	411/100	−5.17/−2.39	2.88/2.46	Single		629	9.2/6.7/10.1	0.68, 0.31	
					Co-host		628	11.6/7.5/11.8		
					Exciplex		633	13.6/9.5/13.8		
132	**1**	417/73	—/—	3.43/2.97	Co-host	Ir(piq)$_3$	—	6.9/3.2/4.5	0.68, 0.32	80
133	**2**	413/54		3.35/2.97				7.1/4.2/4.9		
134	**3**	411/93		3.42/2.97				8.4/5.3/5.5		

One of the standout features of **tpc-CDBP (122)** is its ability to form smooth, uniform thin films, which is crucial for the fabrication of high-quality solution-processable OLEDs. These films allowed for the successful development of multilayer red-phosphorescent OLEDs (using Hex-Ir(phq)$_3$ as the emissive material), with **tpc-CDBP (122)** serving as the hole-transporting host. Remarkably, these devices exhibited minimal colour deviation, demonstrating the versatility and stability of the carbazole dendrimer in OLED applications. OLED devices incorporating **tpc-CDBP (122)** as the host material achieved performance for a current efficiency of 9.9 cd A^{-1} and a power efficiency of 3.3 lm W^{-1}.

Brouillac *et al.* introduced a novel class of carbazole-based nanohoops by comparing the linear analogue *N*-butyl-2,7-quartercarbazole (**[4]L-Bu-Cbz (123)**) with its cyclic counterpart, [4]-cyclo-*N*-butyl-2,7-carbazole (**[4]C-Bu-Cbz (124)**).[161] These compounds were studied for their electronic properties, with cyclic voltammetry revealing the HOMO/LUMO of −5.30/−2.17 eV for **[4]L-Bu-Cbz (123)** and −5.18/−2.40 eV for **[4]C-Bu-Cbz (124)**. Additionally, the T_1 values were determined to be 2.38 eV for **[4]L-Bu-Cbz (123)** and 2.26 eV for **[4]C-Bu-Cbz (124)**. The key innovation in this work lies in the cyclic structure of **[4]C-Bu-Cbz (124)**, in which four carbazole units are assembled into a ring and substituted at the C-2 and C-7 positions. The OLEDs incorporating **[4]C-Bu-Cbz (124)** as the host and Ir(MDQ)$_2$(acac) as the emitter exhibited a higher efficiency of 17.0% (20.6 cd A^{-1} and 25.8 lm W^{-1}), with a low threshold voltage (V_{on}) of just 2.3 V. In comparison, the linear analogue **[4]L-Bu-Cbz (123)**, which shares the same C-2/C-7 linkages but lacks the cyclic structure, showed significantly lower performance under identical conditions with an efficiency of 11.1% (13.0 cd A^{-1} and 15.7 lm W^{-1}). This study not only demonstrates that **[4]C-Bu-Cbz (124)** can efficiently host a phosphorescent emitter in a high-performance PhOLED but also highlights the significant advantages of cyclic (nanohoops) over linear structures.

Liu *et al.* introduced two novel host materials, **DOBCz (125)** and **DSBCz (126)**, by introducing 10*H*-phenoxazine and 10*H*-phenothiazine donor groups at the 9,9′-positions of a 9,9′-bicarbazole core.[162] Both materials exhibit higher thermal stability (T_d/T_g = 394/170 and 394/180 °C) and well-aligned electronic energy levels (HOMO/LUMO/T_1 = −4.96/−1.86/2.70 eV and −4.97/−1.87/2.65 eV, respectively), supporting efficient charge transport and exciton confinement. When evaluated in OLED devices using the red phosphorescent emitter Ir(MDQ)$_2$(acac), **DOBCz (125)** achieved a performance of 13.3% (22.0 cd A^{-1} and 13.1 lm W^{-1}), while **DSBCz (126)** showed a slightly lower performance of 11.7% (19.5 cd A^{-1} and 11.3 lm W^{-1}). These results demonstrate that both materials are promising host materials for red OLEDs, with **DOBCz (125)** showing slightly improved performance.

Zhao *et al.* reported three fused carbazole-based host molecules, **5CzICz (127)**, **Cz$_2$ICz (128)**, and **Cz$_3$ICz (129)**, constructed from an indolo[3,2,1-*jk*]carbazole (ICz) core with different numbers and positions of 9*H*-carbazole substituents.[76] The molecular design aimed to prevent excimer formation commonly observed in ICz-based structures, which typically limits the efficiency of PhOLEDs. By altering the substitution position and reducing the molecular symmetry around the ICz core, steric hindrance was increased, thereby weakening intermolecular interactions between ICz subunits. **5CzICz (127)** incorporates a single 9*H*-carbazole substituent at the 5-position to disrupt molecular symmetry and hinder ordered packing. **Cz$_2$ICz (128)** introduces two 9*H*-carbazole groups, further enhancing steric hindrance while positioning the ICz core closer to the molecular center. **Cz$_3$ICz (129)** contains three 9*H*-carbazole units, providing the greatest steric bulk and moving the ICz core to the molecular center, thereby shielding it from intermolecular interactions. As a result, these materials exhibit high triplet energy (T_1 = 2.83, 2,82, and 2,80 eV for **5CzICz (127)**, **Cz$_2$ICz (128)**, and **Cz$_3$ICz (129)**, respectively) and excellent thermal stability ($T_d \geq 450$ °C and $T_g \geq 101$ °C), enabling effective exciton confinement for various phosphorescent emitters. When applied as the host material in red PhOLEDs with Ir(MDQ)$_2$(acac) as the emitter, the device exhibited a low turn-on voltage, indicating efficient charge injection and

transport. The best performance was achieved with the **Cz_2ICz (128)** host, delivering 20.4% (30.0 cd A^{-1} and 29.3 lm W^{-1}), along with a favourable efficiency roll-off, similar to that of the **5CzICz (127)**-based device, with only 6% and 17% roll-off at luminances of 1000 and 5000 cd m^{-2}, respectively.

Beresneviciute *et al.* synthesized two carbazole-based host materials, **BeCzMFI (130)** and **BbCzMFI (131)**, incorporating a methoxydibenzofuran-carbazole donor core and differentiated by *N*-ethyl and *N*-butyl substituents to improve film-forming properties.[163] Both materials exhibit good thermal stability (T_d/T_g = 360/132 °C for **BeCzMFI (130)** and 411/100 °C for **BbCzMFI (131)**) and suitable electronic characteristics (HOMO/LUMO/T_1 = −5.21/−2.42 eV/2.45 eV and −5.17/−2.93/2.46 eV, respectively). When applied as a host in red PhOLEDs with the $Ir(piq)_2(acac)$ emitter, maximum efficiencies of 8.0% (5.0 cd A^{-1} and 5.7 lm W^{-1}) and 9.2% (6.7 cd A^{-1} and 10.1 lm W^{-1}) were achieved for **BeCzMFI (130)** and **BbCzMFI (131)**, respectively. Further improvements were realized through co-host systems with TAPC and exciplex configurations with CN-T2T. The most significant improvements were observed at CN-T2T : **BbCzMFI (131)** (1 : 1), delivering a performance of 13.6% (9.5 cd A^{-1} and 13.8 lm W^{-1}) and a high luminance of nearly 30 000 cd m^{-2}. These results demonstrate that **BeCzMFI (130)** and **BbCzMFI (131)** are not only effective host materials for phosphorescent OLEDs but also offer substantial advantages when used in exciplex-based systems.

Concluding the discussion on special architecture, our group synthesized three novel host materials (compounds **1–3 (132–134)**) containing electronically isolated carbazolyl fragments.[80] A distinctive feature of these materials is the incorporation of electronically isolated carbazole units, which were strategically designed to optimize the OLED performance. These host materials exhibit high thermal stability, with T_d ranging from 411 °C to 417 °C and T_g varying across the materials: 73 °C for **1 (132)**, 54 °C for **2 (133)**, and 93 °C for **3 (134)**. The difference in T_g is attributed to the molecular structure, with the low T_g values of host materials reflecting the flexible sp^3-centered bonds. Despite these differences, all three materials show a high T_1 of 2.97 eV, which is particularly beneficial for red OLEDs, as this triplet energy is essential for efficient phosphorescent emission. In OLED testing, the three host materials were paired with the red phosphorescent emitter $Ir(piq)_3$, demonstrated a performance of 6.9% (3.2 cd A^{-1} and 4.5 lm W^{-1}) for compound **1 (132)**, 7.1% (4.2 cd A^{-1} and 4.9 lm W^{-1}) for compound **2 (133)**, and 8.4% (5.3 cd A^{-1} and 5.5 lm W^{-1}) for compound **3 (134)**, respectively. The results highlight that these carbazole-based host materials provide sufficient carrier transport capability and suitable triplet energy levels for efficient OLED performance.

4. Evaluation of the molecular design strategy in OLED hosts

Based on the molecular design strategies reviewed above, it is evident that the development of high-performance OLEDs relies on the synergistic interplay between molecular architecture and host material functionality. To critically evaluate the strengths and limitations of different design approaches, it is essential to examine how structural configuration and molecular geometry shape the underlying electronic landscape. In particular, the alignment and spatial distribution of HOMO and LUMO levels govern charge injection, while charge transport is further influenced by intermolecular electronic coupling and molecular packing. Altogether, these factors strongly impact current and power efficiencies. A central challenge in the molecular design of host materials for red-to-NIR emitters lies in balancing the competing requirements of high triplet energy and efficient charge transport. Achieving a high triplet energy typically requires limiting π-conjugation and promoting localized electronic states to preserve a wide energy gap. In contrast, efficient charge transport is often associated with enhanced orbital delocalization and intermolecular interactions, although hopping-mediated transport can still occur in more localized systems. These requirements are not inherently mutually exclusive and can be reconciled through careful molecular design, such as incorporating bipolar architectures or three-dimensional frameworks. This balance is particularly critical for optimizing EQE and suppressing efficiency roll-off, as the host must effectively confine excitons and prevent energy leakage from the emitter.

Push–pull frameworks utilize ICT to spatially separate the HOMO and LUMO, thereby facilitating charge transfer and reducing the driving voltage. However, such systems often exhibit a tendency toward increased molecular planarity, which may promote intermolecular π–π interactions. These interactions can reduce triplet energy and increase the likelihood of exciton quenching, particularly in aggregated states, thereby limiting overall device performance. The structural influence of phenyl π-bridges (*para*-, *meta*-, and *ortho*-substitution) provides a useful means to modulate molecular geometry, enabling a transition from relatively planar to highly twisted conformations. For example, the work by Hu *et al.* (**compounds 33–35**) clearly illustrates the interplay among triplet energy, charge transport, and thermal stability.[103] Notably, despite their distinct geometries, the *para*-bridged (more planar) and *ortho*-bridged (more twisted) systems exhibit nearly identical device performance (EQE ≈ 12%). This observation suggests that while molecular geometry strongly influences intrinsic material properties, the effectiveness of a host material is ultimately determined by how well it enables balanced charge transport and exciton confinement.

Symmetric architectures, composed of identical donor or acceptor units arranged around a central core, typically exhibit a well-balanced electronic framework with significant HOMO–LUMO overlap, which is beneficial for charge transport. However, the high degree of symmetry can also increase the propensity for crystallization and strong intermolecular π–π stacking, potentially reducing triplet energy and enhancing exciton quenching. As demonstrated in our previous work (**compounds 48–53**),[118] introducing steric hindrance through bulky substituents, carbazole linkages, or twisted bridges

effectively disrupts π–π stacking at the cost of reduced conjugation. Although these materials have comparable frontier orbital energy levels, their device performance differs significantly, highlighting that frontier orbital alignment alone is insufficient to predict device behavior. While twisted geometries often correlate with improved performance, linear structures can exhibit either inferior or superior efficiencies depending on how molecular packing is controlled. This underscores that intermolecular interactions, rather than geometry alone, play a decisive role in determining device performance.

Asymmetrical architectures provide a versatile platform by intentionally breaking molecular symmetry to achieve finer control over electronic properties. Through modulation of orbital distribution and steric effects, these systems enable optimization of HOMO and LUMO levels while suppressing excessive crystallization and π–π stacking. The resulting control over molecular packing and charge mobility can improve charge balance within the emissive layer, which is closely associated with enhanced EQE and reduced efficiency roll-off. A representative study by Zheng *et al.* compared asymmetrical (**compound 73**, EQE 17.1%) and push–pull (**compound 40**, EQE 19.4%) systems based on a phenanthro[9,10-*d*]imidazole core.[108] Despite similar energy-level alignment, thermal stability, and highly twisted geometries, their device performances differ slightly. The introduction of an additional ICz unit in **compound 73** increases steric hindrance and enhances electron-blocking properties, likely reducing electron-transport capability and disrupting charge balance. These results highlight that achieving balanced bipolar charge transport is widely recognized as a key factor in realizing high efficiency and operational stability, regardless of the specific architectural category.

Meanwhile, special architectures often exhibit excellent hole-transporting characteristics due to their electron-rich nature, with HOMOs delocalized across the molecular framework. Because the triplet exciton is typically localized on a donor unit, these materials can maintain relatively high triplet energy. However, they generally require a complementary electron-transporting material to ensure efficient carrier recombination. Poor compatibility between components may shift the recombination zone toward interfaces, increasing the likelihood of exciton quenching. To address this issue, co-host and exciplex host systems have emerged as effective strategies for balancing charge transport and improving exciton management. In such systems, charge-transfer states with small ΔE_{ST} can form, while the individual host components retain their intrinsically high triplet energies and favorable charge-transport properties. This synergistic effect improves charge balance, reducing driving voltages, suppressing efficiency roll-off, and enhancing device performance. Despite the effectiveness of these approaches, the development of single-component bipolar host materials remains a key objective. Designing a single molecule that simultaneously provides efficient charge transport and high triplet energy is essential to simplify device architecture and reduce fabrication complexity, thereby enabling large-scale production. Overall, these findings demonstrate that optimizing carbazole-based host materials requires a delicate balance among triplet energy, charge transport, and intermolecular interactions, achieved through precise control of molecular architecture, electronic distribution, and steric configuration.

5. Conclusions, rational design principles, and future perspectives

Based on the systematic classification and comparative analysis presented, four key design guidelines emerge for carbazole-based hosts for red-to-NIR OLEDs: (i) manage S_1/T_1 energy levels to prevent back-energy transfer, (ii) balance hole and electron transport capability, (iii) align HOMO/LUMO levels for efficient charge injection, and (iv) ensure high thermal and morphological stability for operational durability. Carbazole derivatives inherently satisfy these criteria by providing exceptional thermal and morphological stability, with a T_d of 350–550 °C and a T_g of 70–150 °C, while their inherently high triplet energy (~2.9 eV), tunable across 2.20–3.20 eV through appropriate molecular engineering–push–pull, symmetric, asymmetric, or special architectures–ensures effective exciton confinement compatible with red-emitting systems. The electron-rich nitrogen center further enables efficient hole injection and precise energy-level alignment, supporting balanced charge transport.

Despite numerous publications reporting EQE exceeding 20%, carbazole-based red-to-NIR host systems are frequently constrained by an inherently dominant hole-transporting nature and insufficient electron-transport capability. Achieving the requisite bipolar charge balance within the EML requires sophisticated molecular engineering–either utilizing push–pull, symmetric, or asymmetric architectures to achieve a bipolar configuration, or implementing special architecture enabling co-host/exciplex configurations–to enhance electron mobility without compromising triplet energy or thermal stability. To overcome performance limitations, researchers have pivoted toward molecular geometry, employing sterically hindered, 3D architectures that regulate intermolecular distances and suppress excessive π–π stacking. This structural approach facilitates the formation of stable amorphous films and mitigates excimer formation and quenching, which are typically associated with planar molecules. Consequently, the development of high-efficiency red-to-NIR PhOLEDs relies on two synergistic design imperatives: achieving balanced bipolar transport through rational electronic architecture and implementing sterically hindered geometries to optimize exciton confinement and thin-film morphology.

The design of effective red-to-NIR host materials involves a complex trade-off across different architecture types. While push–pull architectures offer straightforward HOMO/LUMO tuning, their excessive charge-transfer character often broadens emission spectra, accelerates non-radiative decay, and promotes π–π stacking induced ACQ. Symmetric architectures mitigate these issues through balanced charge distribution, yet remain prone to high crystallinity and strong intermolecular

π–π stacking, which is problematic in red-to-NIR emission, where the energy-gap law already accelerates non-radiative losses. Asymmetric architectures can disrupt molecular symmetry, thereby suppressing crystallization and π–π stacking and enhancing morphological stability. However, if substitution patterns are not precisely optimized, they can risk energetic disorder, broaden emission profiles, and ultimately compromise operational stability. In contrast, special architectures maintain exceptionally high triplet energy and morphological stability through extended π-conjugation, but require integration into co-host or exciplex-forming systems to achieve charge balance. Furthermore, the absence of a strong dipole moment in these systems limits the solid-state solvation effects required for precise spectral control, while their synthetic complexity remains a significant hurdle for scalability.

Despite significant progress, several challenges remain for red-to-NIR OLED applications. The evolution of host materials should move beyond simple linear or planar motifs toward rigid, sterically hindered 3D frameworks-whether through push–pull, symmetric, asymmetric, or special configurations–to suppress ACQ and disrupt molecular planarity. Future developments should focus on precise control of D–A torsion angle, hybridization with multi-resonance motifs, and rational dipole engineering to minimize non-radiative decay while maintaining the high triplet energy required for effective exciton confinement. Since the energy-gap law not only accelerates non-radiative decay but also promotes chemical degradation, host material properties such as molecular rigidity, charge balance, and morphological stability are crucial in governing both device efficiency and operational lifetime. Therefore, future research should prioritize systematically correlating molecular architecture with efficiency and long-term stability while ensuring that molecular design optimizations remain synthetically accessible and scalable for large-scale industrial OLED production.

Conflicts of interest

There are no conflicts to declare.

Data availability

This article is a review of previously published studies. No new experimental or computational data were generated or analyzed in this work; therefore, data sharing is not applicable.

Acknowledgements

This work was financially supported by the National Science and Technology Council of Taiwan (NSTC 112-2923-E-155-002-MY4, 113-2221-E-155-014-MY3, 114-2923-E-155-001-MY3, 113-2113-M-029-001-, and 114-2113-M-029-011-). Yuan Ze University and Tunghai University are gratefully acknowledged.

References

1 M. J. Schnermann, *Nature*, 2017, **551**, 176–177.
2 A. Zampetti, A. Minotto and F. Cacialli, *Adv. Funct. Mater.*, 2019, **29**, 1807623.
3 K. Sutanto, N. R. Al Amin, C.-H. Chen, D. Luo, C.-H. Chen, S. Biring, C.-C. Lee and S.-W. Liu, *Org. Electron.*, 2022, **103**, 106454.
4 E. H. Cho, H.-R. Choi, Y. Park, S. Y. Jeong, Y. J. Song, Y. H. Hwang, J. Lee, Y. Chi, S.-F. Wang, Y. Jeon, C.-H. Huh and K. C. Choi, *ACS Appl. Mater. Interfaces*, 2023, **15**, 57415–57426.
5 P. L. dos Santos, P. Stachelek, Y. Takeda and P. Pander, *Mater. Chem. Front.*, 2024, **8**, 1731–1766.
6 S. Ahadzadeh, S. Brebels, W. Maes and W. Deferme, *Adv. Funct. Mater.*, 2025, 2419599, DOI: 10.1002/adfm.202419599.
7 Y.-C. Wei, S. F. Wang, Y. Hu, L.-S. Liao, D.-G. Chen, K.-H. Chang, C.-W. Wang, S.-H. Liu, W.-H. Chan, J.-L. Liao, W.-Y. Hung, T.-H. Wang, P.-T. Chen, H.-F. Hsu, Y. Chi and P.-T. Chou, *Nat. Photon.*, 2020, **14**, 570–577.
8 J. V. Caspar, E. M. Kober, B. P. Sullivan and T. J. Meyer, *J. Am. Chem. Soc.*, 1982, **104**, 630–632.
9 X. Zhao, J. Fan, S. Liu, W. Hu and Y. Xu, *Chem. Phys.*, 2025, **598**, 112829.
10 Z. Chen, H. Zhang, D. Wen, W. Wu, Q. Zeng, S. Chen and W.-Y. Wong, *Chem. Sci.*, 2020, **11**, 2342–2349.
11 D. H. Kim, N. S. Cho, H.-Y. Oh, J. H. Yang, W. S. Jeon, J. S. Park, M. C. Suh and J. H. Kwon, *Adv. Mater.*, 2011, **23**, 2721–2726.
12 Q. Wang, F. Lucas, C. Quinton, Y.-K. Qu, J. Rault-Berthelot, O. Jeannin, S.-Y. Yang, F.-C. Kong, S. Kumar, L.-S. Liao, C. Poriel and Z.-Q. Jiang, *Chem. Sci.*, 2020, **11**, 4887–4894.
13 C.-T. Chen, *Chem. Mater.*, 2004, **16**, 4389–4400.
14 C.-H. Fan, P. Sun, T.-H. Su and C.-H. Cheng, *Adv. Mater.*, 2011, **23**, 2981–2985.
15 C. Poriel and J. Rault-Berthelot, *Adv. Funct. Mater.*, 2021, **31**, 2010547.
16 S. Oner and M. R. Bryce, *Mater. Chem. Front.*, 2023, **7**, 4304–4338.
17 Y. Tao, C. Yang and J. Qin, *Chem. Soc. Rev.*, 2011, **40**, 2943–2970.
18 T. Chatterjee and K. T. Wong, *Adv. Opt. Mater.*, 2018, **7**, 1800565.
19 W. Che, Y. Xie and Z. Li, *Asian J. Org. Chem.*, 2020, **9**, 1262–1276.
20 M. Y. Wong and E. Zysman-Colman, *Adv. Mater.*, 2017, **29**, 1605444.
21 S. Hu, J. Zeng, X. Zhu, J. Guo, S. Chen, Z. Zhao and B. Z. Tang, *ACS Appl. Mater. Interfaces*, 2019, **11**, 27134–27144.
22 A. Chaskar, H.-F. Chen and K.-T. Wong, *Adv. Mater.*, 2011, **23**, 3876–3895.
23 R. K. Konidena, K. R. J. Thomas and J. W. Park, *ChemPhotoChem*, 2022, **6**, e202200059.
24 B. Wex and B. R. Kaafarani, *J. Mater. Chem. C*, 2017, **5**, 8622–8653.

25 N. Blouin and M. Leclerc, *Acc. Chem. Res.*, 2008, **41**, 1110–1119.
26 S. L. Lin, L. H. Chan, R. H. Lee, M. Y. Yen, W. J. Kuo, C. T. Chen and R. J. Jeng, *Adv. Mater.*, 2008, **20**, 3947–3952.
27 A. Bree and R. Zwarich, *J. Chem. Phys.*, 1968, **49**, 3355–3358.
28 N. Mataga, Y. Torihashi and K. Ezumi, *Theor. Chim. Acta*, 1964, **2**, 158–167.
29 G. E. Johnson, *J. Phys. Chem.*, 1974, **78**, 1512–1521.
30 M. H. Tsai, H. W. Lin, H. C. Su, T. H. Ke, C. C. Wu, F. C. Fang, Y. L. Liao, K. T. Wong and C. I. Wu, *Adv. Mater.*, 2006, **18**, 1216–1220.
31 T. D. Anthopoulos, J. P. J. Markham, E. B. Namdas, I. D. W. Samuel, S.-C. Lo and P. L. Burn, *Appl. Phys. Lett.*, 2003, **82**, 4824–4826.
32 C. Adachi, M. A. Baldo, S. R. Forrest, S. Lamansky, M. E. Thompson and R. C. Kwong, *Appl. Phys. Lett.*, 2001, **78**, 1622–1624.
33 A. Tsuboyama, H. Iwawaki, M. Furugori, T. Mukaide, J. Kamatani, S. Igawa, T. Moriyama, S. Miura, T. Takiguchi, S. Okada, M. Hoshino and K. Ueno, *J. Am. Chem. Soc.*, 2003, **125**, 12971–12979.
34 M. A. Baldo, S. Lamansky, P. E. Burrows, M. E. Thompson and S. R. Forrest, *Appl. Phys. Lett.*, 1999, **75**, 4–6.
35 S. Madagyal, A. Paul, F.-Y. Yang, C.-H. Huang, P. Verma, P. Chetti, C.-H. Chang, S. Kothavale and A. Chaskar, *ACS Appl. Opt. Mater.*, 2024, **2**, 2248–2261.
36 N. R. Al Amin, C.-Y. Ho, D.-C. Huang, R.-M. Chang, Y.-H. Cheng and C.-H. Chang, *Chem. Eng. J.*, 2025, **505**, 159509.
37 N. R. Al Amin, M.-J. Lin, J.-M. Wang, Z.-P. Yang, H.-C. Su and C.-H. Chang, *ACS Appl. Mater. Interfaces*, 2025, **17**, 40881–40892.
38 T.-H. Chuang, K.-Y. Su, Y.-R. Yang, Y.-T. Chen, C.-Y. Hsu, Z.-R. He, C.-W. Lu and C.-H. Chang, *Opt. Mater.*, 2025, **159**, 116513.
39 C.-H. Chang, Y.-J. Lu, C.-C. Liu, Y.-H. Yeh and C.-C. Wu, *J. Display Technol.*, 2007, **3**, 193–199.
40 D. Tanaka, H. Sasabe, Y.-J. Li, S.-J. Su, T. Takeda and J. Kido, *Jpn. J. Appl. Phys.*, 2007, **46**, L10–L12.
41 S. J. Yeh, M. F. Wu, C. T. Chen, Y. H. Song, Y. Chi, M. H. Ho, S. F. Hsu and C. H. Chen, *Adv. Mater.*, 2005, **17**, 285–289.
42 C.-H. Chien, F.-M. Hsu, C.-F. Shu and Y. Chi, *Org. Electron.*, 2009, **10**, 871–876.
43 H. Kanno, K. Ishikawa, Y. Nishio, A. Endo, C. Adachi and K. Shibata, *Appl. Phys. Lett.*, 2007, **90**, 123509.
44 A. Haldi, B. Domercq, B. Kippelen, R. D. Hreha, J. Y. Cho and S. R. Marder, *Appl. Phys. Lett.*, 2008, **92**, 253502.
45 M. H. Tsai, Y. H. Hong, C. H. Chang, H. C. Su, C. C. Wu, A. Matoliukstyte, J. Simokaitiene, S. Grigalevicius, J. V. Grazulevicius and C. P. Hsu, *Adv. Mater.*, 2007, **19**, 862–866.
46 W. Jiang, L. Duan, J. Qiao, G. Dong, D. Zhang, L. Wang and Y. Qiu, *J. Mater. Chem.*, 2011, **21**, 4918–4926.
47 Y.-C. Chang, S.-C. Yeh, Y.-H. Chen, C.-T. Chen, R.-H. Lee and R.-J. Jeng, *Dyes Pigm.*, 2013, **99**, 577–587.
48 I. Neogi, S. Jhulki, A. Ghosh, T. J. Chow and J. N. Moorthy, *ACS Appl. Mater. Interfaces*, 2015, **7**, 3298–3305.
49 H. Huang, Q. Fu, B. Pan, S. Zhuang, L. Wang, J. Chen, D. Ma and C. Yang, *Org. Lett.*, 2012, **14**, 4786–4789.
50 G. Li, J. Zheng, K. Klimes, Z.-Q. Zhu, J. Wu, H. Zhu and J. Li, *ACS Appl. Mater. Interfaces*, 2019, **11**, 40320–40331.
51 M. M. Raikwar, S. C. Kim, J. Sun, C. Chu and J. Y. Lee, *ACS Appl. Mater. Interfaces*, 2023, **15**, 40809–40816.
52 A. Arai, H. Sasabe, K. Nakao, Y. Masuda and J. Kido, *Chem. – Eur. J.*, 2021, **27**, 4971–4976.
53 Y.-C. Cheng, X.-C. Fan, F. Huang, X. Xiong, J. Yu, K. Wang, C.-S. Lee and X.-H. Zhang, *Angew. Chem., Int. Ed.*, 2022, **61**, e202212575.
54 H. Zhang, Y. Sun, Z. Chen, W. Wang, Q. Wang, S. Chen, Y. Xu and W.-Y. Wong, *Chem. Eng. J.*, 2023, **451**, 138632.
55 H. Wang, J.-X. Chen, L. Zhou, X. Zhang, J. Yu, K. Wang and X.-H. Zhang, *Mater. Horiz.*, 2023, **10**, 2997–3004.
56 X. Yang, S. Xu, Y. Zhang, C. Zhu, L. Cui, G. Zhou, Z. Chen and Y. Sun, *Angew. Chem., Int. Ed.*, 2023, **62**, e202309739.
57 H. Wang, J.-X. Chen, Y.-Z. Shi, X. Zhang, L. Zhou, X.-Y. Hao, J. Yu, K. Wang and X.-H. Zhang, *Adv. Mater.*, 2024, **36**, e2307725.
58 L. Ge, W. Zhang, Y.-H. Hao, M. Li, Y. Liu, M. Zhou and L.-S. Cui, *J. Am. Chem. Soc.*, 2024, **146**, 32826–32836.
59 T. Nishimoto, T. Yasuda, S. Y. Lee, R. Kondo and C. Adachi, *Mater. Horiz.*, 2014, **1**, 264–269.
60 P. Ledwon, *Org. Electron.*, 2019, **75**, 105422.
61 A. Afrin, *Mater. Chem. Front.*, 2025, **9**, 1794–1820.
62 J.-H. Pan, H.-L. Chiu and B.-C. Wang, *J. Mol. Struct. THEOCHEM*, 2005, **725**, 89–95.
63 G. Krucaite and S. Grigalevicius, *Coatings*, 2025, **15**, 398.
64 L. A. T. Allen and P. Natho, *Org. Biomol. Chem.*, 2023, **21**, 8956–8974.
65 K. Brunner, A. van Dijken, H. Borner, J. J. A. M. Bastiaansen, N. M. M. Kiggen and B. M. W. Langeveld, *J. Am. Chem. Soc.*, 2004, **126**, 6035–6042.
66 R. Beresneviciute, D. Tavgeniene, D. Blazevicius, K.-W. Chen, Y.-H. Chen, S. Grigalevicius and C.-H. Chang, *Opt. Mater.*, 2024, **157**, 116273.
67 P. Yu and Y. Xiao, *Materials*, 2021, **14**, 2349.
68 G. Grybauskaite-Kaminskiene, D. Volyniuk, V. Mimaite, O. Bezvikonnyi, A. Bucinskas, G. Bagdziunas and J. V. Grazulevicius, *Chem. – Eur. J.*, 2018, **24**, 9581–9591.
69 S. Macionis, D. Gudeika, O. Bezvikonnyi, S. Melnykov, L. Guminilovych, J. Simokaitiene, S. Sargsyan, R. Keruckiene, D. Volyniuk, P. Stakhira and J. V. Grazulevicius, *Mater. Adv.*, 2024, **5**, 5749–5762.
70 S. Li, Z. Ma, S. Gao, Y. Wang, Z. Mao, J. Zhao and Z. Chi, *Dyes Pigm.*, 2024, **227**, 112172.
71 S.-W. Li, C.-H. Yu, C.-L. Ko, T. Chatterjee, W.-Y. Hung and K.-T. Wong, *ACS Appl. Mater. Interfaces*, 2018, **10**, 12930–12936.
72 B. Patil, J. Lade, S.-S. Chiou, Y.-C. Cheng, Y.-F. Lin, Y. Jadhav, P. Chetti, C.-H. Chang and A. Chaskar, *Org. Electron.*, 2021, **92**, 106090.
73 W. Yuan, S. Hu, Y. Zhang, J. Wang, Y. Wu, W. Yao, C. Shi, N. Sun and Y. Tao, *Org. Electron.*, 2025, **144**, 107288.

74 S. Grigalevicius, *Synth. Met.*, 2006, **156**, 1–12.
75 V. V. Patil, W. P. Hong and J. Y. Lee, *Adv. Energy Mater.*, 2024, **15**, 2400258.
76 C. Zhao, T. Schwartz, B. Stoger, F. J. White, J. Chen, D. Ma, J. Frohlich and P. Kautny, *J. Mater. Chem. C*, 2018, **6**, 9914–9924.
77 D. Tavgeniene, D. Blazevicius, E. Skuodis, S. Grigalevicius, C.-H. Huang, Y.-H. Chen and C.-H. Chang, *Dyes Pigm.*, 2025, **242**, 112965.
78 Z.-J. Gao, T.-H. Yeh, J.-J. Xu, C.-C. Lee, A. Chowdhury, B.-C. Wang, S.-W. Liu and C.-H. Chen, *ACS Omega*, 2020, **5**, 10553–10561.
79 F. Rodella, S. Bagnich, E. Duda, T. Meier, J. Kahle, S. Athanasopoulos, A. Kohler and P. Strohriegl, *Front. Chem.*, 2020, **8**, 657.
80 C.-H. Chang, R. Griniene, Y.-D. Su, C.-C. Yeh, H.-C. Kao, J. V. Grazulevicius, D. Volyniuk and S. Grigalevicius, *Dyes Pigm.*, 2015, **122**, 257–263.
81 A. Islam, K. Usman, Q. M. Kaleem, A. G. Wattoo, K. Javaid, F. E. Alam, S. Y. Ryu, M.-D. Li and Z. Ge, *J. Lumin.*, 2021, **236**, 118088.
82 K. Guo, M. Righetto, A. Minotto, A. Zampetti and F. Cacialli, *iScience*, 2021, **24**, 102545.
83 L. Duan, J. Qiao, Y. Sun and Y. Qiu, *Adv. Mater.*, 2011, **23**, 1137–1144.
84 K. S. Yook and J. Y. Lee, *Chem. Rec.*, 2016, **16**, 159–172.
85 X. Qiu, S. Ying, J. Yao, J. Zhou, C. Wang, B. Wang, Y. Li, Y. Xu, Q. Jiang, R. Zhao, D. Hu, D. Ma and Y. Ma, *Dyes Pigm.*, 2020, **174**, 108045.
86 R. H. Yi, Y. C. Lei, Y. H. Tseng, Y. F. Lin, Y. C. Cheng, Y. C. Fang, C. Y. Ho, W. W. Tsai, C. H. Chang and C. W. Lu, *Chem. – Eur. J.*, 2022, **28**, e202102966.
87 W. Song, Q. Xu, J. Zhu, Y. Chen, H. Mu, J. Huang and J. Su, *ACS Appl. Mater. Interfaces*, 2020, **12**, 19701–19709.
88 Z. Feng, Z. Gao, W. Qu, T. Yang, J. Li and L. Wang, *RSC Adv.*, 2019, **9**, 10789–10795.
89 S. H. Cheng, W. Y. Hung, M. H. Cheng, H. F. Chen, G. H. Lee, C. L. Chung, T. C. Yeh, W. C. Tang, S. L. Huang and K. T. Wong, *Adv. Electron. Mater.*, 2016, **2**, 1500241.
90 H. Y. Park, J. Lee, C. W. Joo, H. Jang, Y. J. Hyeon, B. Sung, H. Park, J. Kim, S.-K. Kwon, J. Lee and Y.-H. Kim, *Dyes Pigm.*, 2025, **239**, 112796.
91 D. Tavgeniene, G. Krucaite, U. Baranauskyte, J.-Z. Wu, H.-Y. Su, C.-W. Huang, C.-H. Chang and S. Grigalevicius, *Dyes Pigm.*, 2017, **137**, 615–621.
92 D. Tavgeniene, D. Blazevicius, M. Kirstukas, G. Krucaite, K. Kazlauskas, D. Banevicius, V. Jankauskas, E. Kamarauskas and S. Grigalevicius, *Synth. Met.*, 2025, **311**, 117822.
93 Y. Hu, Q. Zhang, S. Guo, Z. Huang, W. Shi, H. Zhou, J. Huang, B. Wei and Z. Zhang, *Dyes Pigm.*, 2024, **229**, 112289.
94 B. N. Patil, J. J. Lade, K. S. Vadagaonkar, P. Chetti and A. C. Chaskar, *ChemistrySelect*, 2018, **3**, 10010–10018.
95 J. Lade, N.-Y. Lee, B. Patil, Y. Y. Deshpande, B. Pownthurai, C.-A. Hsieh, S. S. Pingale, L.-Y. Chen and A. Chaskar, *Org. Electron.*, 2021, **92**, 106104.
96 L. Peng, Y. Huo, S. He, Y. Liu, Z. Ren, S. Ying and S. Yan, *J. Mater. Chem. C*, 2022, **10**, 11642–11653.
97 X. Chen, X.-M. Zhuang, Z.-Y. Wang, J.-J. Zhu, S.-S. Tang, X.-H. Zheng, Y. Liu and Q.-X. Tong, *Org. Electron.*, 2019, **69**, 85–91.
98 P. Wang, S. Fan, J. Liang, L. Ying, J. You, S. Wang and X. Li, *Dyes Pigm.*, 2017, **142**, 175–182.
99 C. Wu, Y. Zhang, D. Ma and Q. Wang, *Dyes Pigm.*, 2020, **173**, 107895.
100 H. Wang, Y. Liu, W. Hu, W. Xu, P. Wang, Y. Wang and X. Luan, *Org. Electron.*, 2018, **61**, 376–382.
101 Y. Hou, S. Ye, D. Zhang, Y. Xu, W. Shi, H. Zhou, J. Huang, B. Wei and Z. Zhang, *Dyes Pigm.*, 2025, **242**, 112977.
102 X. Fei, Y.-J. Zhang, X.-Y. Liu, M.-K. Fung and J. Fan, *Tetrahedron*, 2019, **75**, 2664–2669.
103 M. Hu, Q. Xu, Y. Jiang, H. Mu, L. Gao, P. Hu, J. Huang and J. Su, *Dyes Pigm.*, 2018, **150**, 185–192.
104 Y. Li, D. Zhang and L. Duan, *Org. Electron.*, 2018, **57**, 53–59.
105 Y. Li, D. Zhang, Y. Zhang, M. Cai and L. Duan, *Sci. China: Chem.*, 2016, **59**, 684–691.
106 V. V. Patil, J. Lim and J. Y. Lee, *Dyes Pigm.*, 2021, **189**, 109247.
107 H. J. Jang, R. Braveenth, K. Raagulan, S. Y. Choi, Y. H. Park, S. B. Oh, I.-J. Bae, B. M. Kim, Q. Wu, M. Kim and K. Y. Chai, *Dyes Pigm.*, 2020, **182**, 108697.
108 X. H. Zheng, J. W. Zhao, T. T. Huang, X. Chen, C. Cao, G. X. Yang, Z. H. Lin, Q. X. Tong, S. L. Tao and D. Liu, *ChemElectroChem*, 2019, **6**, 5810–5818.
109 O. Bezvikonnyi, R. S. Bernard, V. Andruleviciene, D. Volyniuk, R. Keruckiene, K. Vaiciulaityte, L. Labanauskas and J. V. Grazulevicius, *Materials*, 2022, **15**, 8495.
110 O. Bezvikonnyi, G. Grybauskaite-Kaminskiene, D. Volyniuk, J. Simokaitiene, Y. Danyliv, R. Durgaryan, A. Bucinskas, E. Jatautienė, I. Hladka, J. Scholz, H. Starykov and J. V. Grazulevicius, *Mater. Sci. Eng. B*, 2020, **261**, 114662.
111 J. Wang, C. Jiang, C. Liu, H. Liu and C. Yao, *Mater. Lett.*, 2018, **233**, 149–152.
112 Q. Ran, Y.-L. Zhang, X. Hua, M.-K. Fung, L.-S. Liao and J. Fan, *Dyes Pigm.*, 2019, **162**, 632–639.
113 X.-D. Zhu, Y.-L. Zhang, Y. Yuan, Q. Zheng, Y.-J. Yu, Y. Li, Z.-Q. Jiang and L.-S. Liao, *J. Mater. Chem. C*, 2019, **7**, 6714–6720.
114 H. Inomata, K. Goushi, T. Masuko, T. Konno, T. Imai, H. Sasabe, J. J. Brown and C. Adachi, *Chem. Mater.*, 2004, **16**, 1285–1291.
115 K. S. Son, M. Yahiro, T. Imai, H. Yoshizaki and C. Adachi, *Chem. Mater.*, 2008, **20**, 4439–4446.
116 F. Wang, J. Sun, M. Liu, H. Shi, H. Ma, W. Ye, H. Wang, H. Zhang, Z. An and W. Huang, *J. Mater. Chem. C*, 2020, **8**, 1871–1878.
117 T. Sarmah, C. Srinivas, D. Barman, R. Gogoi, R. Parui, K. Narang, H. Baishya and P. K. Iyer, *J. Mater. Chem. C*, 2025, **13**, 20367–20423.
118 P. Gnanasekaran, Y.-T. Chen, Y.-T. Tseng, K.-Y. Su, Y.-T. Lin, T. C. Yiu, C.-H. Chang and Y. J. Chang, *J. Mater. Chem. C*, 2024, **12**, 2203–2215.

119 T. C. Yiu, P. Gnanasekaran, W.-L. Chen, W.-H. Lin, M.-J. Lin, D.-Y. Wang, C.-W. Lu, C.-H. Chang and Y. J. Chang, *ACS Appl. Mater. Interfaces*, 2023, **15**, 1748–1761.
120 H. Zhou, G. Wang, S. Guo, X. Jin, X. Luo, Y. Miao, J. Huang, H. Wang and J. Su, *New J. Chem.*, 2022, **46**, 15344–15350.
121 S. Park, H. Kwon, S. Park, S. Oh, K. Lee, H. Lee, S. Kang, D. Park and J. Park, *Materials*, 2024, **17**, 4347.
122 Y.-Z. Li, H.-C. Liang, C.-H. Chen, C.-H. Chiu, L.-C. Huang, Y.-T. Lee, Y.-C. Dzeng, C. Chen, B.-Y. Lin, J.-H. Lee, T.-L. Chiu and M.-K. Leung, *Chem. Eng. J.*, 2024, **498**, 155553.
123 C. P. Han, E. H. C. Shi, C. A. Chen, C. H. Hsu, C. H. Chen, C. C. Wu, Y. T. Lee, T. L. Chiu, J. H. Lee, M. K. Leung and P. T. Chou, *Adv. Opt. Mater.*, 2024, **12**, 2303295.
124 G. Li, M. Du, T. Fan, X. Luo, L. Duan and Y. Zhang, *Mater. Today*, 2024, **73**, 30–37.
125 J. Jayabharathi, S. Panimozhi and V. Thanikachalam, *Sci. Rep.*, 2019, **9**, 17555.
126 Y. Liu, J. Yang, Z. Mao, X. Chen, Z. Yang, X. Ge, X. Peng, J. Zhao, S.-J. Su and Z. Chi, *ACS Appl. Mater. Interfaces*, 2022, **14**, 33606–33613.
127 Z. Zhou, J. Pan, C. Guan, Y. Pu, J. Sun, J. Pan, W. Zhu and Y. Liu, *Chem. Eng. J.*, 2025, **523**, 168548.
128 C. Zang, X. Peng, H. Wang, Z. Yu, L. Zhang, W. Xie and H. Zhao, *Org. Electron.*, 2017, **50**, 106–114.
129 W.-C. Chen, Y. Yuan, Z.-L. Zhu, Z.-Q. Jiang, S.-J. Su, L.-S. Liao and C.-S. Lee, *Chem. Sci.*, 2018, **9**, 4062–4070.
130 F. Wang, J. Ye, J. Liu, X. K. Chen, Y. Yang, Z. Bin and J. You, *Angew. Chem., Int. Ed.*, 2025, **64**, e202502380.
131 Z. Zhang, J. Xie, H. Wang, B. Shen, J. Zhang, J. Hao, J. Cao and Z. Wang, *Dyes Pigm.*, 2016, **125**, 299–308.
132 Y. H. Lin, W.-H. Lin, Y.-S. Huang, C.-H. Wu, P. Gnanasekaran, Y.-M. Chang, S.-W. Teng, C.-W. Lu, C.-H. Chang and Y. J. Chang, *J. Mater. Chem. C*, 2023, **11**, 3101–3111.
133 B. Jia, H. Lian, T. Sun, J. Wei, J. Yang, H. Zhou, J. Huang and Q. Dong, *Dyes Pigm.*, 2019, **168**, 212–218.
134 N. Yamada, H. Nakanotani, A. Takagi, M. Mamada, U. Balijapalli, T. Ichikawa, E. Hirata, S. Kaizu, A. Tanaka, K. Itonaga and C. Adachi, *Sci. Adv.*, 2024, **10**, eadj6583.
135 B. Sun, K.-N. Tong, S.-N. Liu, M.-K. Fung and J. Fan, *J. Mater. Chem. C*, 2021, **9**, 2969–2976.
136 Q. Xie, Y. Qu, G. Wang, X. Luo, D. Zhang, H. Zhou, L. Wang, L. Wang, Y. Miao and J. Huang, *Dyes Pigm.*, 2022, **205**, 110559.
137 Y. Hu, X. Yang, Z. Huang, Q. Xie, Y. Chen, Y. Zheng, R. Kabe, D. Zhang, J. Huang, Y. Qu and Z. Zhang, *Synth. Met.*, 2024, **308**, 117712.
138 F. Wang, Y. Zhao, H. Xu, J. Zhang, Y. Miao, K. Guo, R. Shinar, J. Shinar, H. Wang and B. Xu, *Org. Electron.*, 2019, **70**, 272–278.
139 W. Song, L. Shi, L. Gao, P. Hu, H. Mu, Z. Xia, J. Huang and J. Su, *ACS Appl. Mater. Interfaces*, 2018, **10**, 5714–5722.
140 Y. Zhao, C. Wu, P. Qiu, X. Li, Q. Wang, J. Chen and D. Ma, *ACS Appl. Mater. Interfaces*, 2016, **8**, 2635–2643.
141 L. Zhao, X. Cheng, W. Xia, L. Yao, Z. Dou, H. Xue, H. Lian, Y. Qu and Q. Dong, *Thin Solid Films*, 2023, **770**, 139767.
142 B. Patil, B. Pownthurai, S.-S. Chiou, W.-L. Chen, D.-C. Huang, Y. Jadhav, P. Chetti, C.-H. Chang and A. Chaskar, *Org. Electron.*, 2021, **96**, 106217.
143 H.-T. Mao, W.-L. Song, C.-X. Zang, G.-F. Li, G.-G. Shan, H.-Z. Sun, W.-F. Xie and Z.-M. Su, *Org. Electron.*, 2020, **77**, 105513.
144 W. Song, L. Gao, T. Zhang, J. Huang and J. Su, *J. Lumin.*, 2019, **206**, 386–392.
145 Q. Zhang, S. Guo, K. Zhang, C. Yu, H. Zhou, Q. Wang, Z. Zhang, J. Huang, H. Wang and B. Wei, *Dyes Pigm.*, 2024, **222**, 111874.
146 K. Zhang, Q. Luo, G. Li, W. Shi, Z. Huang, Q. Zhang, H. Zhou, J. Huang, B. Wei and H. Wang, *Dyes Pigm.*, 2024, **226**, 112145.
147 Y. Chen, W. Chen, Y. Zheng, Q. Zhang, B. Zhao, L. Chen and J. Huang, *Dyes Pigm.*, 2023, **220**, 111684.
148 P. Zang, Y. Wu, R. Xia, Y. Jiang, P. Wu and Z. Wang, *Dyes Pigm.*, 2024, **230**, 112363.
149 T. Chatterjee, W.-Y. Hung, W.-F. Tang, H.-F. Chen and K.-T. Wong, *Org. Electron.*, 2017, **50**, 204–212.
150 W.-L. Chen, S.-Y. Chen, D.-C. Huang, D. Luo, H.-W. Chen, C.-Y. Wang and C.-H. Chang, *Materials*, 2021, **14**, 5723.
151 G. Krucaite, D. Blazevicius, D. Tavgeniene, S. Grigalevicius, C.-H. Lin, C.-M. Shao and C.-H. Chang, *Opt. Mater.*, 2020, **108**, 110225.
152 S. Grigalevicius, D. Tavgeniene, G. Krucaite, R. Griniene, Y.-P. Wang, S.-R. Tsai and C.-H. Chang, *Dyes Pigm.*, 2018, **159**, 173–178.
153 N. R. Al Amin, K. K. Kesavan, S. Biring, C.-C. Lee, T.-H. Yeh, T.-Y. Ko, S.-W. Liu and K.-T. Wong, *ACS Appl. Electron. Mater.*, 2020, **2**, 1011–1019.
154 C.-H. Chang, S.-W. Wu, C.-W. Huang, C.-T. Hsieh, S.-E. Lin, N.-P. Chen and H.-H. Chang, *Jpn. J. Appl. Phys.*, 2016, **55**, 03CD02.
155 G. Bagdžiūnas, G. Grybauskaitė, N. Kostiv, K. Ivaniuk, D. Volyniuk and A. Lazauskas, *RSC Adv.*, 2016, **6**, 61544–61554.
156 J.-K. Peng, C.-H. Ko, P. Gnanasekaran, C.-H. Ku, J.-R. Zhang, C.-Y. Chen, S.-W. Huang, T. J. Chow, Y.-T. Hung, Y. H. Lin, C.-H. Chang and Y. J. Chang, *Chem. – Asian J.*, 2025, **20**, e00739.
157 R.-H. Yi, Y.-S. Chen, D. Luo, H. Chen, S.-W. Liu and K.-T. Wong, *J. Mater. Chem. C*, 2024, **12**, 18363–18373.
158 Y. Y. Chen, Y. C. Kung, M. Wang, Y. C. Lo, Y. T. Chia, C. K. Wang, D. G. Chen, J. T. Cheng, P. T. Chou, C. Wu, E. Y. Li, B. Hu, W. Y. Hung and K. T. Wong, *Adv. Opt. Mater.*, 2024, **12**, 2303131.
159 Q. Yu, Y. Tamura, H. Nakanotani, M. Mamada and C. Adachi, *Adv. Opt. Mater.*, 2024, **12**, 2400932.
160 Z. A. Hasan, K. L. Woon, W. S. Wong, A. Ariffin and S.-A. Chen, *J. Lumin.*, 2017, **183**, 150–158.
161 C. Brouillac, F. Lucas, D. Tondelier, J. Rault-Berthelot, C. Lebreton, E. Jacques, C. Quinton and C. Poriel, *Adv. Opt. Mater.*, 2022, **11**, 2202191.
162 X.-Y. Liu, Y.-L. Zhang, X. Fei, L.-S. Liao and J. Fan, *Chem. – Eur. J.*, 2019, **25**, 4501–4508.
163 R. Beresneviciute, D. Blazevicius, S. Grigalevicius, Z.-R. He, F.-Y. Yang and C.-H. Chang, *Dyes Pigm.*, 2025, **241**, 112897.